AD-784 979

EXPERIMENTAL EVALUATION OF A SERIES OF SKEWED PROPELLERS WITH FORWARD RAKE: OPEN-WATER PERFORMANCE, CAVITATION PERFORMANCE, FIELD-POINT PRESSURES, AND UNSTEADY PROPELLER LOADING

John J. Nelka

Naval Ship Research and Development Center
Bethesda, Maryland

July 1974

UNCLASSIFIED

SECURITY CLASSIFICATION OF THIS PAGE (When Data Entered)

REPORT DOCUMENTATION PAGE		READ INSTRUCTIONS BEFORE COMPLETING FORM
1. REPORT NUMBER 4113	2. GOVT ACCESSION NO.	3. RECIPIENT'S CATALOG NUMBER AD-784 979
4. TITLE (and Subtitle) EXPERIMENTAL EVALUATION OF A SERIES OF SKEWED PROPELLERS WITH FORWARD RAKE: OPEN-WATER PERFORMANCE, CAVITATION PERFORMANCE, FIELD-POINT PRESSURES, AND UNSTEADY PROPELLER LOADING		5. TYPE OF REPORT & PERIOD COVERED 6. PERFORMING ORG. REPORT NUMBER
7. AUTHOR(s) John J. Nelka		8. CONTRACT OR GRANT NUMBER(s)
9. PERFORMING ORGANIZATION NAME AND ADDRESS Naval Ship Research and Development Center Bethesda, Maryland 20034		10. PROGRAM ELEMENT, PROJECT, TASK AREA & WORK UNIT NUMBERS Task Area ZR 0230101 Work Unit 1-1544-214
11. CONTROLLING OFFICE NAME AND ADDRESS Naval Ship Research and Development Center Bethesda, Maryland 20034		12. REPORT DATE July 1974 13. NUMBER OF PAGES 93
14. MONITORING AGENCY NAME & ADDRESS(if different from Controlling Office)		15. SECURITY CLASS. (of this report) UNCLASSIFIED 15a. DECLASSIFICATION/DOWNGRADING SCHEDULE

16. DISTRIBUTION STATEMENT (of this Report)

APPROVED FOR PUBLIC RELEASE: DISTRIBUTION UNLIMITED

17. DISTRIBUTION STATEMENT (of the abstract entered in Block 20, if different from Report)

18. SUPPLEMENTARY NOTES

19. KEY WORDS (Continue on reverse side if necessary and identify by block number)

Blade Warp
Blade Skew
Open-Water
Cavitation
Field-Point Pressures
Unsteady Propeller Loading

20. ABSTRACT (Continue on reverse side if necessary and identify by block number)

Results are given showing the experimental effect of propeller-blade warp on open-water performance, cavitation performance, unsteady field-point pressures, and unsteady propeller loading for a series of warped propellers. Blade warp is defined as the angular displacement at the midchord point of the blade section from the blade reference line in the plane of rotation.

Open-water results indicate that at the design thrust-loading coefficient and shaft horsepower the warped propellers are as much as 4.5 percent less than the design rpm.

(Continued on reverse side)

DD FORM 1 JAN 73 1473 EDITION OF 1 NOV 65 IS OBSOLETE
S/N 0102-014-6601

UNCLASSIFIED
SECURITY CLASSIFICATION OF THIS PAGE (When Data Entered)

(Block 20 continued)

Cavitation results show a widening of the cavitation-free bucket with increasing warp; however there is some crossover in the inception of back cavitation and tip-vortex cavitation. Field-point pressures and the unsteady propeller forces and moments have been found to decrease with increasing warp to reductions previously achieved with blade skew.

The Naval Ship Research and Development Center is a U. S. Navy center for laboratory effort directed at achieving improved sea and air vehicles. It was formed in March 1967 by merging the David Taylor Model Basin at Carderock, Maryland with the Marine Engineering Laboratory at Annapolis, Maryland.

Naval Ship Research and Development Center

Bethesda, Md. 20034

MAJOR NSRDC ORGANIZATIONAL COMPONENTS

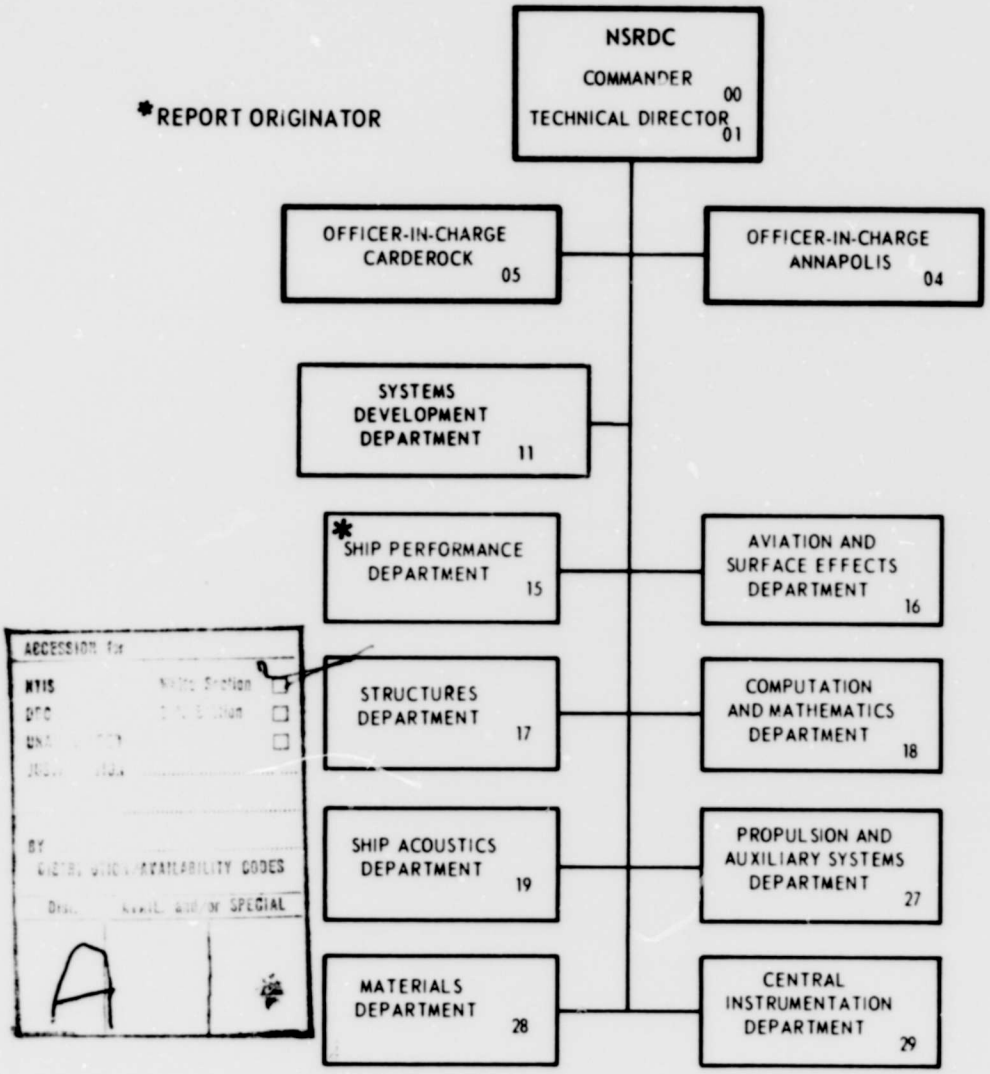

NDW-NSRDC 3960/43b (Rev. 3-
GPO 928-

TABLE OF CONTENTS

LIST OF FIGURES

LIST OF TABLES

Page

NOTATION

A_E	Expanded-blade area
A_E/A_o	Expanded-area ratio
A_m	Fourier sine coefficient of the mth harmonic of the propeller loading
A_o	Disk area of propeller, $A_o = \pi R^2$
a_m	Fourier cosine coefficient of the mth harmonic of the pressure signal
a_0	Constant term of the pressure signal
a_Z	Fourier cosine coefficient of the blade-frequency harmonic of the pressure signal
B_m	Fourier cosine coefficient of the mth harmonic of the propeller loading
b_m	Fourier sine coefficient of the mth harmonic of the pressure signal
b_Z	Fourier sine coefficient of the blade-frequency harmonic of the pressure signal
C_m	Amplitude of the mth harmonic of the pressure signal
C_p	Pressure coefficient, $C_p = (p - p_\infty) \Big/ \left(\frac{1}{2}\rho V_A^2\right)$
C_P	Power coefficient, $C_P = 2\pi NQ \Big/ \frac{\rho}{2} A_o V_A^3$
C_{Th}	Thrust-loading coefficient, $C_{Th} = T \Big/ \frac{\rho}{2} A_o V_A^2$
C_Z	Amplitude of the blade-frequency harmonic of the pressure signal
c	Section chord length
D	Propeller diameter
F	Side force
f_M	Maximum camber of propeller blade section
g	Acceleration due to gravity

h	Hydrostatic head at shaft centerline minus vapor pressure
IVFV	Inception of face vortex cavitation
IVTV	Inception of tip vortex cavitation
J	Advance coefficient, $J = V_A/ND$
J_D	Design value of J
K_p	Nondimensional pressure coefficient, $K_p = p/\rho N^2 D^2$
K_{p_Z}	Nondimensional blade-frequency pressure coefficient, $K_{p_Z} = C_Z/\rho N^2 D^2$
K_Q	Torque coefficient, $K_Q = Q/\rho N^2 D^5$
K_{QD}	Design value of K_Q
K_T	Thrust coefficient, $K_T = T/\rho N^2 D^4$
K_{TD}	Design value of K_T
$\bar{K}_T$	Mean thrust coefficient
L	Loading
M	Bending moment
N	Propeller revolutions per unit time, positive in direction propelling ship forward
N_D	Design value of N
n	Order of wake harmonic
P	Propeller section pitch
P_D	Power delivered to the propeller, $P_D = 2\pi QN/550$
p	Pressure
p_∞	Free-stream pressure
$\bar{p}$	Mean pressure
$\tilde{p}$	Unsteady pressure

Q	Propeller torque, positive in direction propelling ship forward
R	Propeller radius
R_n	Reynolds number at 0.7R, $R_N = c_{0.7} \frac{\sqrt{V_A^2 + (0.7\pi ND)^2}}{\nu}$
r	Radial distance from propeller axis
T	Propeller thrust, positive in direction propelling ship forward
t	Maximum thickness of propeller-blade section
V	Ship speed
V_A	Speed of advance of propeller, positive forward, $V_A = (1 - w)V$
V_D	Design value of V_A
$V_L(r,\theta)$	Local longitudinal inflow velocity to propeller plane, based on results of wake survey
$[V_L(r)]_n$	Fourier coefficient of the nth harmonic of the longitudinal wake velocity
V_{VM}	Volume mean velocity into propeller disk
V_∞	Free-stream velocity
w	Taylor wake fraction, based on thrust identity, $w = (V - V_A)/V$
x	Nondimensional radius, $x = r/R$
x/R	Nondimensional axial distance from propeller plane
Z	Blade number; subscript denoting blade-frequency
β	Advance angle
β_I	Hydrodynamic flow angle
γ	Dummy phase angle
η_o	Propeller open-water efficiency, $\eta_o = (J/2\pi)K_T/K_Q$
θ	Angular coordinate about shaft axis; positive clockwise looking upstream ($\theta = 0$ for vertical upward)
θ_{C_p}	Phase angle of maximum pressure coefficient amplitude relative to reference line

θ_p	Propeller angular position about shaft axis; positive clockwise looking upstream (θ_p = 0 for vertical upward)
θ_S	Projected skew angle at radius r relative to reference line
θ_Z	Phase angle of peak blade-frequency pressure amplitude relative to reference line
ν	Kinematic viscosity of water
ρ	Density of water
σ	Cavitation number based on vapor pressure, $\sigma = 2g\nu/V_A^2$
Φ	Geometric angle by which the blade-rate propeller loading leads the same frequency component of the longitudinal velocity
ϕ	Propeller angular coordinate about shaft axis; positive counter-clockwise looking upstream (ϕ = 0 for vertical upward)
ϕ_w^n	Phase angle of nth harmonic of wake
ϕ_m	Phase angle of the mth harmonic of propeller loading, relative to the radial line through the midchord of the root section of the propeller blade (ϕ_m = 0 for vertical upward), positive clockwise looking upstream
ϕ_{ZW}	Phase angle of the blade-rate harmonic of the wake velocity, measured at r/R = 0.7 relative to the upward vertical

Subscripts

H	Horizontal direction with respect to fixed axes
m	Order of propeller-loading harmonic
n	Order of wake-velocity harmonic
V	Vertical direction with respect to fixed axes
W	Wake
Z	Order of blade-frequency harmonic
1,2	Horizontal and vertical directions rotating with propeller
–	Mean component
~	Fluctuating or unsteady component

ABSTRACT

Results are given showing the experimental effect of propeller-blade warp on open-water performance, cavitation performance, unsteady field-point pressures, and unsteady propeller loading for a series of warped propellers. Blade warp is defined as the angular displacement at the midchord point of the blade section from the blade reference line in the plane of rotation.

Open-water results indicate that at the design thrust-loading coefficient and shaft horsepower the warped propellers are as much as 4.5 percent less than the design rpm. Cavitation results show a widening of the cavitation-free bucket with increasing warp; however, there is some crossover in the inception of back cavitation and tip-vortex cavitation. Field-point pressures and the unsteady propeller forces and moments have been found to decrease with increasing warp to reductions previously achieved with blade skew.

ADMINISTRATIVE INFORMATION

The work reported herein was authorized and funded by the in-house independent research program of the Naval Ship Research and Development Center under Task Area Z-R023 01 01, Work Unit 1-1544-214 (544-214 before 1 January 1971).

INTRODUCTION

Various categories of propeller-blade distortions are being evaluated by the Naval Ship Research and Development Center to determine their effect in reducing propeller cavitation as well as unsteady propeller pressures and bearing forces and moments. One kind of blade distortion, skew,[1] can provide significant decreases in propeller force and moment fluctuations,[2] decreases in propeller-induced pressures,[3,4] and delays in the inception of propeller-blade cavitation.[5,6]

---

[1]Cumming, R. A. et al., "Highly Skewed Propellers," Transaction of Society of Naval Architects and Marine Engineers, Vol. 80 (1972). A complete listing of references is given on pages 79 and 80.

[2]Boswell, R. J. and M. L. Miller, "Unsteady Propeller Loading Measurement, Correlation with Theory, and Parametric Study," NSRDC Report 2625 (Oct 1968).

[3]Denny, S. B., "Comparisons of Experimentally Determined and Theoretically Predicted Pressures in the Vicinity of a Marine Propeller," NSRDC Report 2349 (May 1967).

[4]Teel, S. S. and S. B. Denny, "Field Point Pressures in the Vicinity of a Series of Skewed Marine Propellers," NSRDC Report 3278 (Aug 1970).

[5]Denny, S. B., "Cavitation and Open-Water Performance of a Series of Propellers Designed by Lifting-Surface Methods," NSRDC Report 2878 (Sep 1968).

[6]Boswell, R. J., "Design, Cavitation Performance and Open-Water Performance of a Series of Research Skewed Propellers," NSRDC Report 3339 (Mar 1971).

Propeller-blade skew is defined as the displacement at the midchord point of the blade section from the blade reference line along the pitch helix. Generally, the value of the angular displacement in the projected view at the tip of the blade is used as a measure of the skew. The resulting axial displacement of the blade sections is sometimes referred to as skew-induced rake.

The benefits of skew described previously cannot always be obtained for existing ships inasmuch as the axial displacement of the blades associated with skew may cause clearance problems in an existing propeller aperture. In addition, the stress in propellers with large amounts of skew may be larger than those in unskewed propellers.[7,8,9] Hence, other forms of blade distortion should be evaluated. Warp, the angular displacement of the blade sections in the plane of rotation without axial displacement, may exhibit the advantages of skew without the aforementioned disadvantages. Figure 1 shows various types of blade distortion. This project was undertaken to determine if the aforementioned benefits of blade skew were also associated with blade warp.

In this report, the effect of blade warp on open-water performance, cavitation performance, the propeller-induced pressure field, and fluctuations of propeller force and moment is evaluated for a series of warped propellers.

More specifically, the open-water and cavitation performance of two warped propellers (36° and 72°) will be compared with the open-water and cavitation performance of two skewed propellers (36° and 72°). The designations shown in Table 1, which directly indicate whether the propeller is warped or skewed, will be used instead of model numbers in referring to the propellers.

For the propeller-induced pressures, a series of warped propellers (0°, 36°, and 72° blade warp) is evaluated. Total fluctuating pressures are measured on a flat plate adjacent to a model propeller operating in the 24-inch water tunnel. The amplitude and phase of the blade-frequency portions of the measured induced pressures are determined for operation in uniform flow at two propeller-tip clearances and in nonuniform flow at one propeller-tip clearance.

Finally the results of the effect of propeller-blade warp on the unsteady forces and moments acting on a propeller operating in nonuniform flow are presented. The warped-propeller results are compared to those of an existing series of skewed propellers, evaluated previously.

---

[7]Boswell, R. J., "Static Stress Measurements on a Highly Skewed Propeller Blade," NSRDC Report 3247 (Dec 1969).

[8]Boswell, R. J. et al., "Experimental Measurements of Static Stresses In a Series of Research Skewed Propellers with and without Forward Rake," NSRDC Report 3804 (in preparation).

[9]Ma, J. H., "Stress Analysis of Complex Ship Components by Numerical Procedure Using Curved Finite Elements," NSRDC Report 4057 (Jul 1973).

The warped propellers were derived from the skewed propellers mentioned previously by removing the skew-induced rake while other characteristics were unchanged. It is known that such a change will affect pitch and camber; however, methods to compute these effects were not available at the time, and it was not clear in any event whether the effects would be significant. Methods[10,11] for the design of warped propellers have become available, however, since these propellers were evaluated, and the methods have been used to calculate the pitch and camber which should be used on such propellers. The results indicate that the camber is too high, particularly near the root, for the propellers reported herein and that the pitch is also somewhat high. These results are generally substantiated by the results of the open-water and cavitation characteristics of these propellers. The lack of proper pitch and camber corrections will also have a measurable effect on the field-point pressures inasmuch as the radial distribution of loading is not the same for similarly warped and skewed propellers at the same value of thrust coefficient. This fact should be kept in mind by the reader when comparing the field point pressure results for the warped propellers with those for the skewed propellers.

PROPELLER CHARACTERISTICS

The warped propeller series consists of a parent propeller (Propeller 4381) with no warp or skew and two propellers (Propellers 4497 and 4498) with 36° and 72° of blade warp derived from Propellers 4382 and 4383, 36° and 72° skew, respectively. Table 2 presents the geometry of these skewed and warped propellers, and Figures 2 and 3 present their photograph and blade outline. Propellers 4381, 4382, and 4383 were the skewed propeller series evaluated by Teel and Denny[4] and Boswell.[6]

Propellers 4382 and 4383 were designed using the lifting-surface procedure of Cheng[12] together with the thickness corrections of Kerwin and Leopold.[13] All parameters, except skew (and pitch and camber corrections due to skew), were held constant for Propellers 4382 and 4383.

---

[10]Kerwin, J. E., "Computer Techniques for Propeller Blade Section Design," Presented at Second LIPS Propeller Symposium, Drunen, Netherlands (May 1973).

[11]Pien, P. C., Discussion of Paper, "Highly Skewed Propellers," by Cumming, R. A. et al., Transactions of Society of Naval Architects and Marine Engineers, Vol. 80 (1972).

[12]Cheng, H. M., "Hydrodynamic Aspect of Propeller Design Based on Lifting-Surface Theory, Part II – Arbitrary Chordwise Load Distribution," David Taylor Model Basin Report 1803 (Jun 1965).

[13]Kerwin, J. E. and R. Leopold, "Propeller-Incidence Correction Due to Blade Thickness," Journal of Ship Research, Vol. 7, No. 2 (Oct 1963).

As mentioned previously, Propeller 4497 (36° warp) and Propeller 4498 (72° warp) were derived from Propellers 4382 and 4383, respectively, by removing the skew-induced rake while all other characteristics were unchanged. The absence of rake in Propellers 36W and 72W may be clearly seen in Figures 4a through 4f.

EXPERIMENTAL PROCEDURE

OPEN-WATER PERFORMANCE

Open-water performance of the two warped and two skewed model propellers in two quadrants was measured in the Center deepwater basin. Instruments in the propeller boat included a gravity dynamometer for the forward quadrants and a transmission dynamometer for the backing quadrants. The forward quadrants for the warped propellers were run at 7.8 rps and at a speed of advance V_A, ranging from 3 to 10 feet per second, resulting in a range of Reynolds number R_n from 6.1×10^5 to 6.9×10^5. The backing quadrants were run at −8.33 rps and at V_A ranging from −3.0 to −9.5 feet per second, resulting in a range of R_n from 6.4×10^5 to 7.4×10^5. The rps and speed of advance for the forward and backing quadrants were measured to within ±0.01 rps and ±0.001 feet per second, respectively.

CAVITATION PERFORMANCE

The cavitation performance of Propellers 36S, 36W, 72S, and 72W was measured in the 24-inch variable pressure water tunnel at the Center in uniform flow, using the open-jet test section and a downstream shaft driven by a 150-horsepower dynamometer. At the design thrust coefficient, the measurement of dynamometer thrust was within ±0.6 percent of the design thrust.

Each propeller was evaluated over a range of advance coefficients J and cavitation numbers σ. For each advance coefficient, the tunnel water speed was calibrated by setting thrust and rps based on the open-water experiment for the propeller. The tunnel water velocity was measured, using a pitot tube and a mercury-filled manometer. The nose of the pitot tube was located in the propeller plane approximately 9 inches from the axis of the propeller. In general, the maximum difference between the thrust-identity, open-water velocity and the measured tunnel water velocity was ±3 percent. The thrust-identity, open-water velocity was used in all calculations.

At each advance coefficient, the cavitation experiments were conducted by starting from a noncavitating condition and reducing the tunnel pressure (and thus σ) until cavitation appeared and/or until the cavitation pattern changed significantly. The cavitation patterns at these pressures were photographed and sketched, and the propeller thrust and torque were recorded. The cavitation experiments for all propellers were run at n = 14 to 20 rps and V_A = 7 to

26 feet per second, i.e., $R_n = 1.09 \times 10^6$ to 1.77×10^6. The total air content, as measured with a Van Slyke apparatus, was maintained at 25 to 30 percent of saturation at atmospheric pressure.

FIELD-POINT PRESSURES

Experiments were run in a closed-jet test section of the previously described water tunnel with propellers fitted on the downstream shaft. A flat plate was mounted parallel to the propeller axis; the plate contained five pressure transducers, located on a line nearest and parallel to the propeller axis. Recorded pressure amplitudes from the transducers were measured to within ±0.01 pounds per square inch. Flat-plate dimensions, transducer locations, and placement in the water tunnel are shown in Table 3 and Figure 5. A plane through the hub midlength and perpendicular to the shaft axis was used as a reference plane for the presentation of data. This plane intersected the flat plate at $x/R = 0.06$ upstream of transducer 4. The plate was positioned at two propeller-tip clearances, 10 and 30 percent of the propeller radius.

Advance coefficients for the experiments were determined by setting a thrust identity with the open-water results. Nonuniform flow was generated by use of a wake screen,[14] and the advance coefficients were then based on a mean thrust coefficient. Thrust coefficients established during the experiments on all propellers were $K_T = 0.0$, 0.1, 0.214 (Design K_T = 0.214), 0.300, and 0.375. Table 4 indicates the $K_T - J$ relations in open water for the three propellers. Shaft revolutions were maintained at 14.0 rps for all conditions so that all loading conditions could be obtained without overloading the drive motor of the 10-horsepower dynamometer. At design K_T, thrust was measured to within ±0.6 percent of the design thrust.

In nonuniform-flow experiments with the 4-cycle wake screen, the effect of each distinct flow region on induced pressures was investigated. Limited availability of the 24-inch water tunnel due to scheduling allowed for only position 3 of the 5-cycle wake to be evaluated for its effect on the induced pressures. Figure 6 presents the diagrams of the wake screens. The positions designated on the diagrams are those directly upstream of and in line with the five pressure transducers. Figure 7 presents the harmonic content of the wakes generated by the 4- and 5-cycle wake screens.

---

[14] McCarthy, J. H., "A Method of Wake Prediction in Water Tunnel," David Taylor Model Basin Report 1785 (Oct 1963).

UNSTEADY PROPELLER LOADING

The warped-propeller series was evaluated in nonuniform flow in the 24-inch water tunnel to determine the effect of warp on unsteady loading. The six-component propeller dynamometer and the procedures described in Reference 2 were used. Since the propellers had five blades, a five-cycle wake screen was used to excite blade-frequency thrust and torque fluctuations; a four-cycle screen was used to excite blade-frequency side forces and bending moments.[15] Wake screens are shown in Figure 6.

The velocity field due to the wake screen can be expressed as

$$V_L(r,\theta) = [V_L(r)]_o + \sum_{n=1}^{\infty} [V_L(r)]_n \sin(n\theta + \phi_{nw}) \qquad (1)$$

where $V_L(r,\theta)$ = local longitudinal inflow velocity to the propeller plane

$[V_L(r)]_n$ = Fourier coefficient of the nth harmonic of the longitudinal wake velocity

θ = angular coordinate about shaft axis, positive clockwise looking upstream (θ = 0 for vertical upward)

ϕ_{nw} = phase angle of the nth harmonic of the wake.

The volume mean velocity over the propeller plane is

$$V_{VM} = \left[\int_0^{2\pi} \int_{r_h}^{R} V_L(r,\theta)\, r\, dr\, d\theta / 2\pi(R^2 - r_h^2) \right] \qquad (2)$$

where V_{VM} = volume mean velocity into the propeller disk

R = radius of the propeller

r_h = radius of the hub.

Figure 7 shows the phase angles and nondimensionalized amplitudes of the principal harmonic components of the two wakes. The phase angles are relative to the radial line directed vertically upward from the propeller axis. Other harmonic components were present; however, they were small and not significant to the results of the experiments since only the fifth harmonic of the five-cycle wake and the fourth and sixth harmonics of the four-cycle wake contributed to the blade-frequency results reported.

---

[15] Hadler, J. B. and H. M. Cheng, "Analysis of Experimental Wake Data in Way of Propeller Plane of Single and Twin-Screw Ship Models," Transactions of Society of Naval Architects and Marine Engineers, Vol. 73 (1965).

Figure 8 defines the three forces and three moments acting on the propeller. Note that what is called horizontal bending moment is not a horizontal moment vector but a moment produced by a horizontal force.

The propellers were evaluated at a constant rotational velocity N of 14 revolutions per second. By changing the water speed, the mean-thrust coefficient $\bar{K}_T$ was varied from zero to nearly twice the design $\bar{K}_T$ of 0.214. This resulted in a Reynolds number $R_{n_{0.7}}$ of at least 10^6 for all conditions. Since the mean tunnel speed could not be measured directly, a thrust identity was used to determine the advance coefficients. It was assumed that the advance coefficient was the same as that which would have resulted in the same thrust coefficient in an open-water experiment.

DATA ANALYSIS

FIELD-POINT PRESSURES

Pressure measured at each transducer was (1) recorded on magnetic tape to be later digitized and analyzed, and (2) digitized and analyzed online by an analog digital converter and an Interdata Model 4 Minicomputer. Figure 9 shows the instrumentation. The magnetic tape pressure results, which were digitized using the XDS-910 system and were then analyzed using a CDC 6700 digital computer, showed excellent agreement with the pressure results obtained from the online data analysis system.

For the magnetic tape, the records of at least 200 revolutions at each condition were digitized and averaged, and the average waveform data were then entered into a harmonic analysis program. For the data that were digitized online, the records of at least 800 revolutions were digitized, averaged, and stored in the memory system of the Interdata Model 4 Minicomputer. The average waveform data were then entered into a harmonic analysis program.

Although the number of revolutions for data collection differed for the two methods of data analyses, no significant difference in the induced pressure results was apparent.

In general, the blade-frequency harmonic was the most significant for all the experimental results. The two times blade-frequency harmonic was usually 10 to 20 percent of the blade-frequency harmonic, and the three times blade-frequency harmonic was usually 5 to 15 percent of the blade-frequency harmonic.

The total pressure at each transducer consists of a periodic time-dependent fluctuation $\tilde{p}$ about a mean value $\bar{p}$ and can be represented by a Fourier series as:

$$p = a_o/2 + \sum_{m=1}^{\infty} [a_m \cos m\phi + b_m \sin m\phi] \qquad (3)$$

where $\bar{p} = a_o/2$

$$\tilde{p} = \sum_{m=1}^{\infty} [a_m \cos m\phi + b_m \sin m\phi]$$

By letting

$$a_m/C_m = \cos \gamma_m \text{ and } b_m/C_m = \sin \gamma_m$$

where $C_m = [a_m^2 + b_m^2]^{1/2}$

Equation (1) then becomes

$$p = a_o/2 + \sum_{m=1}^{\infty} C_m [a_m/C_m \cos m\phi + b_m/C_m \sin m\phi]$$

or

$$p = a_o/2 + \sum_{m=1}^{\infty} C_m \cos (m\phi - \gamma_m) \tag{4}$$

where $\gamma_m = \tan^{-1} (b_m/a_m)$

Thus, the unsteady pressure at each transducer is defined as the total pressure less the mean pressure

$$\tilde{p} = p - \bar{p} = \sum_{m=1}^{\infty} C_m \cos (m\phi - \gamma_m) \tag{5}$$

If Z is the number of blades of the propeller then the amplitude of the blade-frequency pressure fluctuation is given by C_Z, and the phase angle of that harmonic is given by γ_Z; thus

$$p_Z = C_Z \cos (Z\phi - \gamma_Z) \tag{6}$$

The maximum blade-frequency signal occurs when $Z\phi - \gamma_Z = 0$. Therefore, the phase angle for which p_Z is a maximum is defined to be

$$\theta_Z = \gamma_Z/Z \tag{7}$$

The amplitude of the blade-frequency harmonic has the dimensions of pressure and is nondimensionalized as follows

$$K_{p_Z} = C_Z/\rho N^2 D^2 \tag{8}$$

It should be noted that the phase angle result of Kerwin[13] is for the angle at which the pressure coefficient is a maximum and, according to Kerwin, is defined to be

$$C_p = \frac{p_\infty - p}{\left(\frac{1}{2}\right)\rho V_A^2} \tag{9}$$

If Equation 2 is used to represent the propeller-induced pressure p, then Equation (6) becomes

$$C_p = \frac{1}{\left(\frac{1}{2}\right)\rho V_A^2}\left[p_\infty - a_o/2 - \sum_{m=1}^{\infty} C_m \cos(m\phi - \gamma_m)\right] \tag{10}$$

If all terms are neglected, except those of blade frequency, then Equation (7) becomes

$$C_{p_Z} = \frac{1}{\left(\frac{1}{2}\right)\rho V_A^2}\left[-C_Z \cos(Z\phi - \gamma_Z)\right] \tag{11}$$

The maximum positive value of the blade-frequency pressure coefficient occurs when $Z\phi - \gamma_Z = \pi$. Therefore, when $\phi = (\pi + \gamma_Z)/Z$, the phase angle for which C_p is a maximum is equal to $\theta_{C_p} = (\pi + \gamma_Z)/Z$ or, using the results of Equation (4)

$$\theta_{C_p} = \pi/Z + \theta_Z \tag{12}$$

where θ_Z represents the phase angle of maximum induced pressure amplitude relative to the blade-reference line. Thus, the maximum pressure-coefficient amplitude and the maximum induced-pressure amplitude are out of phase by π/Z.

UNSTEADY PROPELLER LOADING

The signals from the six-component balance along with phase-reference pulses were recorded on magnetic tape for digital computer analysis. The balance was designed so that the transverse-force and bending-moment sensors would rotate with the propeller. These sensors were used to measure force and moment along a pair of orthogonal axes. Hence, transverse-force and bending-moment vectors rotating with the propeller were measured. A propeller position ($\theta_p = 0$) is defined as that at which the rotating axis coincides with the (fixed) horizontal and vertical axes; then

$$\tilde{M}_1 = \tilde{M}_V ; \tilde{M}_2 = \tilde{M}_H ; \tilde{F}_1 = \tilde{F}_V ; \tilde{F}_2 = \tilde{F}_H \tag{13}$$

where $\tilde{M}_1$, $\tilde{M}_2$, $\tilde{F}_1$, and $\tilde{F}_2$ are forces and moments with respect to the rotating axes. The angle θ_p is the propeller angular position about the shaft axis positive clockwise looking upstream, $\theta_p = 0$ for vertical upward. At any θ_p, the forces and moments with respect to the fixed axes are

$$\begin{aligned} M_V &= M_1 \cos\theta_p + M_2 \sin\theta_p \\ M_H &= -M_1 \sin\theta_p + M_2 \cos\theta_p \\ F_V &= F_1 \cos\theta_p - F_2 \sin\theta_p \\ F_H &= F_1 \sin\theta_p + F_2 \cos\theta_p \end{aligned} \tag{14}$$

For the computer analysis, the tape record was digitized at 80 points per revolution. These values were averaged for 200 revolutions and were scaled to obtain 80 points at 4.5° intervals of an average cycle. The values for the six channels were then multiplied by a 6 by 6 calibration matrix to obtain values of thrust and side forces in pounds and torque and bending moment in foot-pounds.

Another computer operation resolved the rotating side-force and bending-moment vectors into vertical and horizontal components. The amplitudes of the first 20 harmonic components were then computed along with the phase angle relative to the propeller position at which the single-tooth pulse was generated. The position at which the single-tooth pulse was generated occurred at the vertical upward position of the midchord of the root section of the propeller blade.

On-the-spot readings of the amplitude and phase of the dominant harmonic component of each signal were also made. In addition, the waveforms of the signals were recorded photographically from an oscilloscope.

Concurrent with this investigation, the field-point pressures were measured on a flat plate near the propellers. The same conditions and phase-reference pulses were used, and the data were recorded on the same magnetic tape. Additional pressure measurements were made with several different angles between the wake screen and the pressure measuring position as well as with uniform flow.

A periodic loading can be expressed as

$$L = a_o/2 + \sum_{m=1}^{\infty} [A_m \sin m\theta_p + B_m \cos m\theta_p] \qquad (15)$$

where $\bar{L} = a_o/2$

$$\tilde{L} = \sum_{m=1}^{\infty} [A_m \sin m\theta_p + B_m \cos m\theta_p]$$

By letting

$$A_m/C_m = \cos\phi \text{ and } B_m/C_m = \sin\phi$$

where $C_m = [A_m^2 + B_m^2]^{1/2}$

Equation (15) becomes

$$L = a_o/2 + \sum_{m=1}^{\infty} C_m [A_m/C_m \sin m\theta_p + B_m/C_m \cos m\theta_p]$$

or

$$L = a_o/2 + \sum_{m=1}^{\infty} C_m \sin (m\theta_p + \phi_{mL}) \qquad (16)$$

where $\phi_{mL} = \tan^{-1} (B_m/A_m)$

Thus the unsteady thrust may be expressed as

$$\tilde{T} = T - \bar{T} = \sum_{m=1}^{\infty} \tilde{T}_m \sin(m\theta_p + \phi_{mT}) \tag{17}$$

where $\tilde{T}_m$ is the amplitude of the mth harmonic of the unsteady thrust, and ϕ_{mT} is the phase angle of the mth harmonic of the unsteady thrust.

Similarly the equations for unsteady torque, side force, and bending moment, are

$$\tilde{Q} = Q - \bar{Q} = \sum_{m=1}^{\infty} \tilde{Q}_m \sin(m\theta_p + \phi_{mQ}) \tag{18}$$

$$\tilde{F} = F - \bar{F} = \sum_{m=1}^{\infty} \tilde{F}_m \sin(m\theta_p + \phi_{mF}) \tag{19}$$

$$\tilde{M} = M - \bar{M} = \sum_{m=1}^{\infty} \tilde{M}_m \sin(m\theta_p + \phi_{mM}) \tag{20}$$

where $\tilde{Q}_m$, $\tilde{F}_m$, $\tilde{M}_m$ are the amplitudes of the mth harmonic of the unsteady torque, side forces, and bending moments, and ϕ_{mQ}, ϕ_{mF}, ϕ_{mM} are the phase angles of the mth harmonic of the unsteady torque, side force, and bending moment.

EXPERIMENTAL RESULTS

OPEN-WATER PERFORMANCE

Figures 10 and 11 present the forward and backing open-water propulsion characteristics, respectively, of Propellers 36S and 72S and Propellers 36W and 72W.

The open-water data of Propellers 36S and 72S presented in Figures 10 and 11 differ slightly from those of Reference 6. The open-water experiments of these propellers were repeated inasmuch as a more accurate comparison could be made when the propeller results were compared from the same experimental setup.

The forward open-water thrust and torque coefficients of Propellers 36W and 72W were, in general, greater than those of Propellers 36S and 72S, respectively. The open-water torque coefficient for Propeller 72W was greater than that of Propeller 36W for all forward advance coefficients, and the forward open-water thrust coefficients for Propellers 36W and 72W were approximately equal for advance coefficients less than 0.7. However, the thrust coefficient of

Propeller 72W was greater than that of Propeller 36W for advance coefficients greater than 0.7.

Table 5 presents a comparison of the four propellers at the design condition. In all instances, the skewed propellers perform nearer to design than do the warped propellers. Table 5 shows that Propellers 36S, 72S, 36W, and 72W operate within 1, 1, 2.5, and 4.5 percent of design rpm, respectively, while absorbing design shaft horsepower. Table 5 also shows that the propellers operate within 1 percent of the design forward velocity when absorbing the design shaft horsepower. It must be mentioned that the data presented in Table 5 are based on open-water results. No propulsion experiments were conducted.

Figure 11 presents the backing open-water performance of the four propellers. The backing open-water thrust and torque coefficients of Propellers 36W and 72W are, in general, less negative than those of Propellers 36S and 72S, respectively. The backing open-water thrust and torque coefficients of 72W are lower in absolute value than those of Propeller 36W for all advance coefficients tested. Table 6 shows the effect of skew and warp on speed at constant power and constant thrust-loading coefficient. Table 6 was computed by entering the backing open-water curves at a constant thrust-loading coefficient, $C_{Th} = 8K_T/\pi J^2$. At the corresponding advance coefficient J, the power coefficient $C_p = [2\pi NQ/(1/2)\rho V_A^3 A_o] = 16K_Q/J^3$ was obtained from the open-water curves. Constant power, $P_D = 2\pi NQ/550$, and diameter were specified; therefore, the speed of advance for each propeller was $V_A = [P_D/(1/2)\rho C_p A_o]^{1/3}$. The data show that the backing speed decreased with increasing skew and warp, and the amount of reduction was insensitive to the thrust-loading coefficient in the region from $C_{Th} = 0.2$ to $C_{Th} = 1.6$. The backing speeds with 36° and 72° skew and 36° and 72° warp were approximately 1.5, 7, 6, and 8 percent less, respectively, than the backing speed with zero skew or warp.

CAVITATION PERFORMANCE

Figure 4, Figures 12 through 22, and Table 7 show the cavitation-inception results of Propellers 36S, 36W, 72S, and 72W. Sketches and photographs of the cavitation at selected advance coefficients and cavitation numbers are given in Figures 4a through 4f. For Figures 12 through 20, a curve marked with one radius means that the propeller was cavitating from that radius to the tip. Curves showing the inception of a separate inner cavity are marked with the radial extent of the inner cavity. This occurs only on Propeller 72S. In general, sheet cavitation on the back (suction side) started near the tip and proceeded to lower radii with decreasing cavitation number. On the face, initial sheet cavitation extended from an inner radius to approximately 0.95 propeller radius. As the pressure was lowered, the inner part of the cavity extended to a larger radius. When the outer end of the cavity extended

slightly beyond r/R = 1.0, and a tip vortex occurred, face vortex cavitation inception was said to occur. Visual tip-vortex inception on the back of a propeller blade occurred when the tip-vortex cavity appeared to attach itself to the propeller blade near the tip with the length of the tip-vortex cavity extending downstream parallel to the leading edge but not adhering to it. For the propellers evaluated, inception does not occur simultaneously on all blades for the same cavitation number; therefore, the curves of Figures 12 through 22 represent cavitation inception on at least three of the five propeller blades unless otherwise noted.

Figures 12 through 14 present the cavitation results of Propellers 36W and 72W. It can be seen in Figure 14 that a widening of the cavitation-free bucket occurs with increasing warp. However, some crossover in the inception of back-sheet and tip-vortex cavitation occurred for the warped propellers so that at the design thrust-loading coefficient, back-sheet cavitation was delayed most on Propeller 36W. For the warped propellers, inception of the tip-vortex cavitation occurred on each blade at nearly the same radius, x = 0.9. Back bubble cavitation on Propeller 72W occurred at higher cavitation numbers than for Propeller 36W for all advance coefficients tested as shown in Figure 15. Back bubble on the warped propellers generally started midchord of the propeller blade near the root ($0.2 < x < 0.4$) and proceeded to 100 percent chord and larger radii with decreasing cavitation number.

Cavitation results of Propellers 36S and 72S are presented in Figures 16 through 18 with comparison of back bubble-inception results presented in Figure 15. In Figure 18, it can be seen that a widening of the cavitation-free bucket occurs with increasing skew, similar to the result obtained for increasing warp. A crossover, similar to that of the warped propellers, in the inception of back-sheet and tip-vortex cavitation occurred for the skewed propellers; thus, at the design thrust-loading coefficient, sheet cavitation was delayed most on Propeller 36S. Tip vortex-cavitation inception occurred at x = 0.9 for Propeller 36S and at the blade tip (x = 1.0) for Propeller 72S. Figure 15 shows that back bubble-cavitation inception occurred on Propeller 72S at slightly lower cavitation numbers than Propeller 36S for advance coefficients greater than 0.85; however, the values for advance coefficients were similar at less than 0.85. Table 7 gives results of back bubble-cavitation inception for the skewed and warped propellers.

For Propellers 72S and 72W, another type of cavitation called back-trailing edge occurred; see Figure 13. This type of cavitation occurred near the root of the trailing edge of the back of the propeller blade and had the appearance of sheet rather than bubble cavitation.

Differences in the cavitation-inception characteristics of the skewed and warped propellers are presented in Figures 19 through 22. It is known that the method used to design the warped propellers will affect the radial load distribution. Thus, some of the differences in the cavitation inception characteristics due to blade warp, especially back bubble-cavitation inception, may be due to using an inadequate design method for the warped propellers.

Comparison of Propellers 36S and 36W at a given advance condition showed that back-sheet and vortex cavitation occurred at a higher cavitation number for Propeller 36S, while face-sheet and face-vortex cavitation occurred at approximately the same cavitation number for a given advance condition for both Propellers 36S and 36W. Comparison of Propellers 72S and 72W showed that cavitation results similar to those for Propellers 36S and 72S as reported by Boswell[6] differed slightly from the results presented herein. However, trends associated with increasing skew are the same. The differences in the present cavitation results of Propellers 36S and 72S and of Boswell could have been caused by the following:

- Use of different open-water results to calculate the speed of advance V_A; thus, changing the inception cavitation number.
- Changes in propeller-blade surface. A number of experiments have been conducted on Propellers 36S and 72S, and the surface finish of the blades was not as good as that for the blades of Propellers 36W and 72W.
- Unknown and unrecorded changes in the water that may have altered the cavitation number for inception.
- Experimental technique that may have differed between experimenters, for example, pressures may have been decreased at different rates.
- Cavitation results that depended ultimately on the subjective evaluation of the observer-experimenter. For this experiment, it was found that for each propeller evaluated, the inception of a particular type of cavitation did not occur on all blades at the same cavitation number. Also, the radial and chordwise extent of cavitation on each propeller blade was not identical for the same cavitation number. Thus, it was necessary to average the cavitation number for a particular type of cavitation pattern. When a particular cavitation pattern appeared on at least three of the five propeller blades, that type of cavitation was said to occur. This observation is subject to personal interpretation.

FIELD-POINT PRESSURES

Uniform Flow—Design Advance Coefficient

Total blade-frequency-induced pressure amplitudes and phases were measured on a flat plate with the propeller operating at design thrust coefficient (K_T = 0.214). Only the 0° blade-warp results could be compared with theoretical results since no theory existed for determining induced pressures of warped propellers at the time. Blade-frequency results of pressure amplitude and phase for the unwarped parent propeller (Model 4381) agreed well with Kerwin theoretical predictions and experimental results of Denny and Teel.[4]

Figures 23 and 26 compare experimental results and theoretical predictions for 0° blade warp for propeller-tip clearance of 10- and 30-percent radius, respectively. Figures 24 and 27 present the experimental results of the propellers with 36° blade warp at propeller tip

clearances of 10 and 30 percent, respectively, while Figures 25 and 28 present experimental results for 72° blade warp. The experimental results have been connected by curves for visual clarity and are not, in general, intended to depict trends in the axial pressure distribution. The pressure amplitudes are presented in the form of nondimensionalized blade-frequency coefficients as shown in Equation (8). The plots show amplitude and phase versus axial distance from the propeller plane with the x/R = 0 position designating the propeller-reference plane. Phase θ_f is defined as the angular difference between the circumferential location of the maximum blade-frequency pressure and a reference line extending from the hub center through the blade-hub sections midchord and lying in the propeller reference plane.

Figures 23 through 28 present θ_{C_p} at which C_p is maximum (minimum p). Figures 23 and 26 show that the measured blade-frequency pressure amplitudes and phases agree very well with the Kerwin theory. Uniform flow-phase angle results indicate that in the propeller plane, the minimum induced blade-frequency pressure occurs at the instant the blade tip passes the pressure transducer.

A comparison of Figures 23 through 25 and 26 through 28 indicates a large decrease of blade-frequency pressure amplitude with increased clearance from the blade tip. The increase in clearance from 10 to 30 percent of the propeller radius reduced the maximum pressures 60 to 70 percent for the three propellers. The measured pressure coefficient at the radius tip clearance of 10 percent shows a decrease for increasing blade warp.

Uniform Flow--Range of Advance Coefficients

Figures 29 and 30 show the measured blade-frequency amplitudes for the propellers with 36° and 72° of blade warp, respectively, operating at K_1 of 0.375, 0.300, 0.214, 0.100, and 0.0 at 10- and 30-percent R tip clearance.

Figure 31 shows the measured blade-frequency pressure amplitudes for all the propellers of the warped series at 10-percent R tip clearance and at K_1 = 0.375, 0.214, 0.100, and 0.0.

For the various uniform flows, the induced pressures showed similar trends in that the maximum values of the induced field pressures were greater at low advance coefficients (highly loaded conditions) and were lessened at high advance coefficients (lightly loaded conditions).

The effect of blade warp was such that at the higher blade loadings, increasing blade warp reduced the blade-frequency pressures; however, as the loading decreased to zero the 36° warped propeller induced higher blade-rate pressures downstream than either the 0° or 72° warped propellers. This effect could be attributed to a change in the loading distribution at the low-loading, off-design conditions where the contributions of thickness and loading might combine in such a way as to result in a maximum blade-frequency pressure for 36° warp.

Nonuniform Flow

Figure 32 compares the results of induced pressure measurements on a flat plate for Propellers 4381 (0° warp), 4497 (36° warp), and 4498 (72° warp) run at design thrust coefficient (K_T = 0.214) for each distinct position of the 4-cycle wake screen (refer to Figure 6 for wake position) and at 10-percent R tip clearance. Position 4 produced the largest values of blade-frequency-induced pressures, followed in magnitudes by values ootained at Positions 1, 3, and 2 in that order. Position 4 corresponded to the region of heaviest propeller-blade loading since the inflow velocity was the least through that region of the screen. Position 2 was the region of highest inflow velocity and the propeller-blade loading was least in that region. The other positions were combinations of the high and low inflow regions, and values of blade-frequency-induced pressures were between those obtained at Positions 4 and 2. Except for the 36° propeller at Position 2, the nonuniform-flow results showed reductions in blade-frequency pressures with increasing blade warp, a trend also observed in the uniform-flow results.

Figures 33 and 34 present the values of blade-frequency pressures, measured on the flat plate for the propellers with 0°, 36°, and 72° blade warp, operating in nonuniform flow created by the 4- and 5-cycle wake screens at 10-percent R tip clearance and at several advance conditions. Results are given for measurements obtained while the 5-cycle wake screen was in Position 3, and the 4-cycle wake screen was in Position 4.

The nonuniform-flow results of Figure 33 (5-cycle wake, Position 3) show reductions in blade-frequency pressures with increasing blade warp. However, results from Figure 33 also indicate that for the 36° and 72° warped propellers, the induced pressures upstream of the propeller plane decrease with decreasing thrust coefficient; whereas, the downstream induced pressures increase with decreasing thrust coefficient. Only marginal reductions of the blade-frequency-induced pressures were noted for the various loading conditions for the 0° warped propeller, operating in the 5-cycle wake at Position 3.

The nonuniform-flow results of Figure 34 (4-cycle wake, Position 4) show reductions in blade-frequency pressures with increasing blade warp and decreasing mean thrust coefficient (increasing advance coefficient).

Comparison of Skew and Warp

Results of the blade-frequency pressure amplitude obtained by Teel and Denny [4] for a skewed-propeller series were compared with blade-frequency pressure amplitude results of a series of warped propellers. Figures 35 through 38 present the comparison of blade-frequency pressure amplitudes for 36° and 72° skewed propellers and 36° and 72° warped propellers operating in uniform and nonuniform flow.

Results show a greater reduction of propeller-induced pressures with increasing blade warp than with equal amounts of blade skew. This may be due to the different load distribution on the warped and skewed propellers as mentioned in the introduction. It should be noticed that the maximum blade-frequency pressure is not displaced downstream for increasing blade warp as with increasing blade skew.

UNSTEADY PROPELLER LOADING

The unsteady loading results for a series of warped propellers are presented in Figures 39 and 46. Figures 39 and 40 show the amplitudes of the blade-frequency harmonics of the unsteady thrust and torque relative to the steady values at the design thrust coefficient. The results are shown as a function of $\bar{K}_T$, instead of $J = V_A/ND$, because the operating advance coefficient varied for the warped propellers due to differences in their open-water characteristics. The increase in blade-frequency thrust and torque coefficients with decreasing mean thrust coefficient was due to the increased fluctuations in flow angle.

A phase angle Φ_L will now be defined as

$$\Phi_L = (\phi_{ZL} - \phi_{ZW})/Z \tag{21}$$

where Φ_L = geometric angle by which the blade rate-propeller loading leads the same frequency component of the longitudinal velocity

ϕ_{ZW} = phase angle of the blade-rate harmonic of wake velocity at r/R = 0.7

ϕ_{ZL} = phase angle of the blade-rate harmonic of the propeller loading

Z = order of the blade-rate harmonic.

The 5-cycle wake screen was rotated so that the phase angle of the blade frequency component of the longitudinal velocity at r/R = 0.7 was 0° with respect to the vertical upward position. This was done to obtain the Φ_L directly from the unsteady loading measurements, that is,

$$\Phi_L = (\phi_{ZL} - \phi_{ZW})/Z$$

since

$$\phi_{ZW} = 0$$

then

$$\Phi_L = \phi_{ZL}/Z$$

where a positive angle Φ_L denotes the angle by which the blade frequency-propeller loading leads the same frequency component of the longitudinal velocity. Since the phase angle of the blade-frequency component of the longitudinal velocity was 0° at r/R = 0.7 for the 4-cycle wake screen; no rotation of the 4-cycle wake screen was necessary.

The phase angles Φ_T' and Φ_Q' in Figure 41 are for the negative of the thrust and torque. This sign convention is used because blade-frequency fluctuations of thrust and torque for a very narrow unwarped blade are 180° out of phase with the velocity fluctuations in the wake. Thus

$$\Phi_T' = [(\pi + \phi_{ZT}) - \phi_{ZW}]/Z \tag{22}$$

$$\Phi_Q' = [(\pi + \phi_{ZQ}) - \phi_{ZW}]/Z \tag{23}$$

The amplitudes of the blade-frequency components of side forces and bending moments are shown in Figures 42 and 43. Their directions are defined in Figure 8.

The phase angles Φ_L and Φ_M of the blade-frequency side forces (positive) and bending moments are shown in Figures 44 and 45, respectively. The angles of the vertical side forces and horizontal bending moments have been shifted by 18° to permit the two force-component phase angles and the two moment-component phase angles to be plotted together. The difference in phase is due to the fact that the blade spacing of 72° is 18° less than the difference between the vertical and horizontal axes. Similar to the skewed-propeller results of Boswell and Miller,[2] the side-force phase angles showed an unexpected value at $\bar{K}_T$ = 0.375. This result may have been due to low amplitude of the unsteady side forces at that particular loading condition, making it difficult to accurately determine the phase angles.

Theoretical and experimental unsteady propeller-loading results for a series of skewed propellers are presented in Reference 16.

Theoretical unsteady loading predictions were not calculated for the warped propellers. Since the existing theory does not consider rake, it is not clear that this theory can properly differentiate between blade warp and blade skew. However, the geometry of the skewed and warped propellers indicates that there should be no significant differences between the unsteady thrust, torque, and side forces of the skewed and warped propellers; however, there should be some differences in their bending moments. Therefore, theoretical unsteady loading results of Reference 16 for the skewed-propeller series may be used for comparison

---

[16] Cox, G. G. and Wm. B. Morgan, "The Use of Theory in Propeller Design," Marine Technology, Vol. 9, No. 4 (Oct 1972).

with the warped-propeller experimental results, except the bending moments. It is recommended that present unsteady loading theory be extended to include the effect of rake on unsteady loading.

In Figure 46 the warped-propeller results are compared with the skewed-propeller results of Reference 16. In general, warped and skewed propellers show comparable reduction with increasing warp and skew. However, it should be noted that the unsteady thrust and side forces of the 36° warped propeller are greater than those of the 36° skewed propeller.

SUMMARY

A modification of the basic lifting-surface programs has been developed by Kerwin to compute the necessary pitch and camber corrections for skewed propellers with arbitrary rake.[6] The modified program derived by Kerwin accounts for the effect of radial induced velocities for propellers whose surface normal has a component in the radial direction; whereas, the lifting-surface program used in the design of the skewed-propeller series[6] does not. The Kerwin results show that the camber in the vicinity of the root needs to be significantly reduced with increasing forward rake. Thus, Propellers 36W and 72W apparently have too much camber near the blade root. The pitch is also predicted to be somewhat high. This result is consistent with the present cavitation results since inception of back-bubble cavitation of the 72° warped propeller is seen to occur much earlier than for the 72° skewed propeller (with the proper pitch and camber corrections), particularly at the root. Because of the excessive camber at the root of the warped propellers, the loading at the tip is reduced, which is consistent with the later onset of back tip-vortex cavitation for the warped propellers. The earlier onset of face cavitation at the outer radii, except 72W at 0.7R, Figure 14a, is also consistent with this reasoning.

OPEN-WATER AND CAVITATION PERFORMANCE

Analysis of the open-water data shows that incorporation of forward rake in highly skewed propellers sufficient to place the blade centerline in a single plane will change the propulsive performance of the propeller if appropriate pitch and camber corrections are not made. Rational techniques for such corrections have been developed by Kerwin[10] and Pien.[11]

The change in the thrust and torque coefficients of the warped propellers were such that the 36° and 72° warped propellers were estimated to be 2.5 and 4.5 percent, respectively, lower than design rpm at design power. The corresponding skewed propellers were both within 1 percent of design rpm. All propellers were estimated to produce within 1.5 percent of the design speed at the design power.

A widening of the cavitation-free region occurs for both increasing warp and increasing skew.

Back bubble-cavitation inception occurs at higher cavitation numbers for increasing warp; however, this may be due to neglecting the effect of rake in the design of the warped propellers.

A crossover in the inception of back-sheet and tip-vortex cavitation occurred for the warped propellers so that at design thrust-loading coefficient, sheet cavitation at the design advance coefficient was delayed most on Propeller 36W. A similar crossover occurred for the skewed propellers, i.e., sheet cavitation was delayed most on Propeller 36S.

Although, the cavitation results of Propellers 36S and 72S reported by Boswell[6] differed from the present results, it was confirmed that the cavitation bucket became wider for increasing skew.

FIELD-POINT PRESSURES

Induced pressures were measured on a flat plate near warped propellers. There were essentially no harmonics in the pressure signal of comparable size to the blade-frequency harmonic. Experimental results of Propeller 4381, 0° blade warp, from the uniform-flow experiments at the advance coefficient of propeller design compared very well in phase and amplitude to the Kerwin predictions of blade-frequency pressure.

Significant decreases in measured amplitude of blade-frequency pressure were found to occur for increasing values of blade warp.

Results of blade-frequency phase angle indicate that the minimum blade-frequency pressure in the propeller plane occurs at the instant the propeller blade tip passes the pressure transducer.

A sizable decay of the blade-frequency-induced pressure was apparent at a 30-percent, propeller radius tip clearance, compared to the 10-percent clearance when the propeller was operating at the same advance coefficient.

Results of nonuniform-flow experiments indicated that a change of the wake region in line with the pressure transducers had essentially the same effect on the maximum blade-frequency pressure amplitudes as changing the loading by changing the advance coefficient in uniform flow.

In general, results of both uniform and nonuniform flows showed that the maximum blade-frequency-induced pressures increased with an increase in blade loading.

UNSTEADY PROPELLER LOADING

The investigation has shown that blade warp has considerable effect in reducing the blade-frequency forces and moments acting on a propeller in nonuniform flow. For the propellers evaluated, warp equal to the blade spacing reduced the blade frequency thrust and torque to about 25 percent of that of an unwarped propeller, the blade-frequency bending

moment to 35 percent, and the blade-frequency side force to 15 percent. However, unsteady thrust and side forces for the 36° warped propellers were greater than those of the 36° skewed propeller.

CONCLUSIONS

The following conclusions have been drawn from the present study.

1. A propeller design procedure similar to that of Kerwin or Pien must be used to properly design warped propellers.

2. The cavitation-free bucket becomes wider with increasing warp.

3. In general, it appears that if warped propellers are designed using the now available pitch and camber corrections, there will be little difference in either the propulsive or cavitation performance of skewed and warped propellers.

4. The radial load distributions of the warped and skewed propellers are apparently different for the same value of thrust coefficient, K_T. This fact should be kept in mind when comparing the field-point pressure results for the warped propellers with those of the skewed propellers.

5. Depending on propeller placement on a ship, sufficient propeller-blade warp could be beneficial in reducing hull vibration created by the induced pressure fluctuations.

6. The induced pressures were found to decrease with increasing propeller-tip clearance.

7. For a given propeller-loading condition, phase angle results indicate that the angular position of minimum blade-frequency pressure is a function of warp angle.

8. A slightly greater reduction of propeller-induced pressures result with increasing blade warp as compared with increasing blade skew.

9. To more accurately determine trends in the axial pressure distribution at off-design conditions, more pressure transducers are required.

10. In general, for increasing warp, the results of warped-propeller unsteady loading showed comparable reduction as did increasing skew for skewed propellers.

ACKNOWLEDGMENTS

The author thanks Messrs. Dennis Crown and Kenneth Remmers, who conducted the open-water experiments of the warped and skewed propellers, Thomas A. LaFone for his assistance in the cavitation experiments and data reduction, Marlin Miller, who conducted the unsteady propeller loading measurements, and Stephen B. Denny who provided invaluable guidance during the experimental phases of this project.

VIEWS LOOKING FORWARD

VIEWS LOOKING TO PORT

1. UNDISTORTED PROPELLER–Blade sections are centered on straight radial lines and lie in a single plane

2. RAKED PROPELLER–Blade sections are displaced in axial direction and need not be linear such as shown above (positive rake is toward stern).

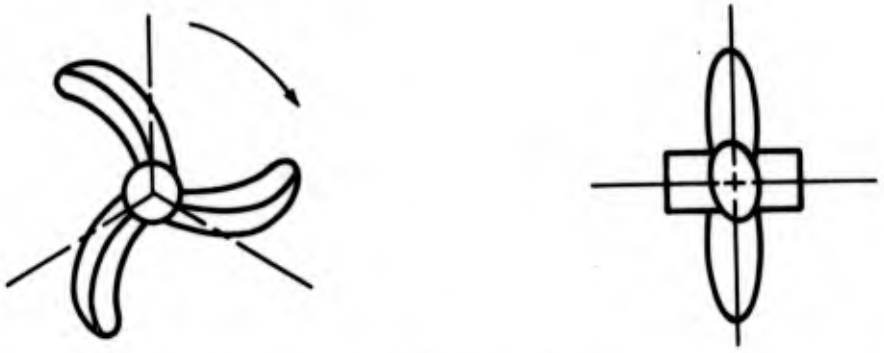

3. WARPED PROPELLER–Angular displacement of blade sections in plane of rotation (positive warp is opposite to direction of rotation)

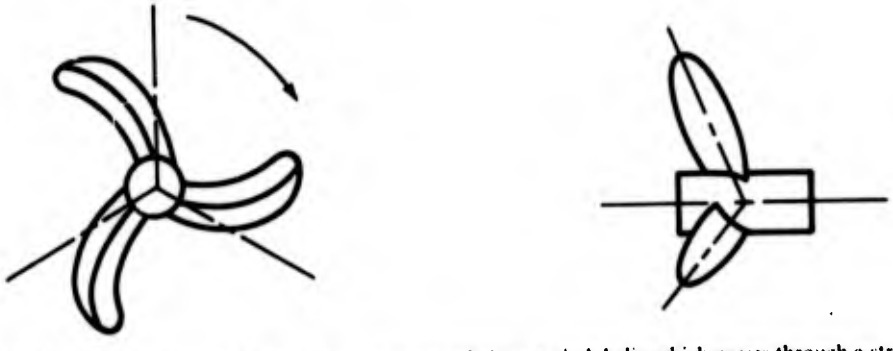

4. SKEWED PROPELLER–Blade mid-chord points are displaced along a pitch helix which passes through a straight radial line in the propeller planetcombination of rake and warp).

Figure 1 – Various Types of Propeller Blade Distortion

Figure 2 – Skewed and Warped Propellers

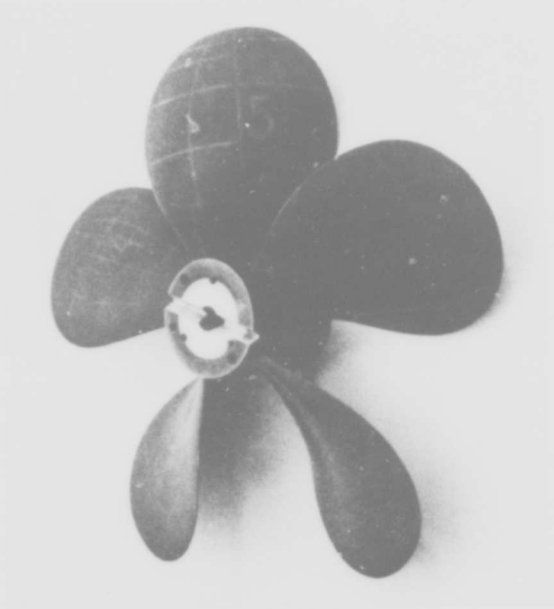

Figure 2a – Parent Propeller –0° Skew or Warp

Figure 2 (Continued)

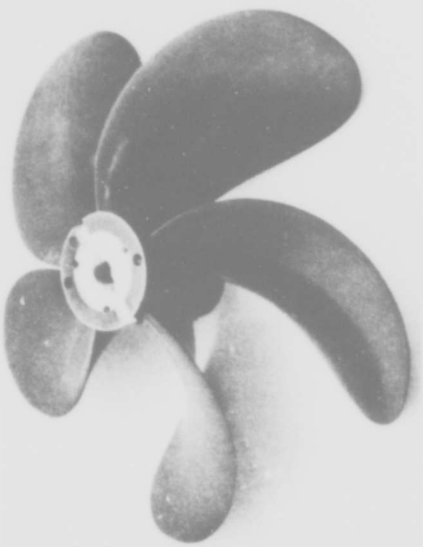

Figure 2b – Propeller 36S

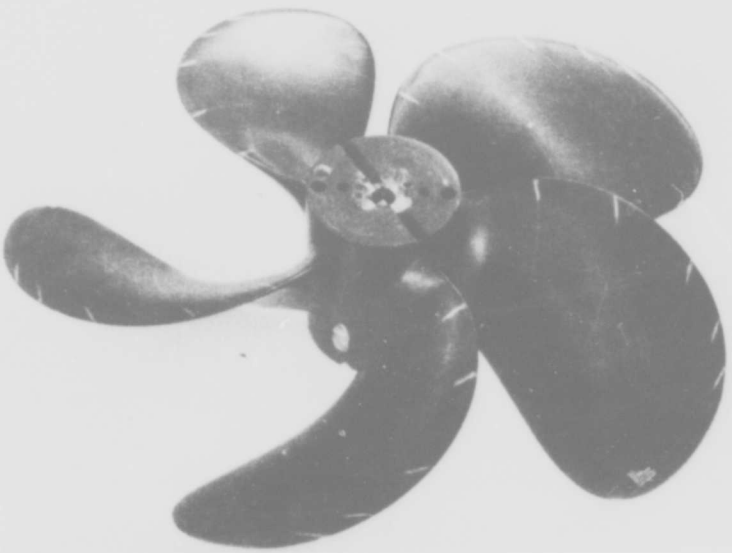

Figure 2c – Propeller 36W

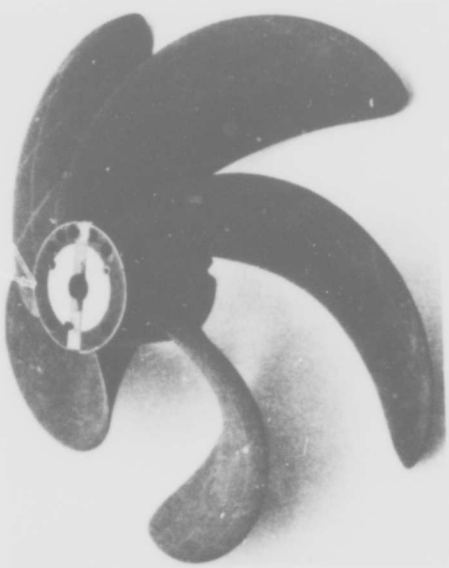

Figure 2d – Propeller 72S

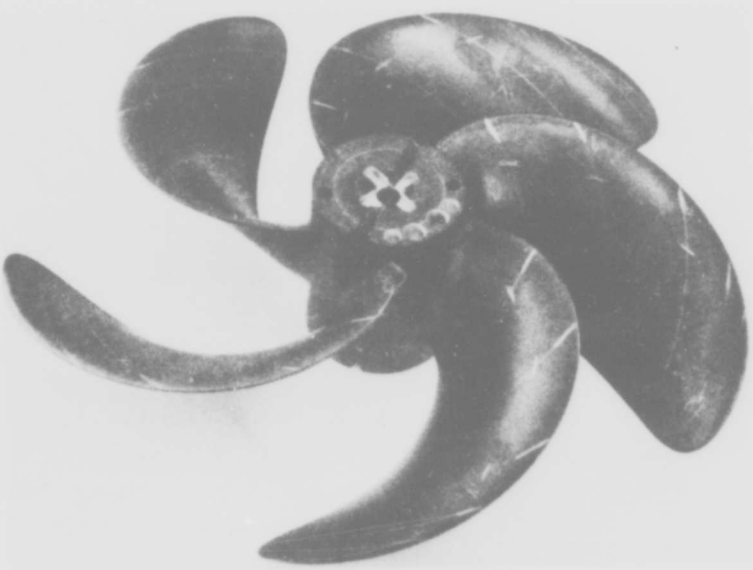

Figure 2e – Propeller 72W

Figure 3 – Blade Outline of Parent Propeller and Propellers 36S, 36W, 72S, and 72W

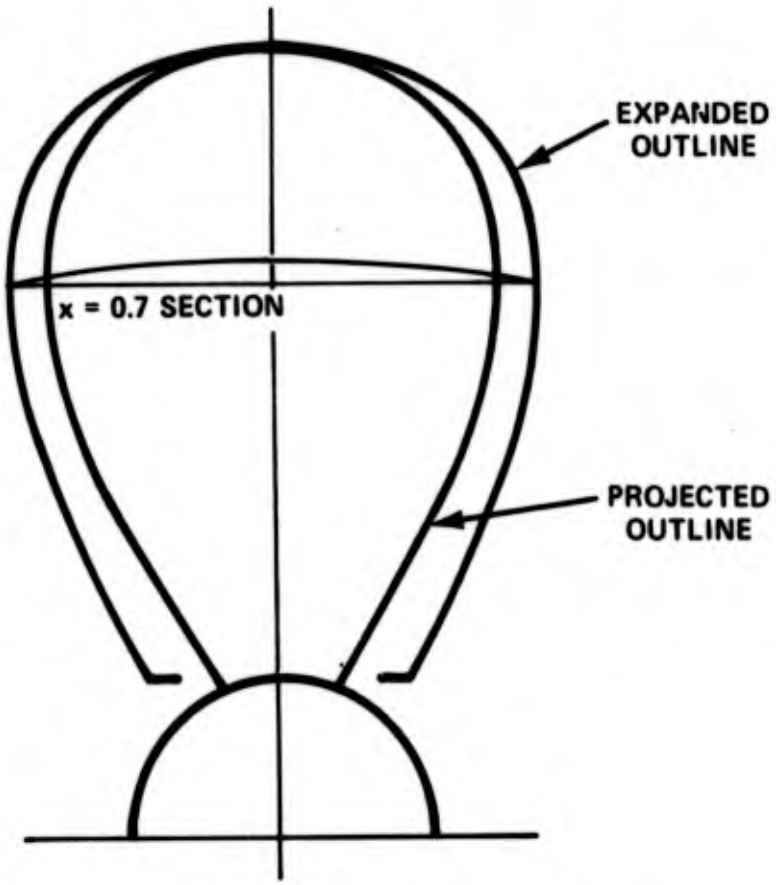

Figure 3a – Parent Propeller -0° Skew or Warp

Figure 3 (Continued)

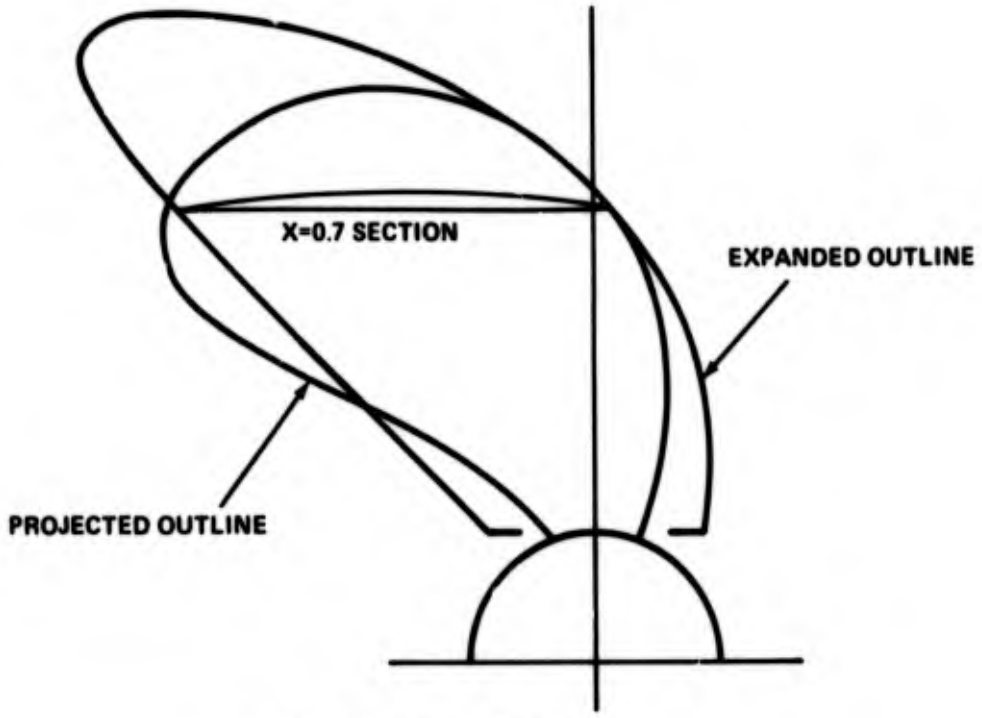

Figure 3b – Propeller 36S or 36W

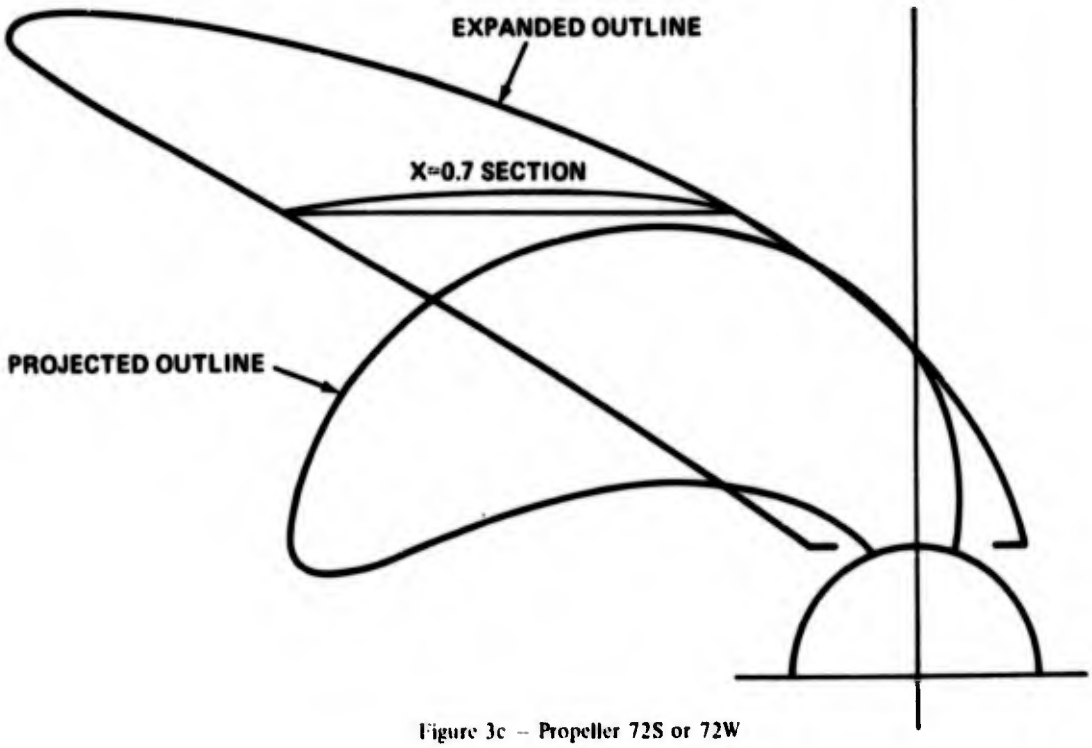

Figure 3c – Propeller 72S or 72W

Figure 4 – Cavitation at Selected Advance Coefficients J and Cavitation Numbers σ

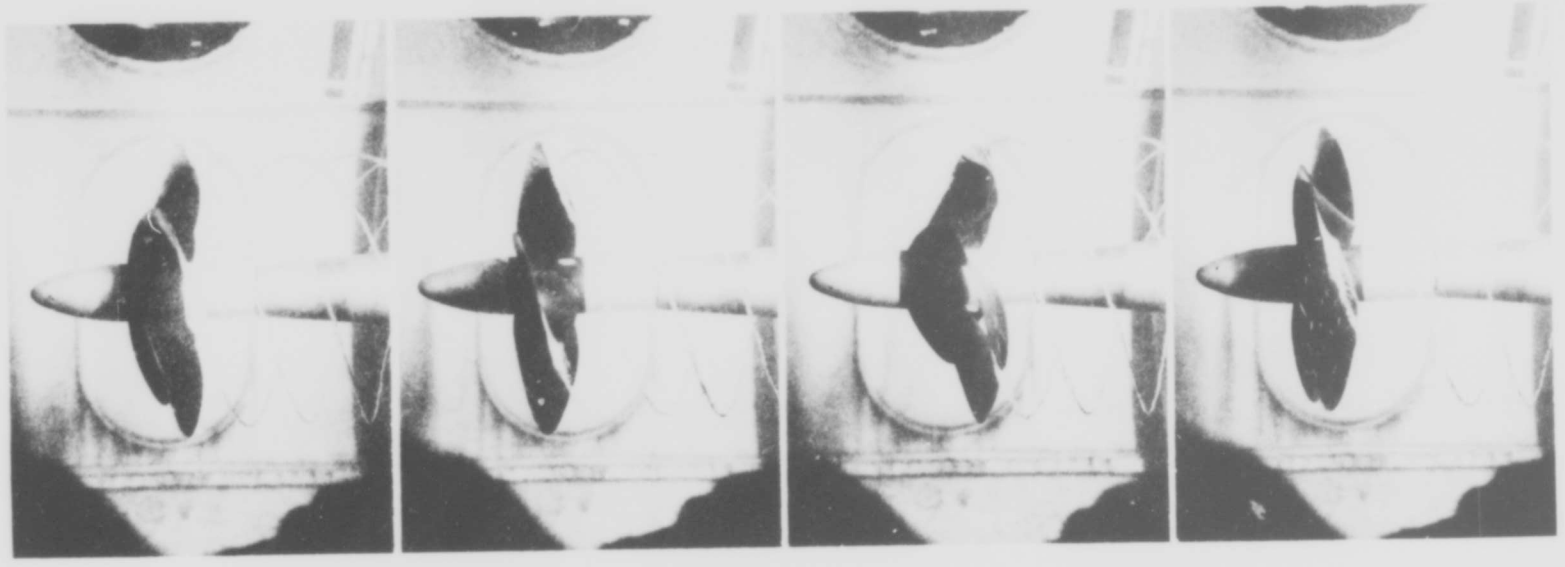

Figure 4a – J = 0.7, σ = 3.5 (Sketches Show Back Cavitation)

Figure 4 (Continued)

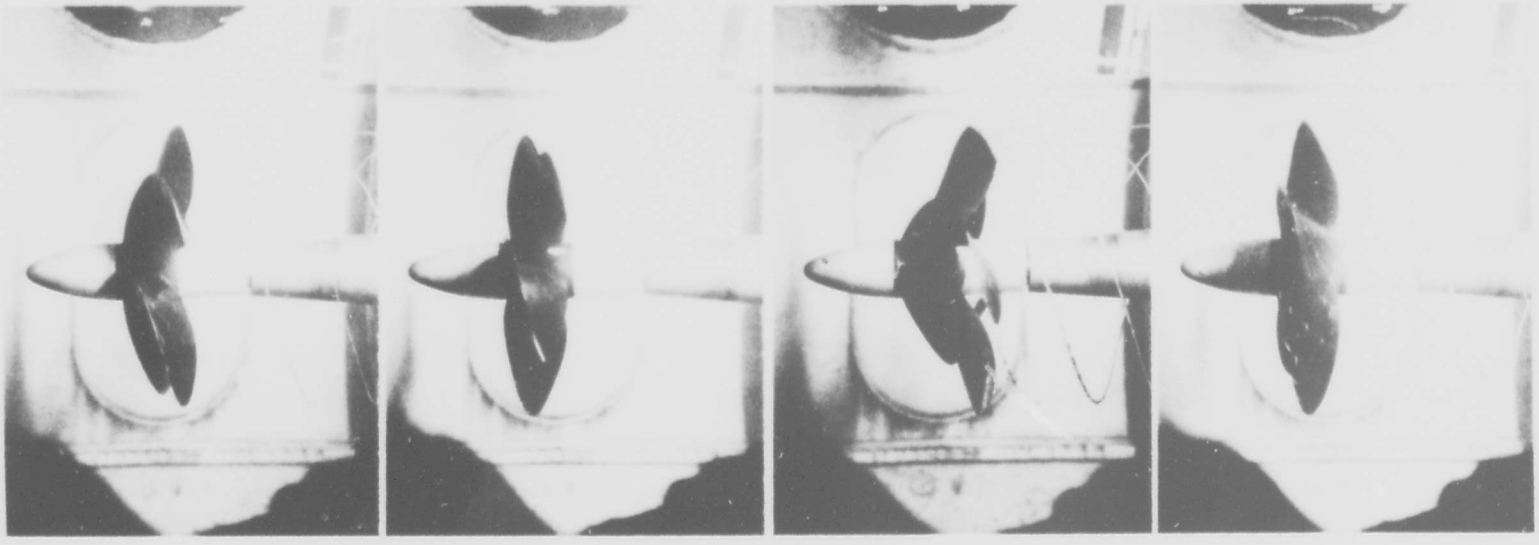

36S 36W 72S 72W

J = 0.8 σ = 3.5

(SKETCHES SHOW BACK CAVITATION)

Figure 4b — J = 0.8, σ = 3.5 (Sketches Show Back Cavitation)

Figure 4 (Continued)

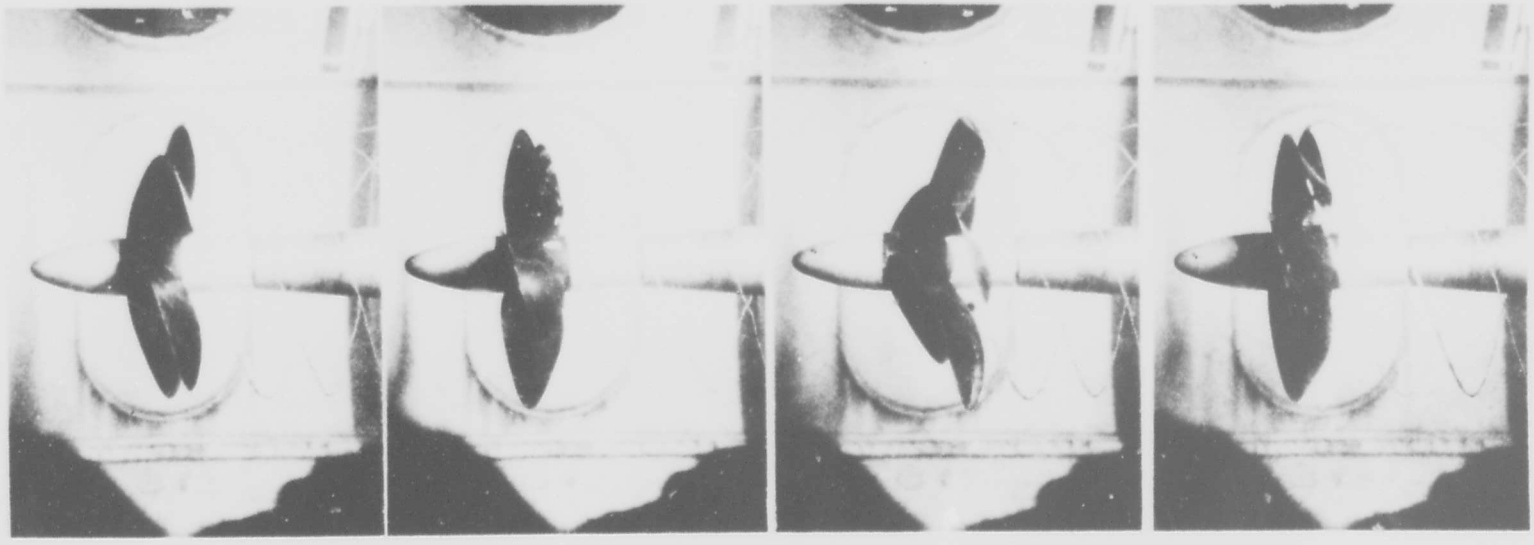

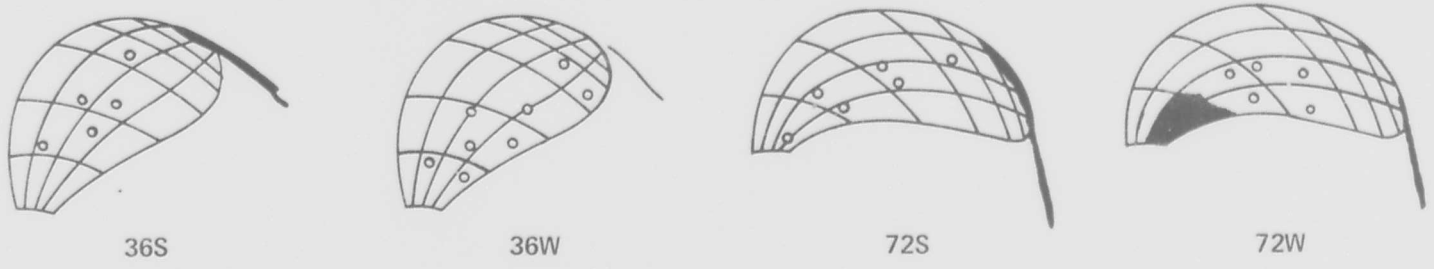

J = 0.875 σ = 1.4

(SKETCHES SHOW BACK CAVITATION)

Figure 4c – J = 0.875, σ = 1.4 (Sketches Show Back Cavitation)

Figure 4 (Continued)

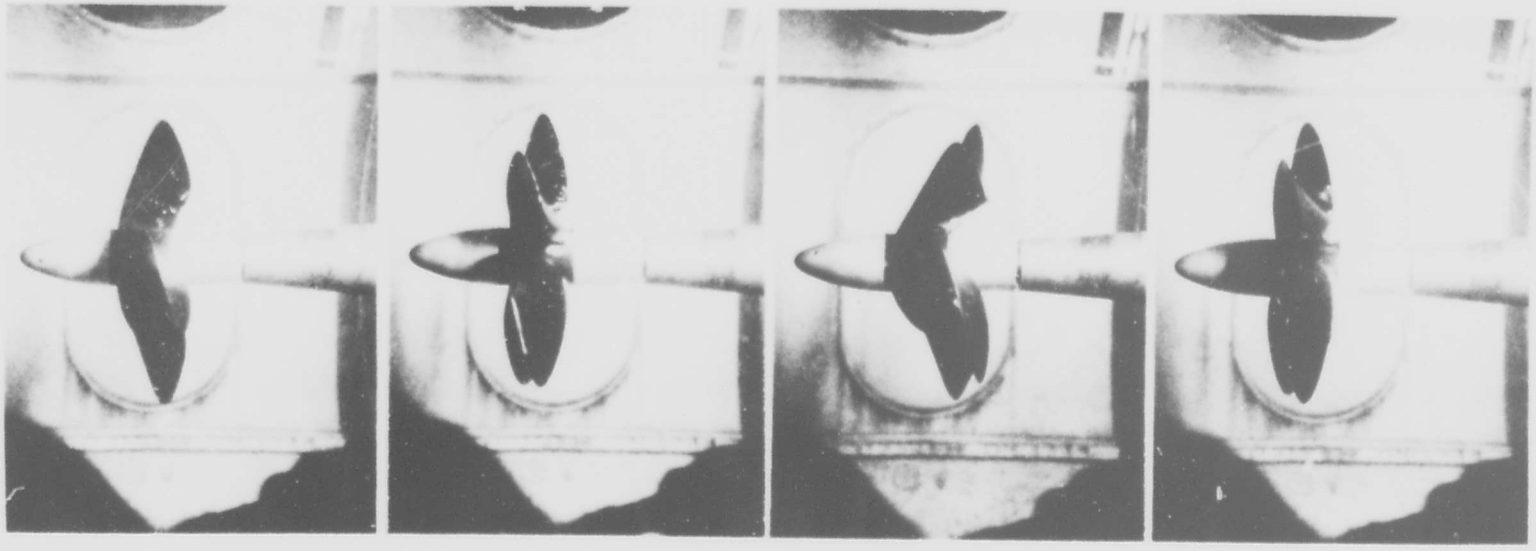

36S 36W 72S 72W

J = 1.0 σ = 0.9

(SKETCHES SHOW BACK CAVITATION)

Figure 4d – J = 1.0, σ = 0.9 (Sketches Show Back Cavitation)

Figure 4 (Continued)

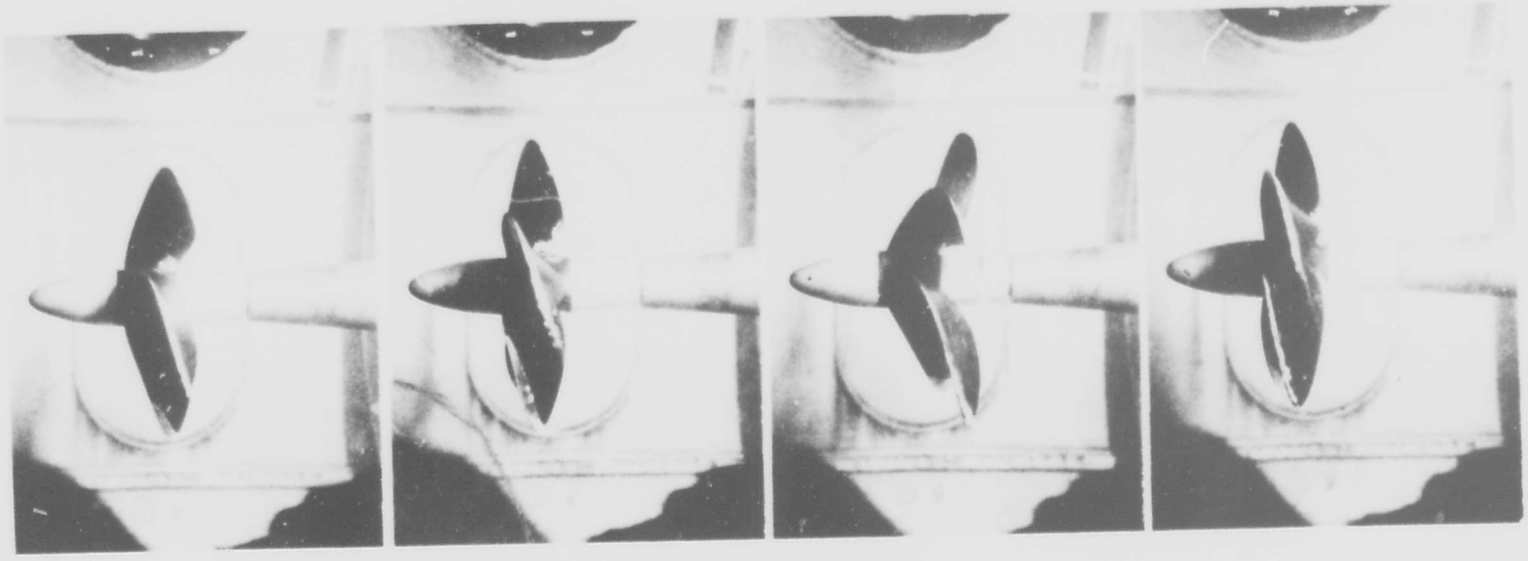

36S 36W 72S 72W

J = 1.1 σ = 0.8

(SKETCHES SHOW FACE CAVITATION)

Figure 4e – J = 1.1, σ = 0,8 (Sketches Show Face Cavitation)

Figure 4 (Continued)

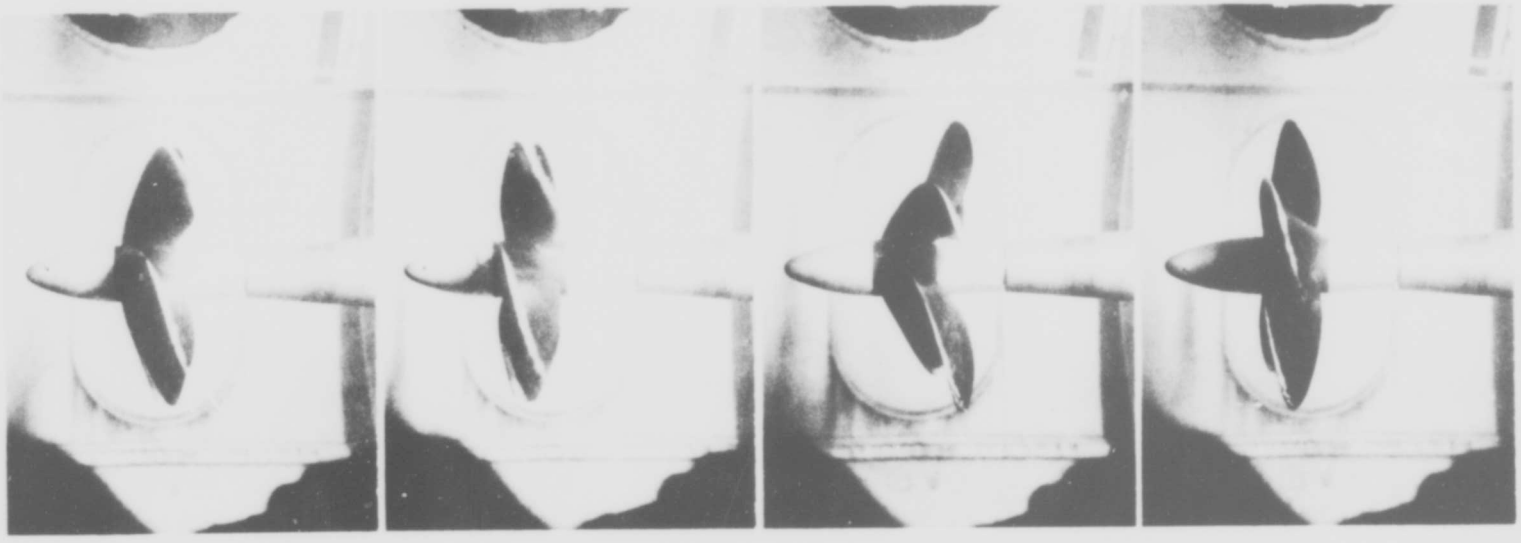

36S 36W 72S 72W

J = 1.2 σ = 1.7

(SKETCHES SHOW FACE CAVITATION)

Figure 4f – J = 1.2, σ = 1.7 (Sketches Show Face Cavitation)

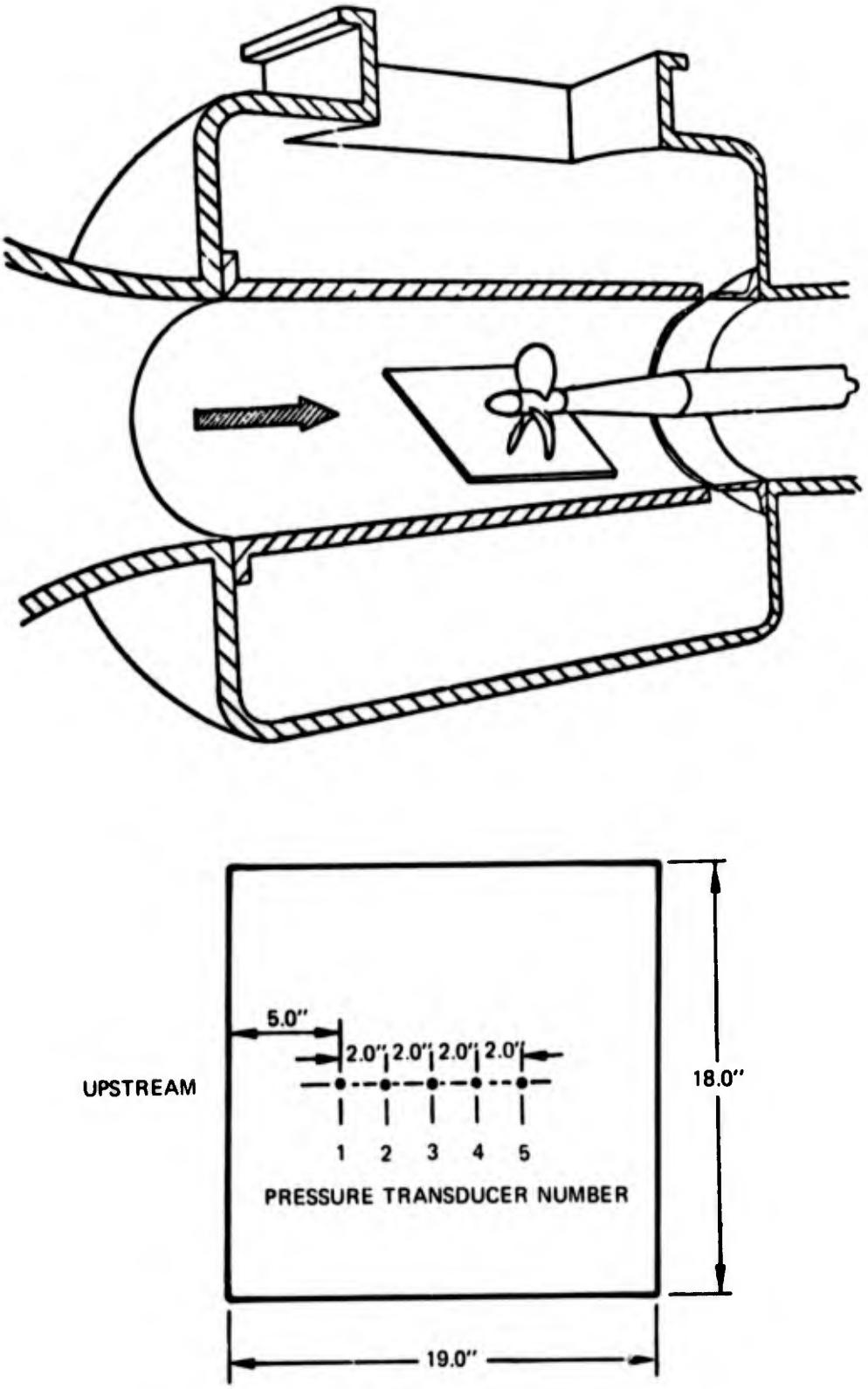

Figure 5 – Flat-Plate Dimensions and Placement in the Water Tunnel

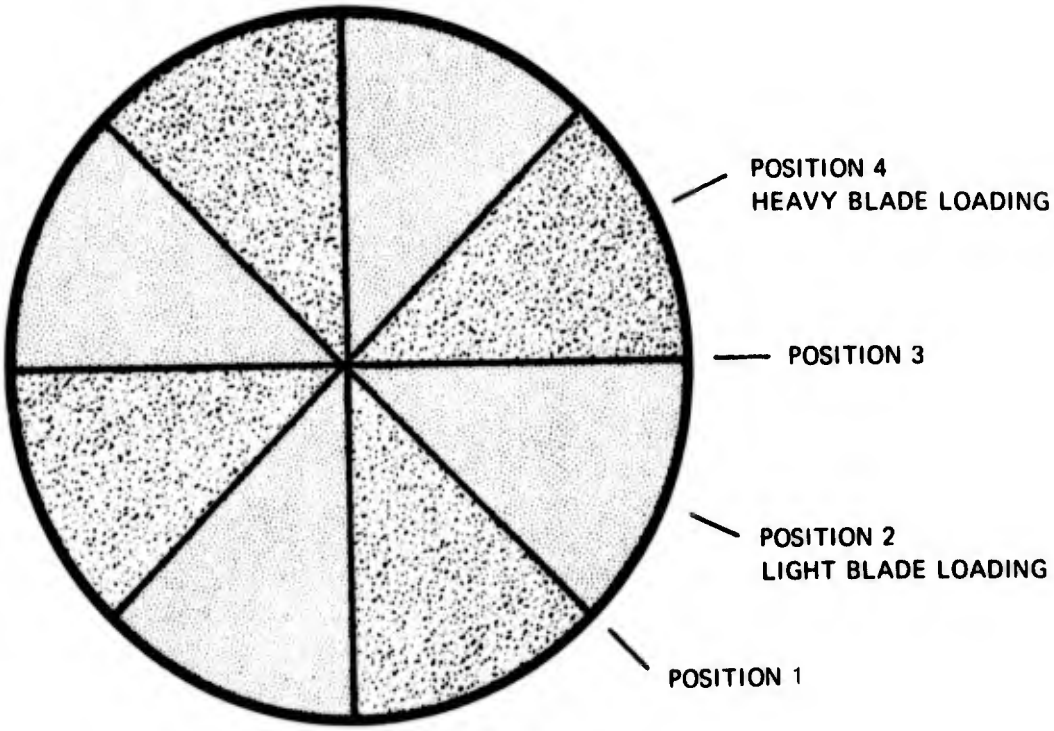

4-CYCLE WAKE SCREEN

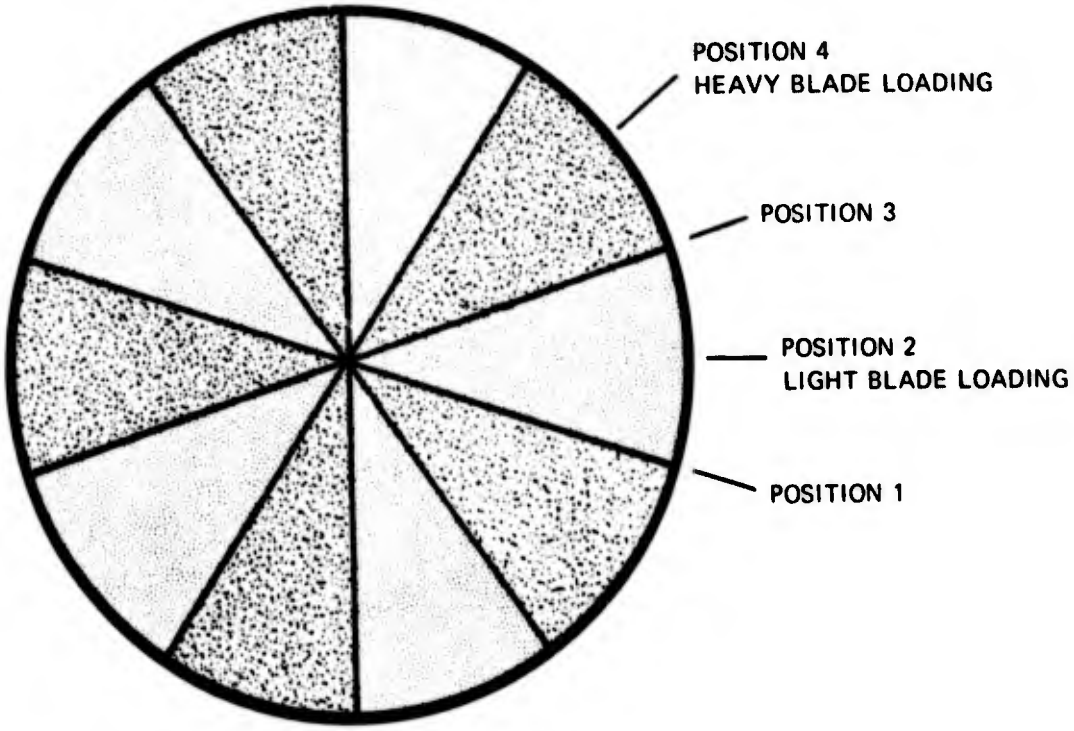

5-CYCLE WAKE SCREEN

Figure 6 – Four- and Five-Cycle Wake Screens, Showing Distinct Regions of Flow

Figure 7 – Harmonic Content of 4- and 5-Cycle Wakes

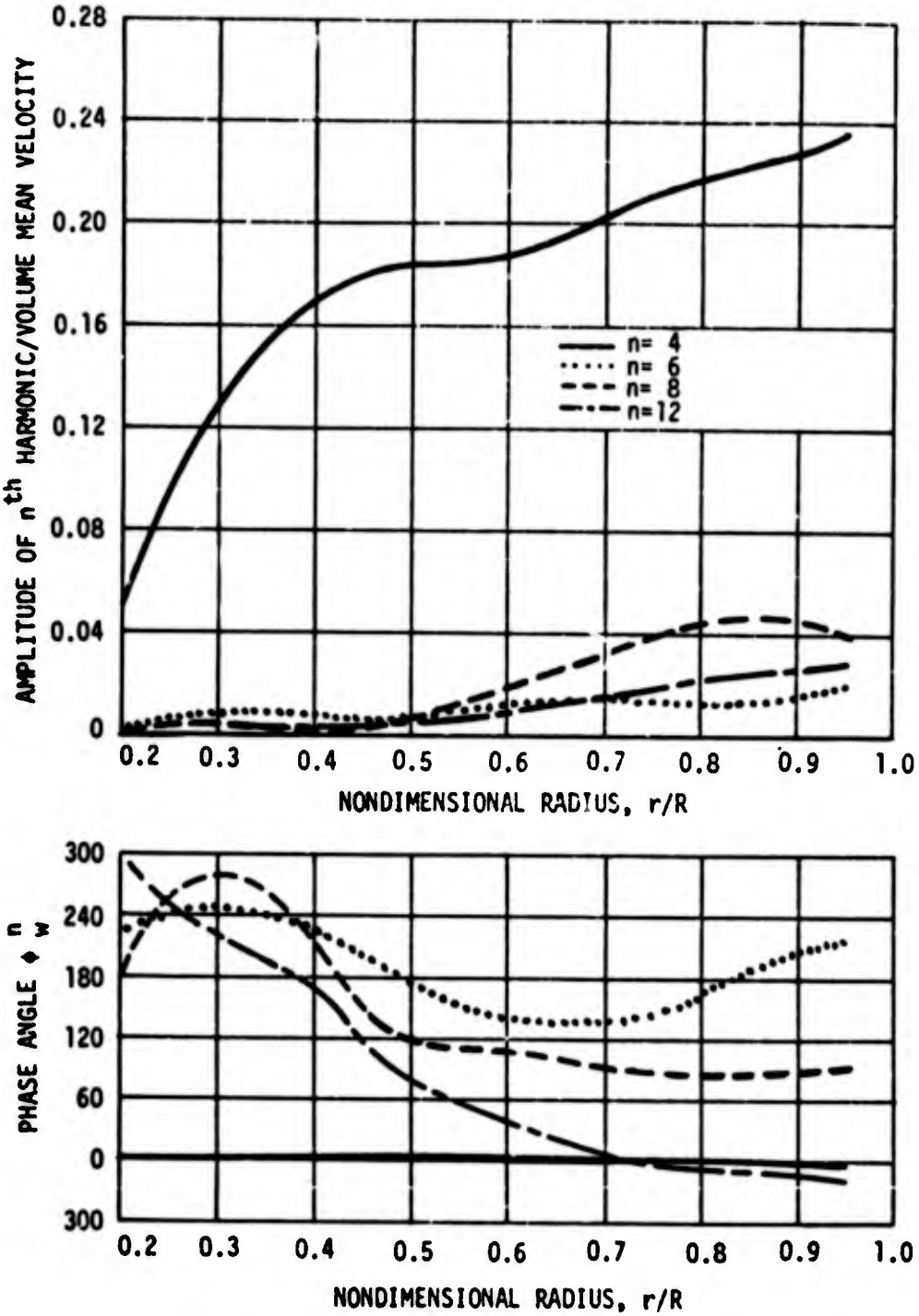

Figure 7a - Four-Cycle Wake

Figure 7 (Continued)

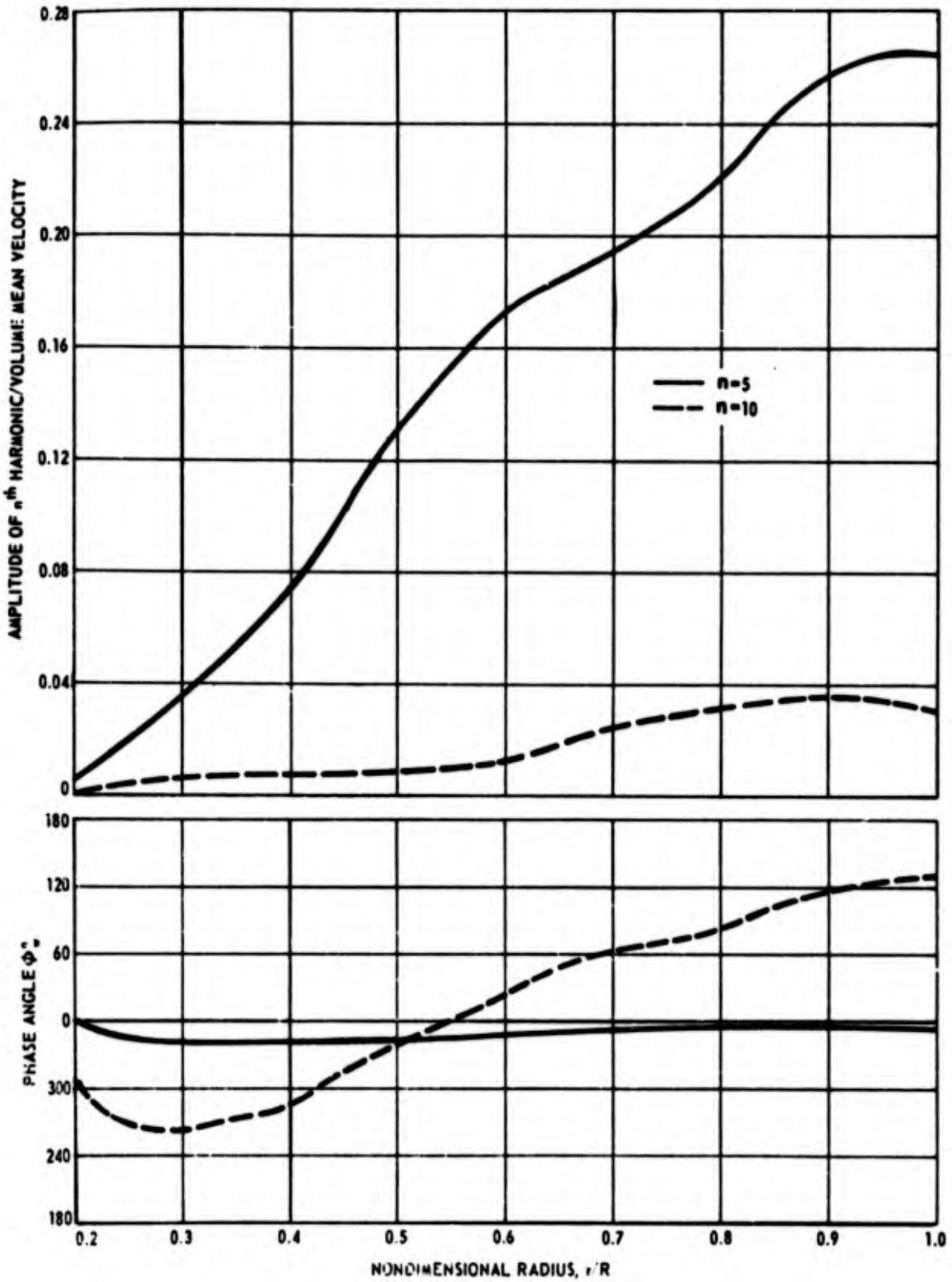

Figure 7b – Five-Cycle Wake

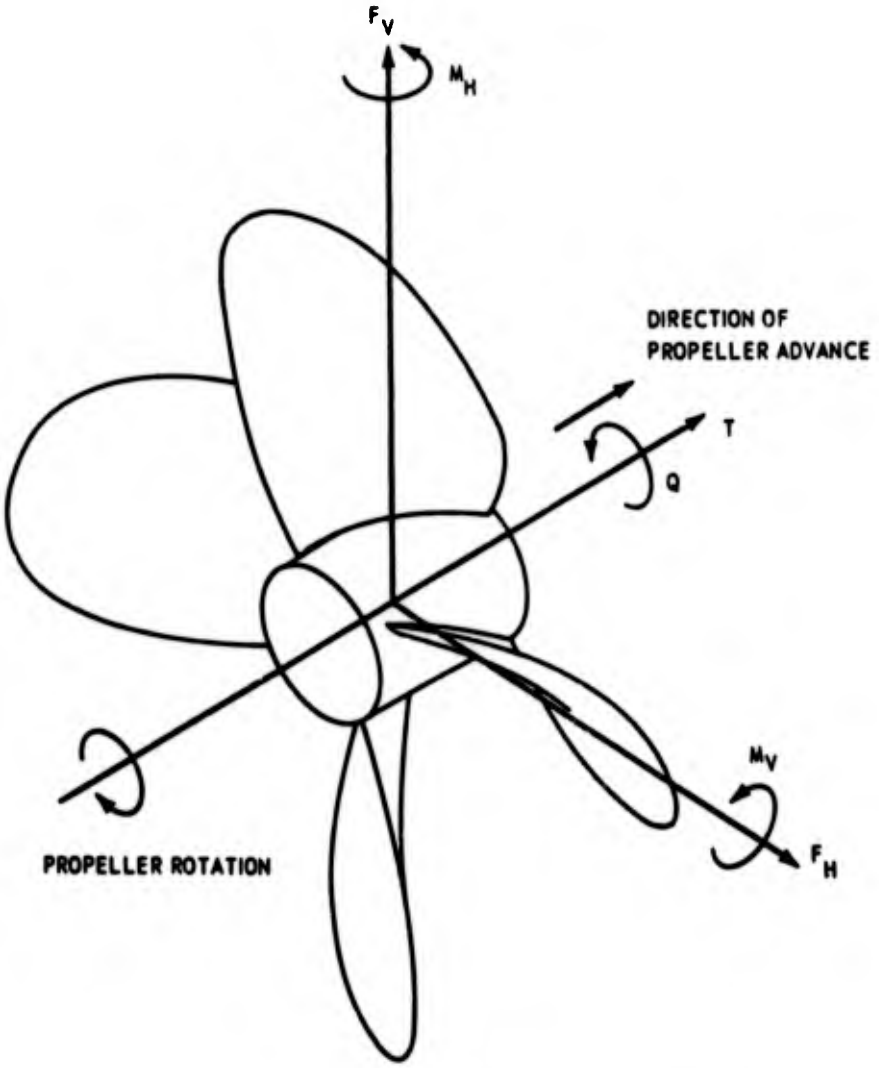

Figure 8 – Forces and Moments Acting on Propeller

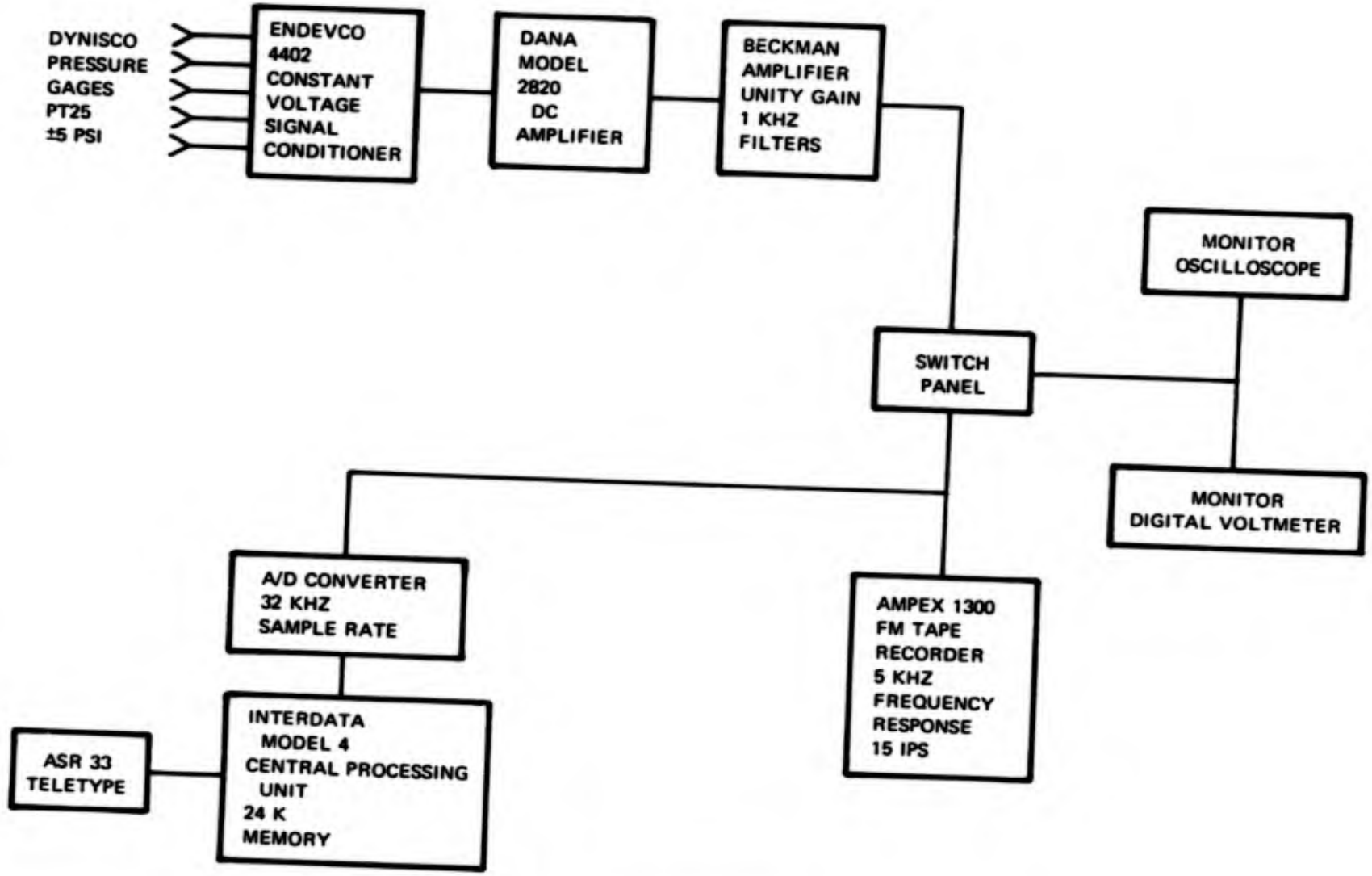

Figure 9 – Instrumentation

Figure 10 – Forward Open-Water Characteristics of Propellers 36S, 36W, 72S, and 72W

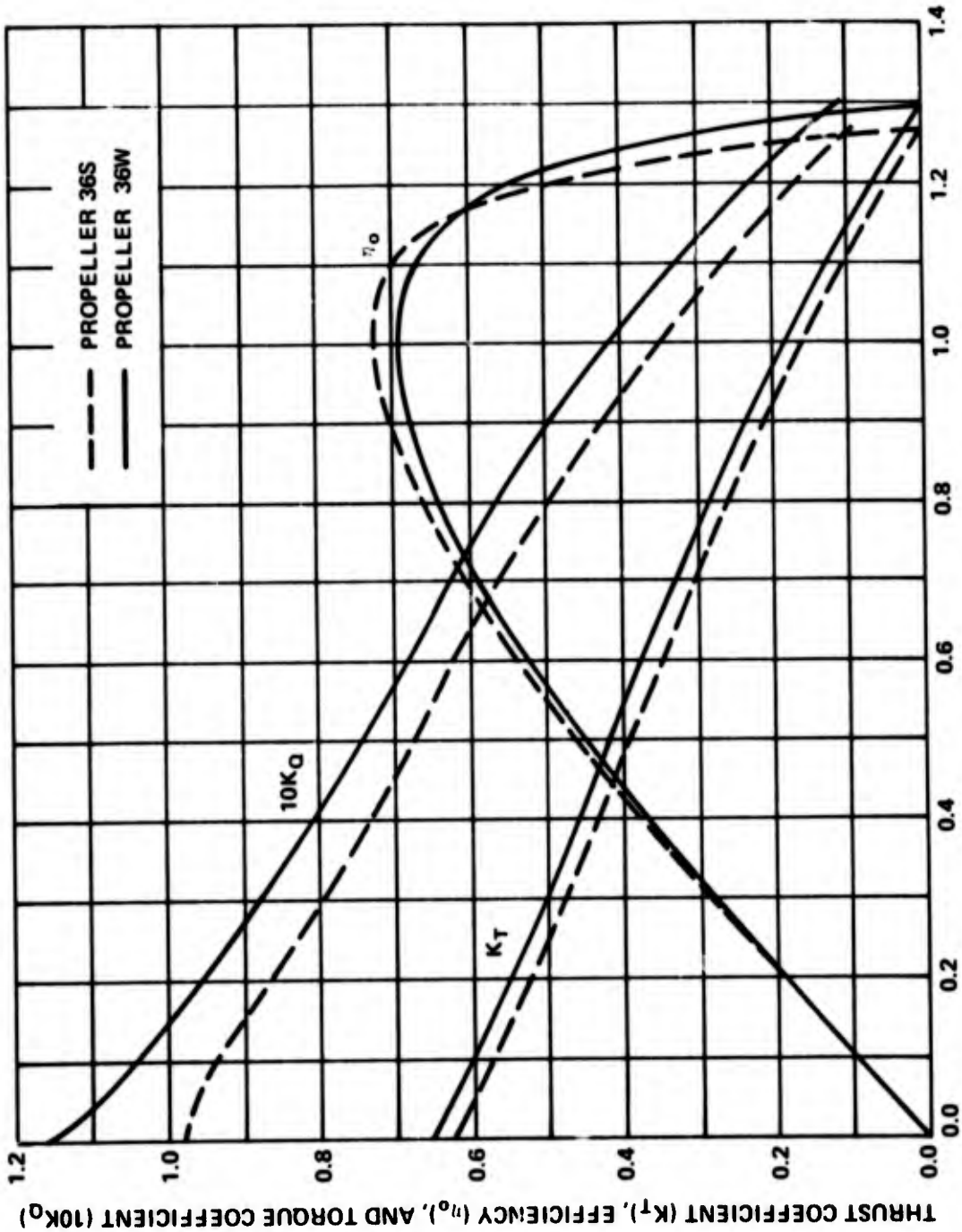

Figure 10a – Propellers 36S and 36W

Figure 10 (Continued)

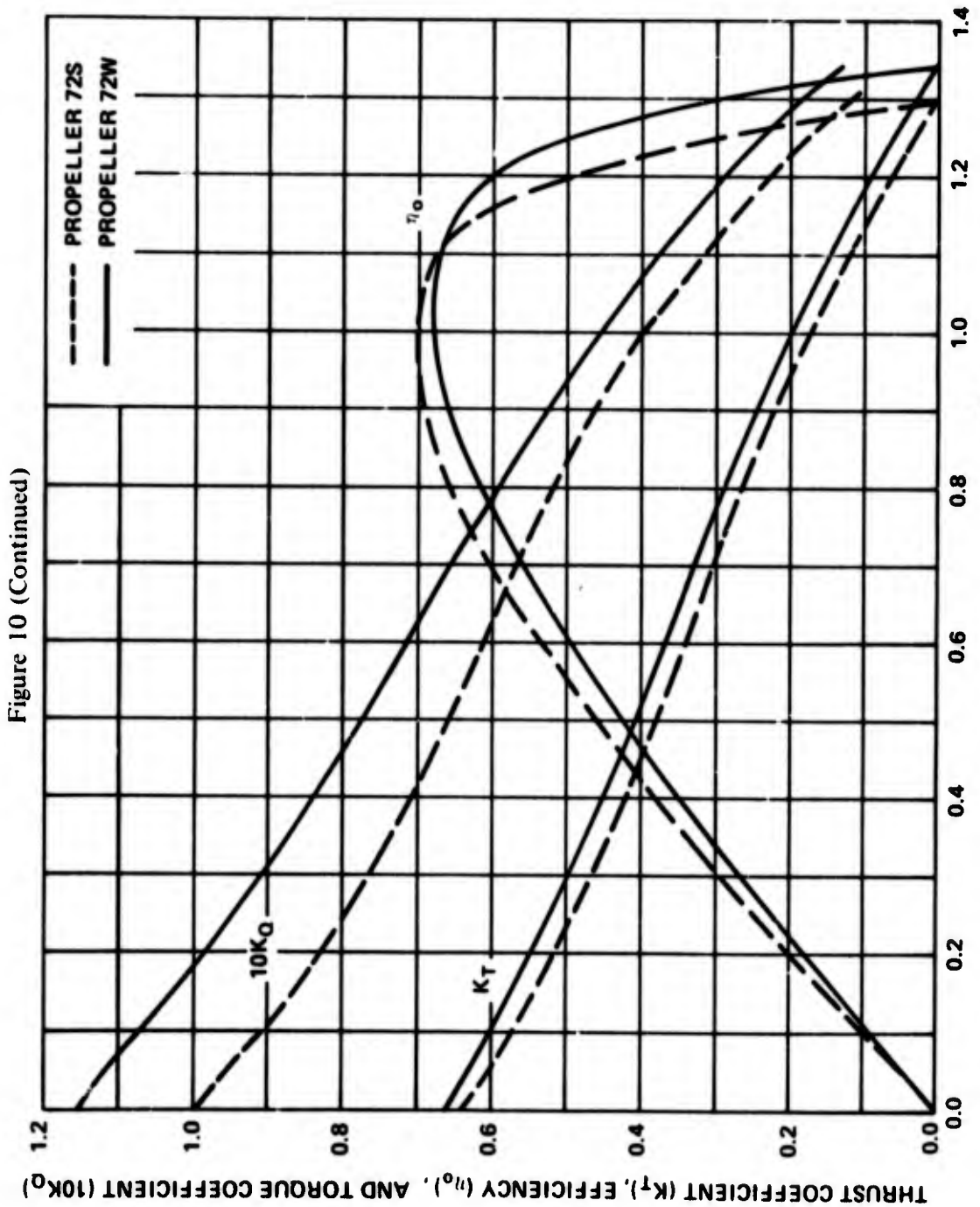

Figure 10b – Propellers 72S and 72W

Figure 10 (Continued)

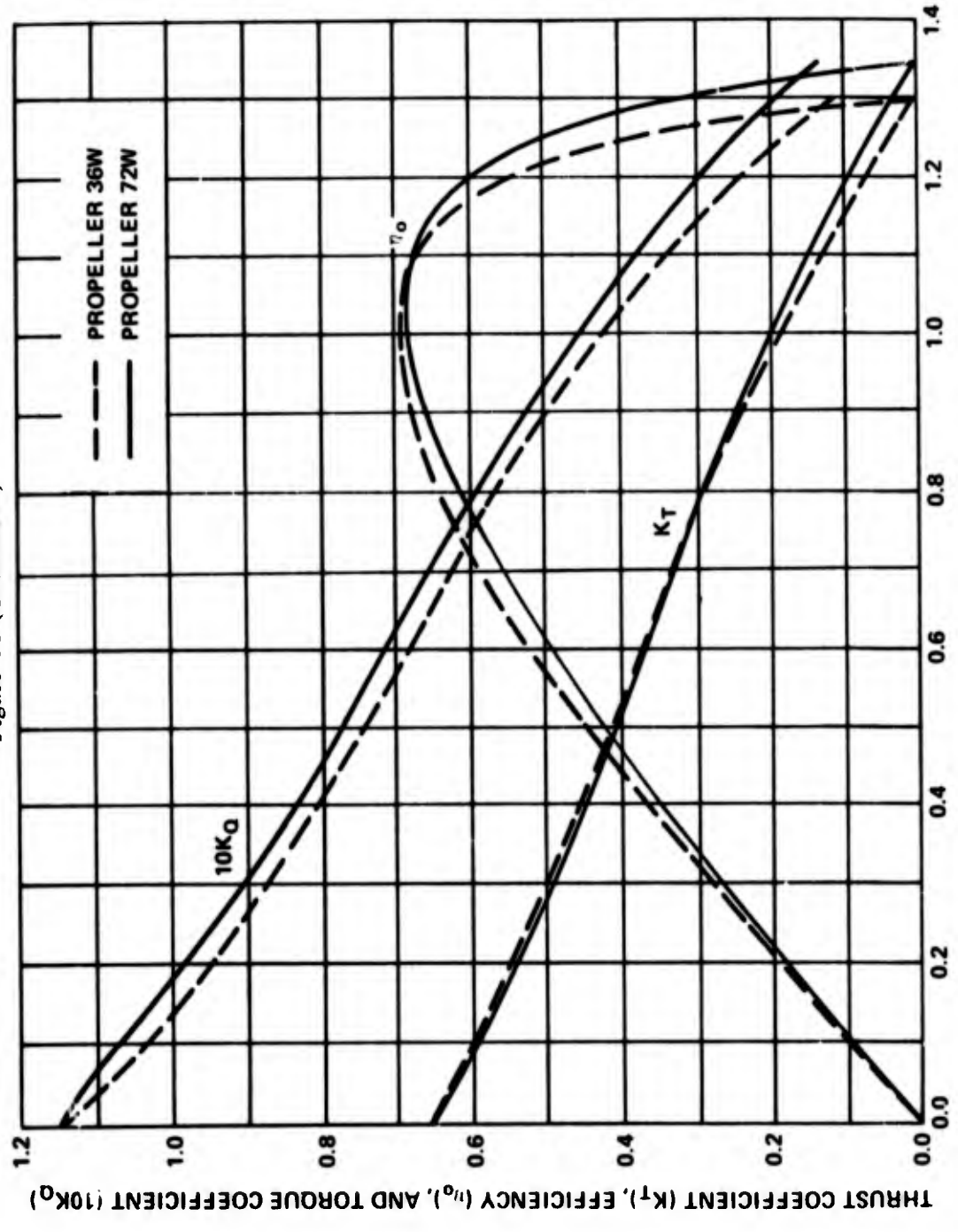

Figure 10c – Propellers 36W and 72W

Figure 11 – Backing Open-Water Characteristics of Propellers 36S, 36W, 72S, and 72W

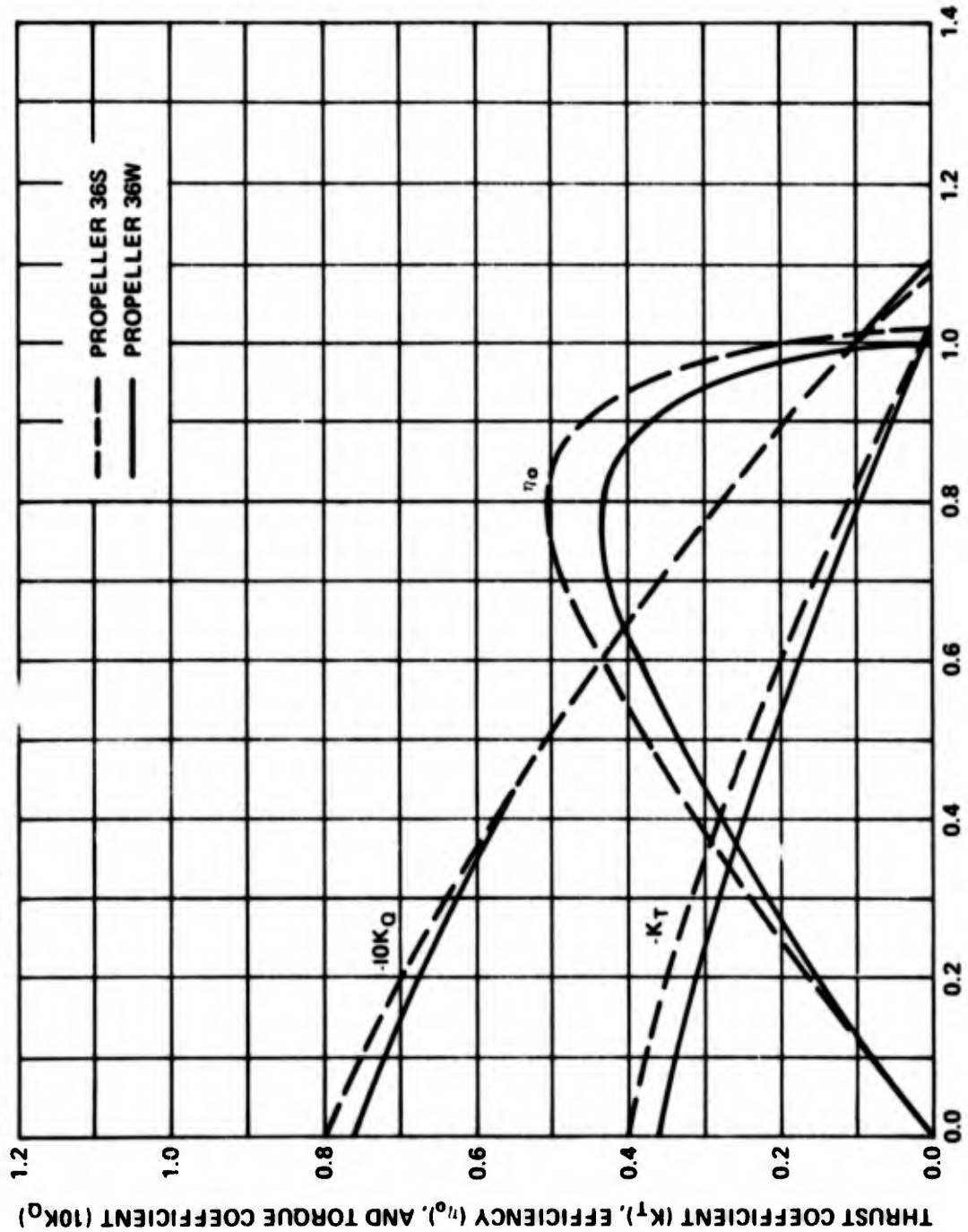

Figure 11a – Propellers 36S and 36W

Figure 11 (Continued)

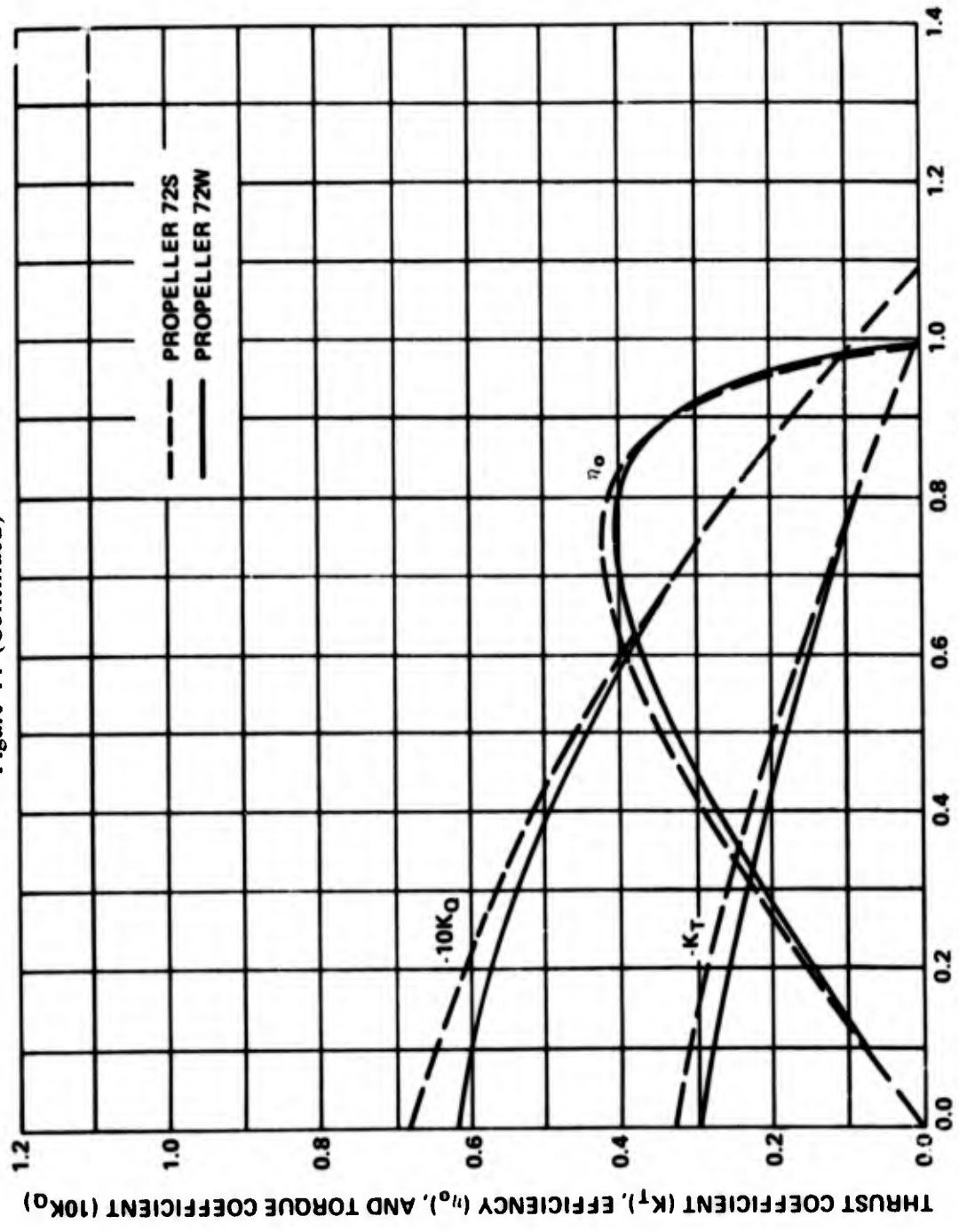

Figure 11b – Propellers 72S and 72W

Figure 11 (Continued)

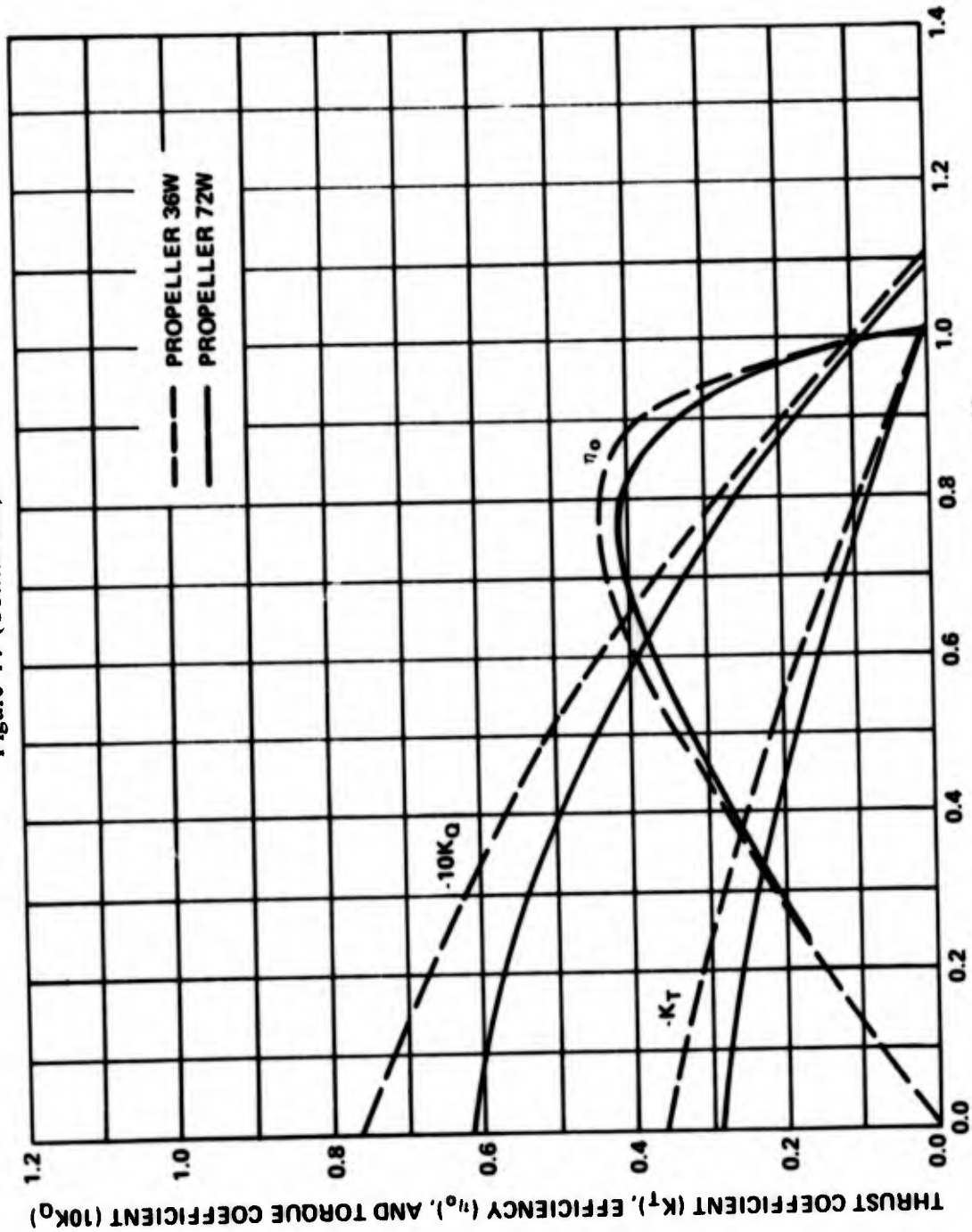

Figure 11c – Propellers 36W and 72W

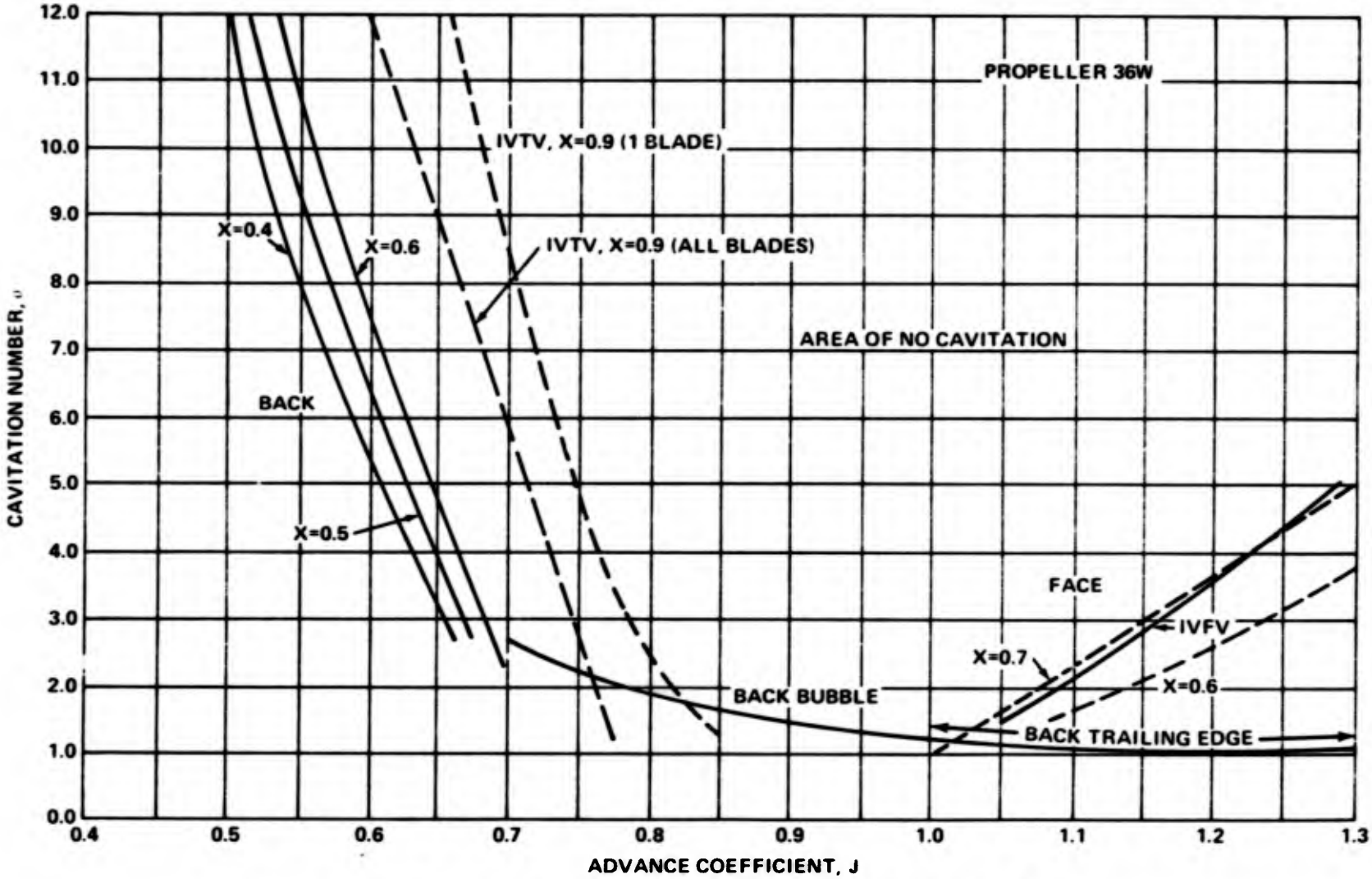

Figure 12 – Cavitation Inception on Propeller 36W at Various Radii

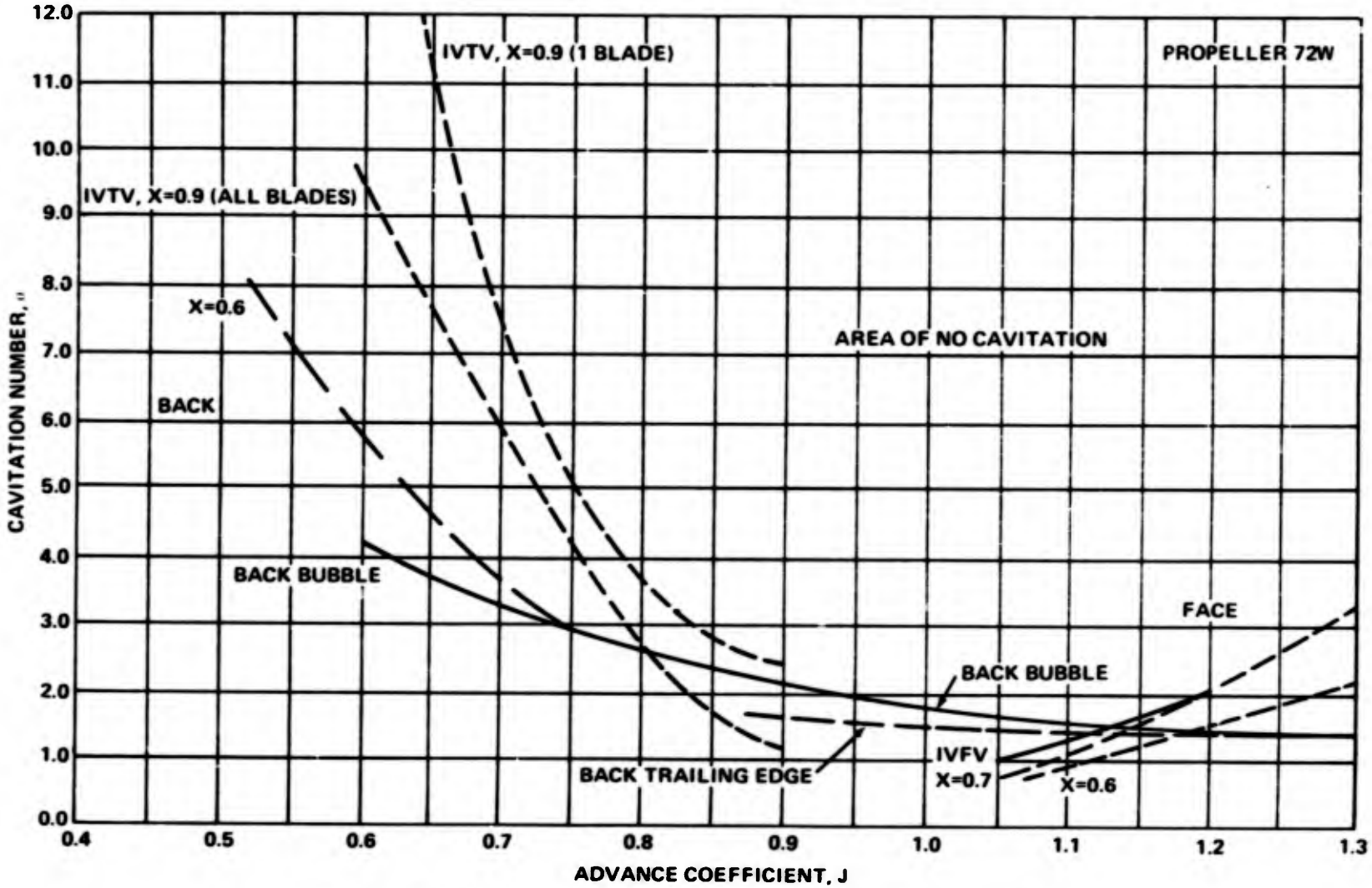

Figure 13 – Cavitation Inception on Propeller 72W at Various Radii

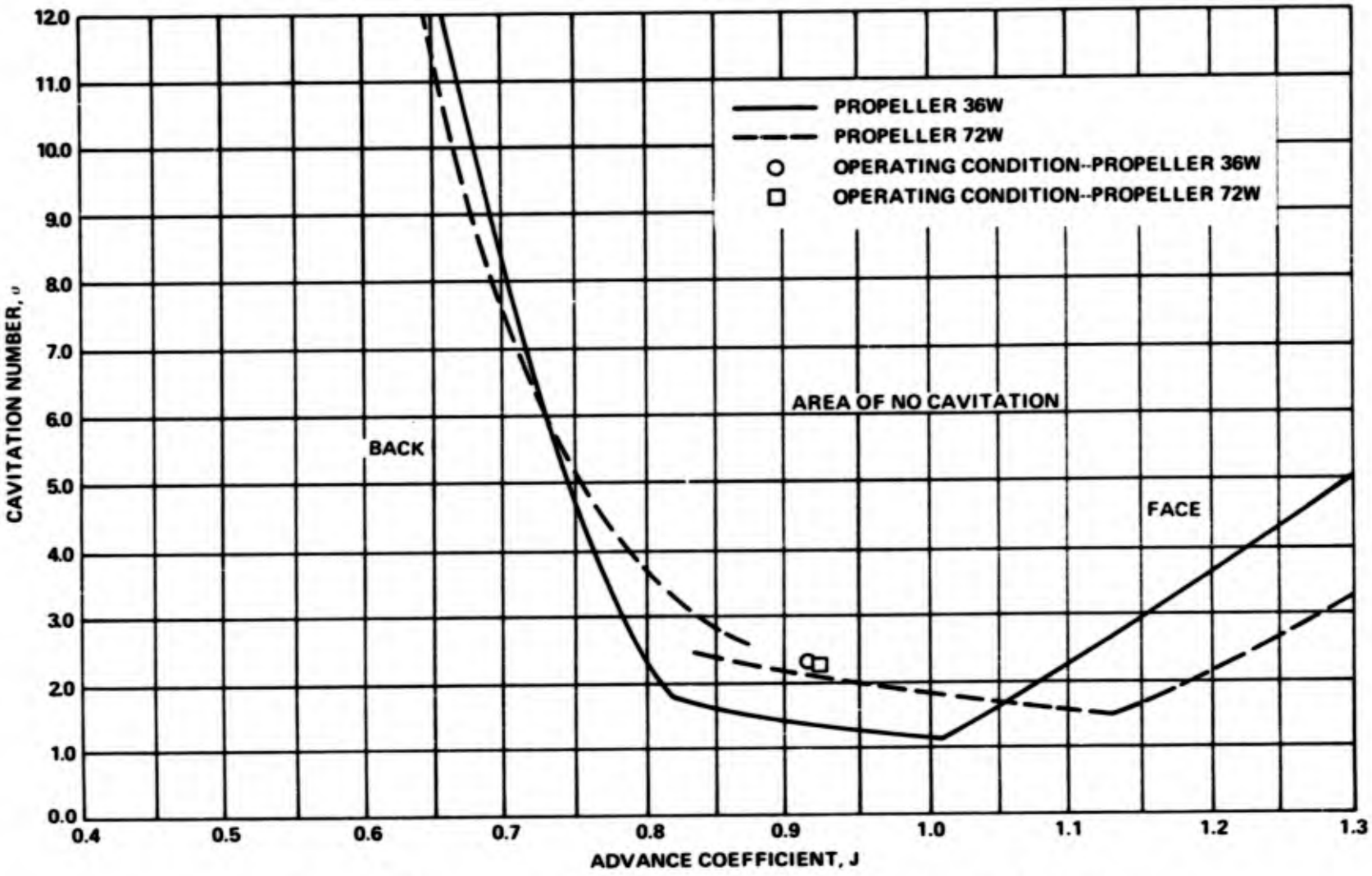

Figure 14 – Comparison of Cavitation Inception on Propellers 36W and 72W

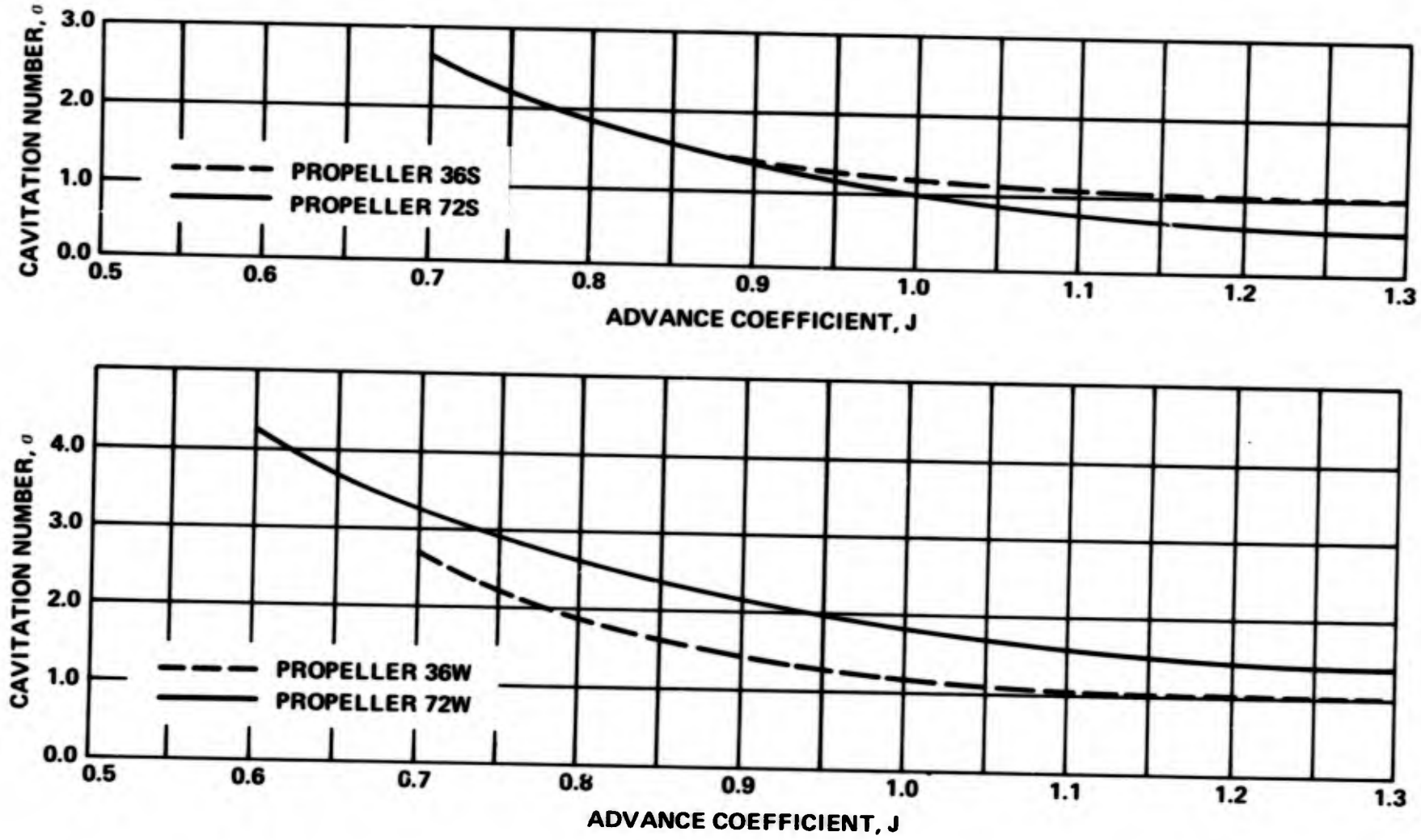

Figure 15 – Effect of Skew Angle on Back Bubble-Cavitation Inception on Propellers 36S, 72S, 36W, and 72W

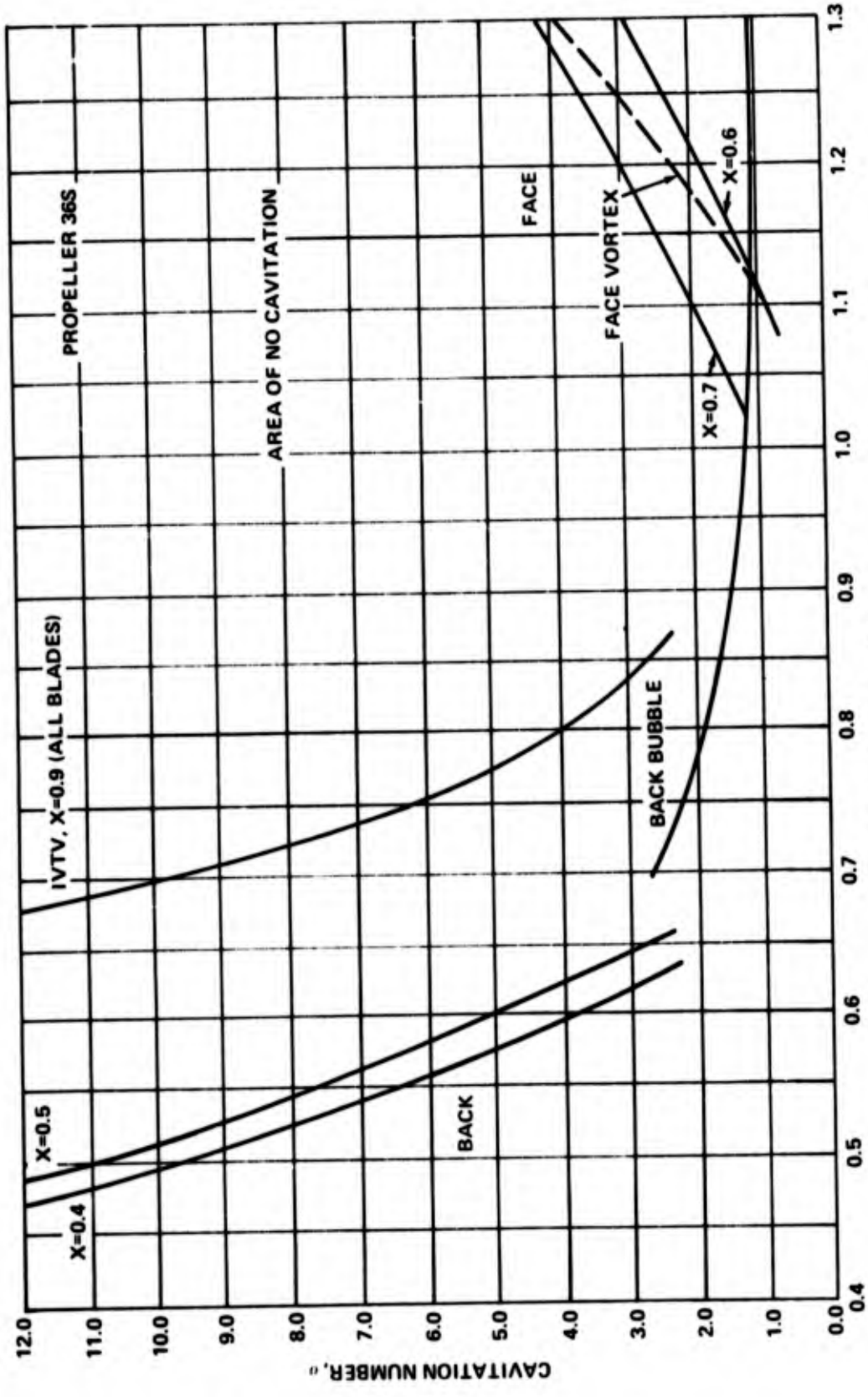

Figure 16 – Cavitation Inception on Propeller 36S at Various Radii

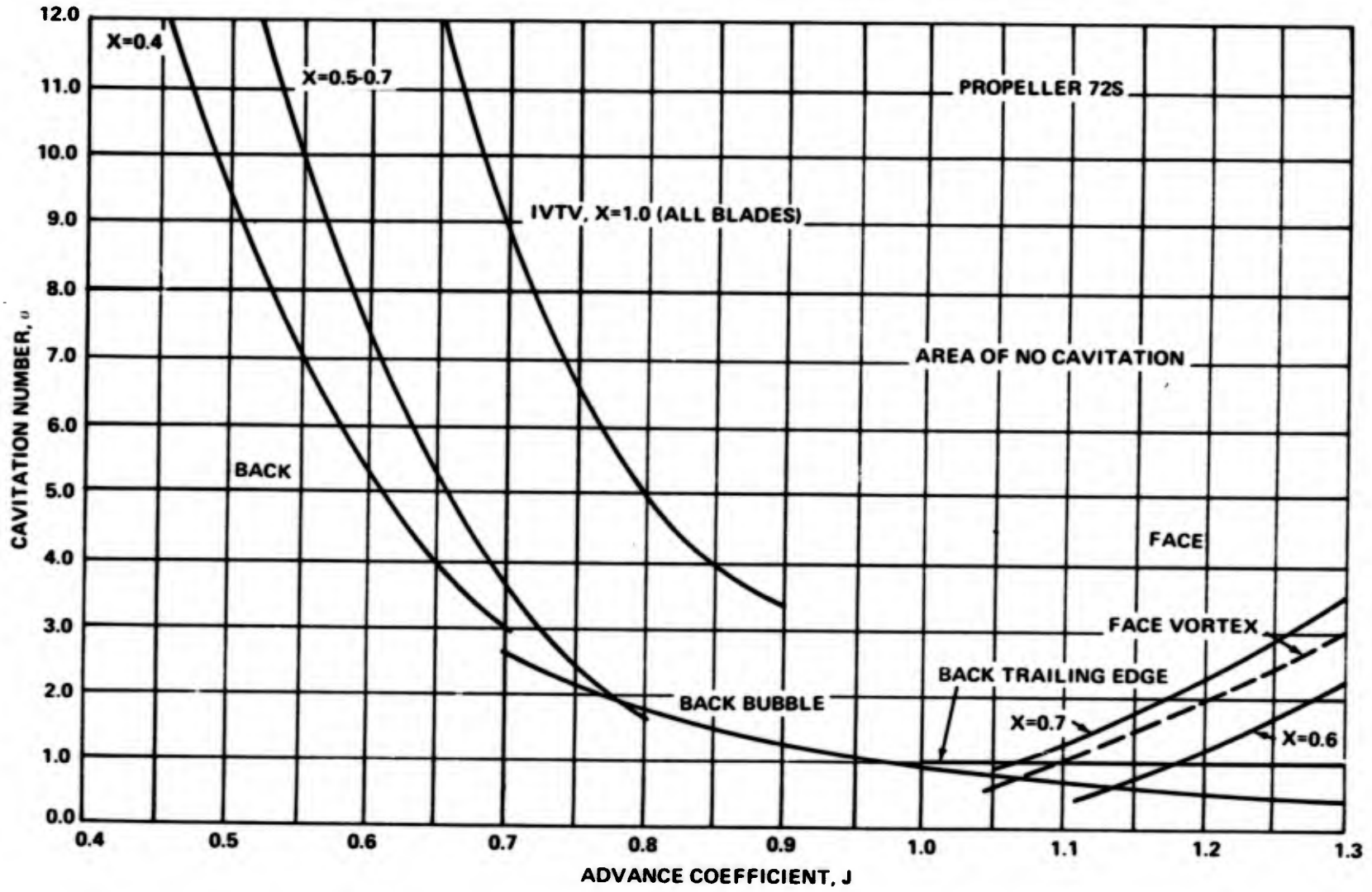

Figure 17 – Cavitation Inception on Propeller 72S at Various Radii

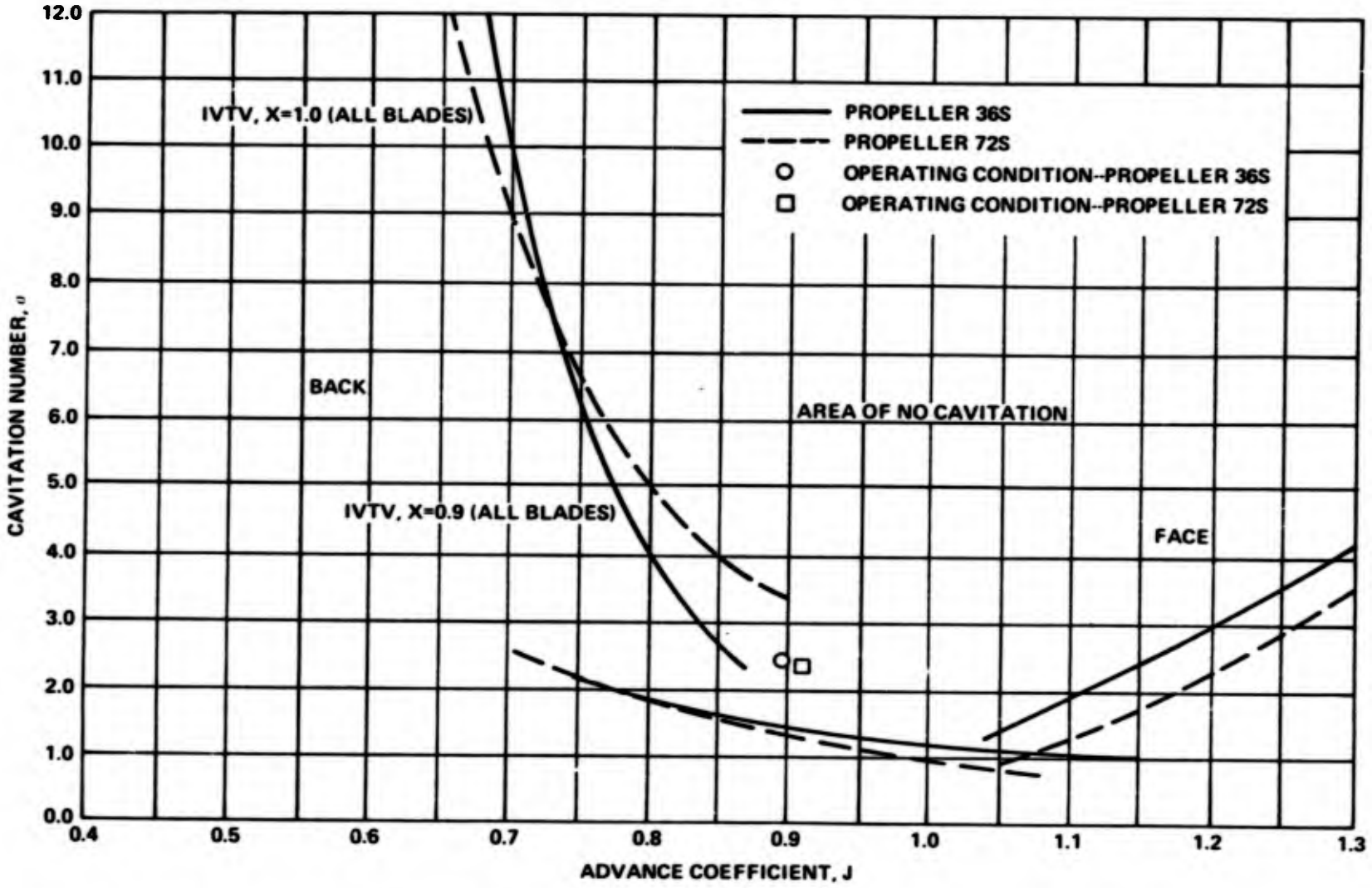

Figure 18 – Comparison of Cavitation Inception on Propellers 36S and 72S

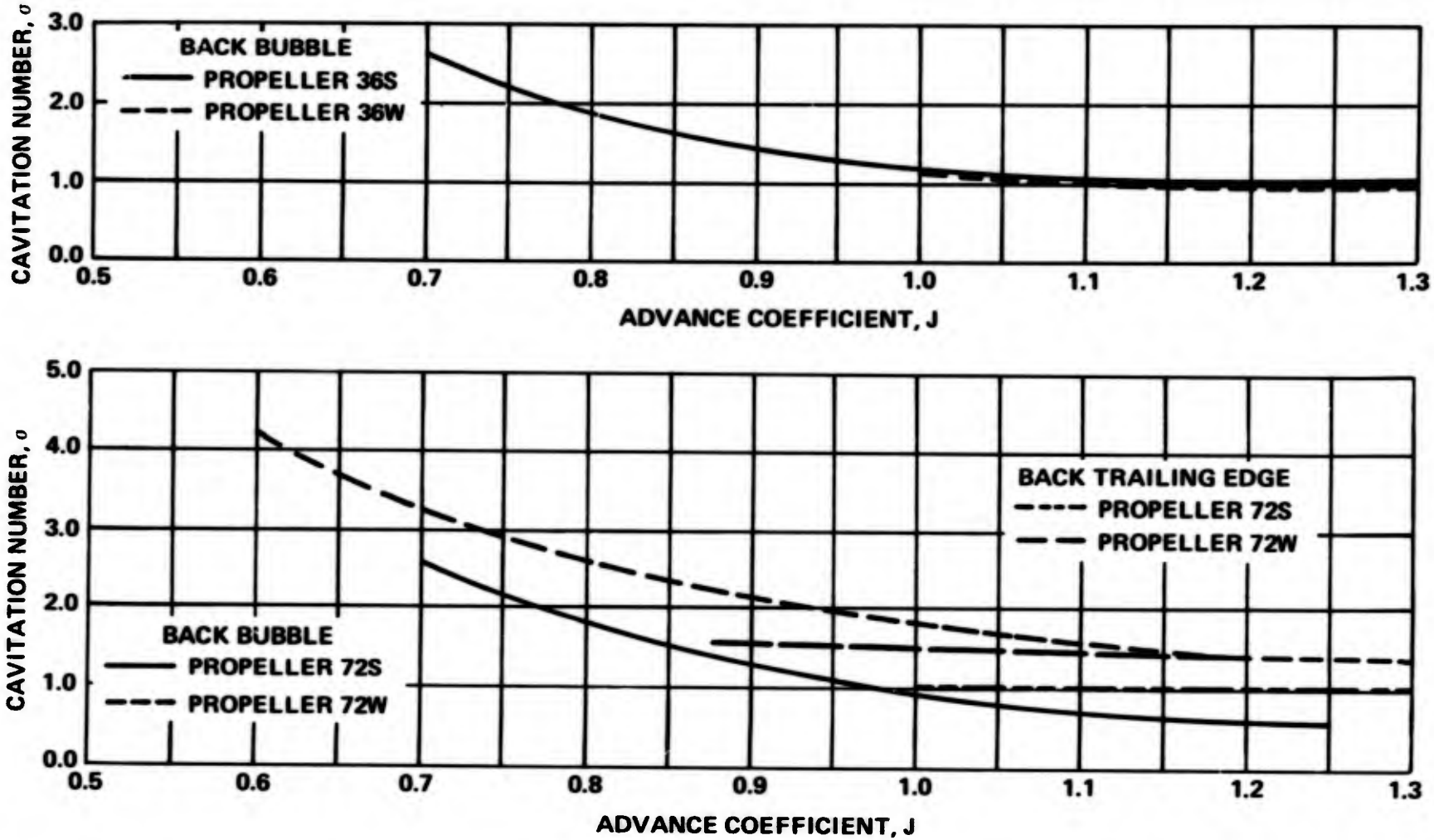

Figure 19 – Effect of Propeller-Blade Distortion on Back Bubble-Cavitation Inception for Propellers 36S, 36W, 72S, and 72W

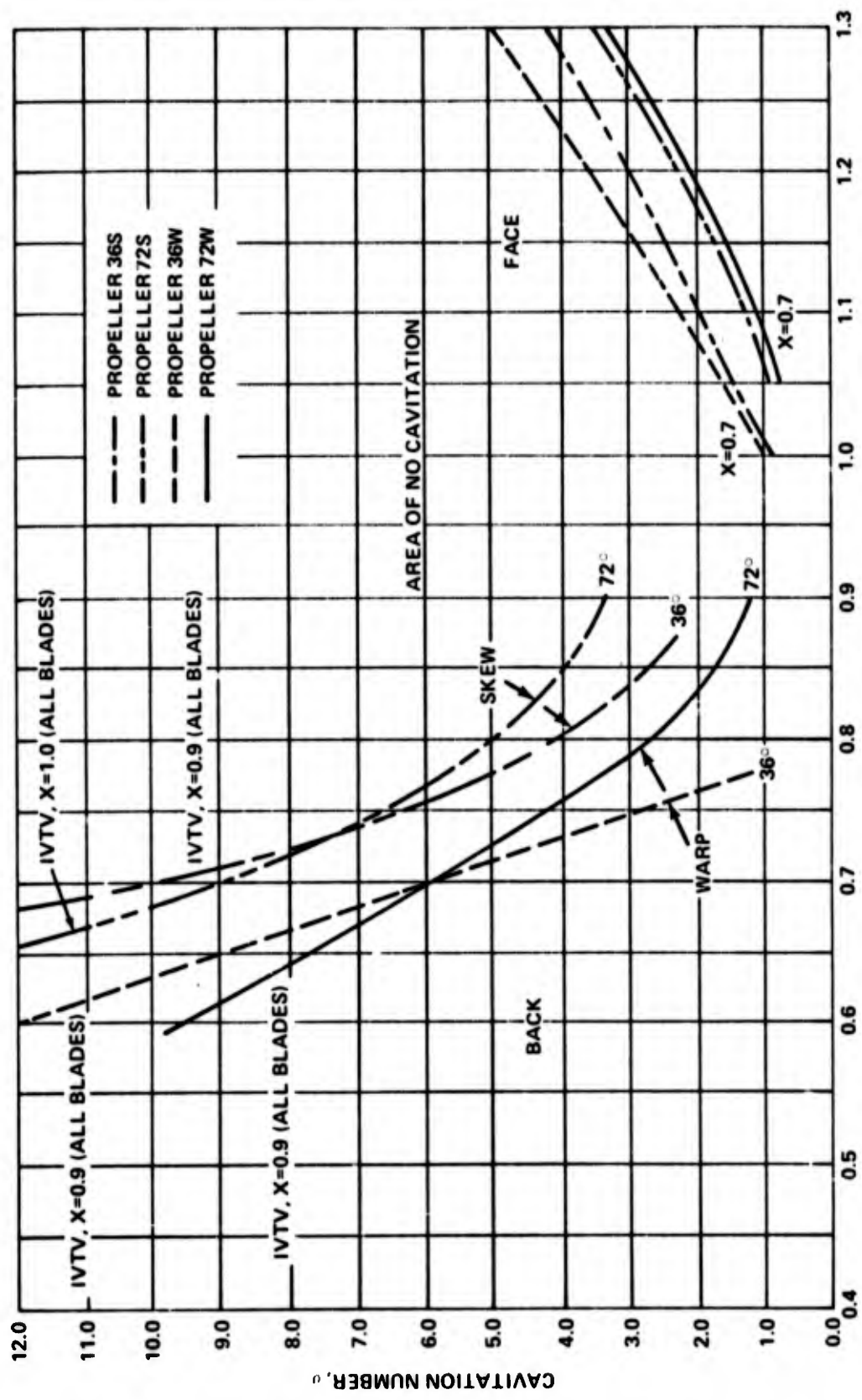

Figure 20 – Comparison of Cavitation Inception on Propellers 36S, 36W, 72S, and 72W

(Except back bubble-cavitation inception)

Figure 21 – Comparison of Face Cavitation Inception on Propellers 36S, 36W, 72S, and 72W

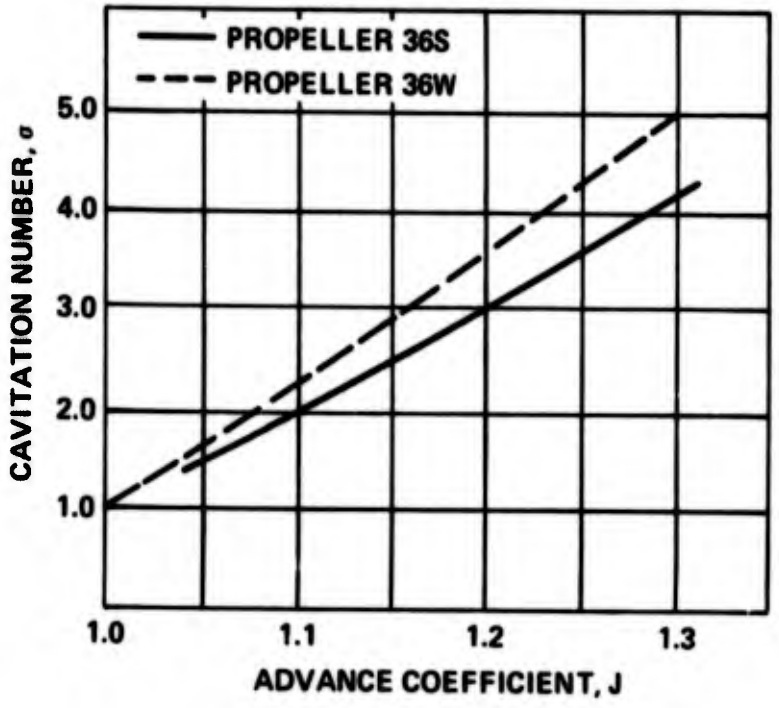

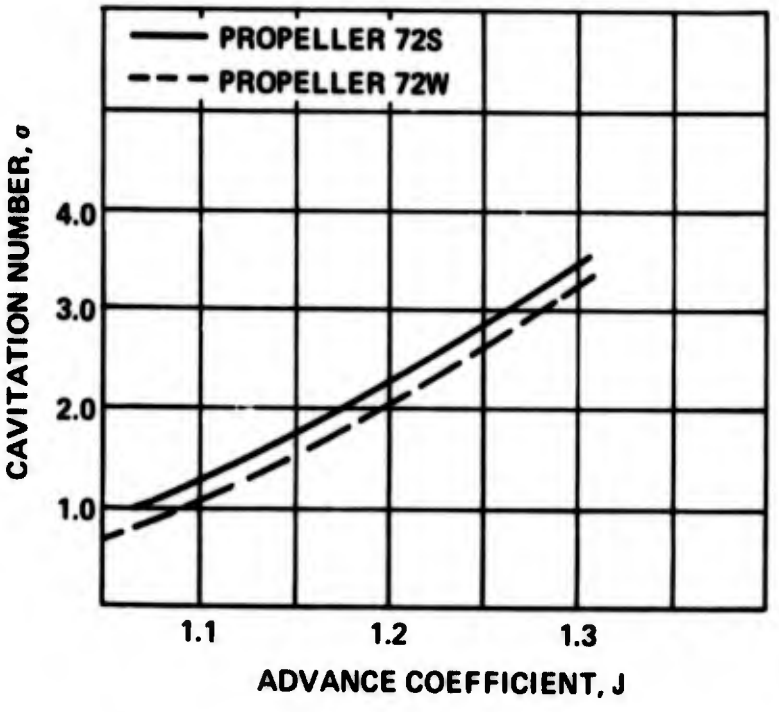

Figure 21a – Face Cavitation, X = 0.7

Figure 21 (Continued)

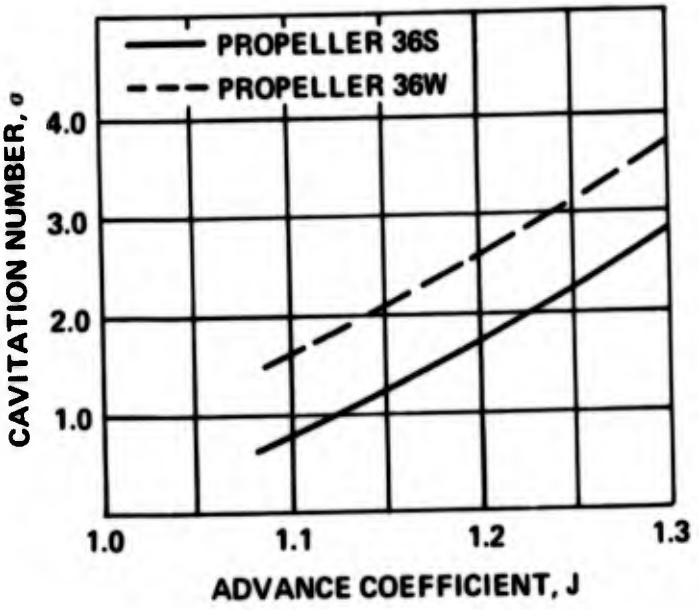

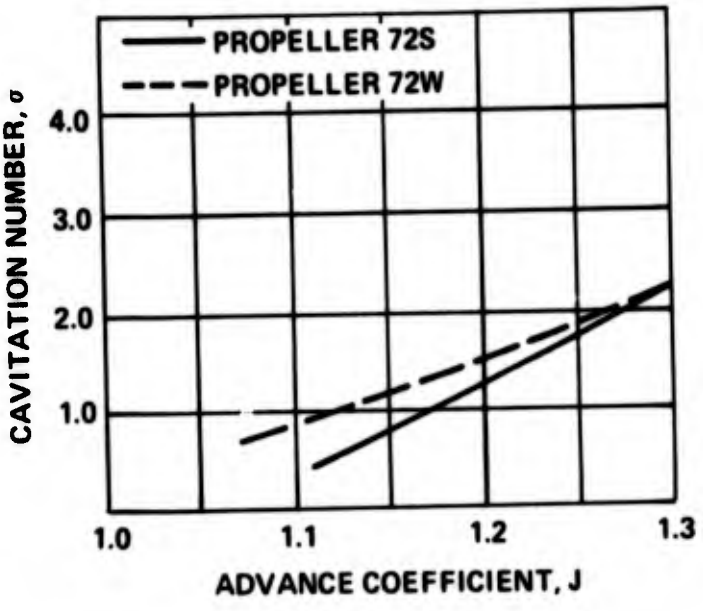

Figure 21b – Face Cavitation, X = 0.6

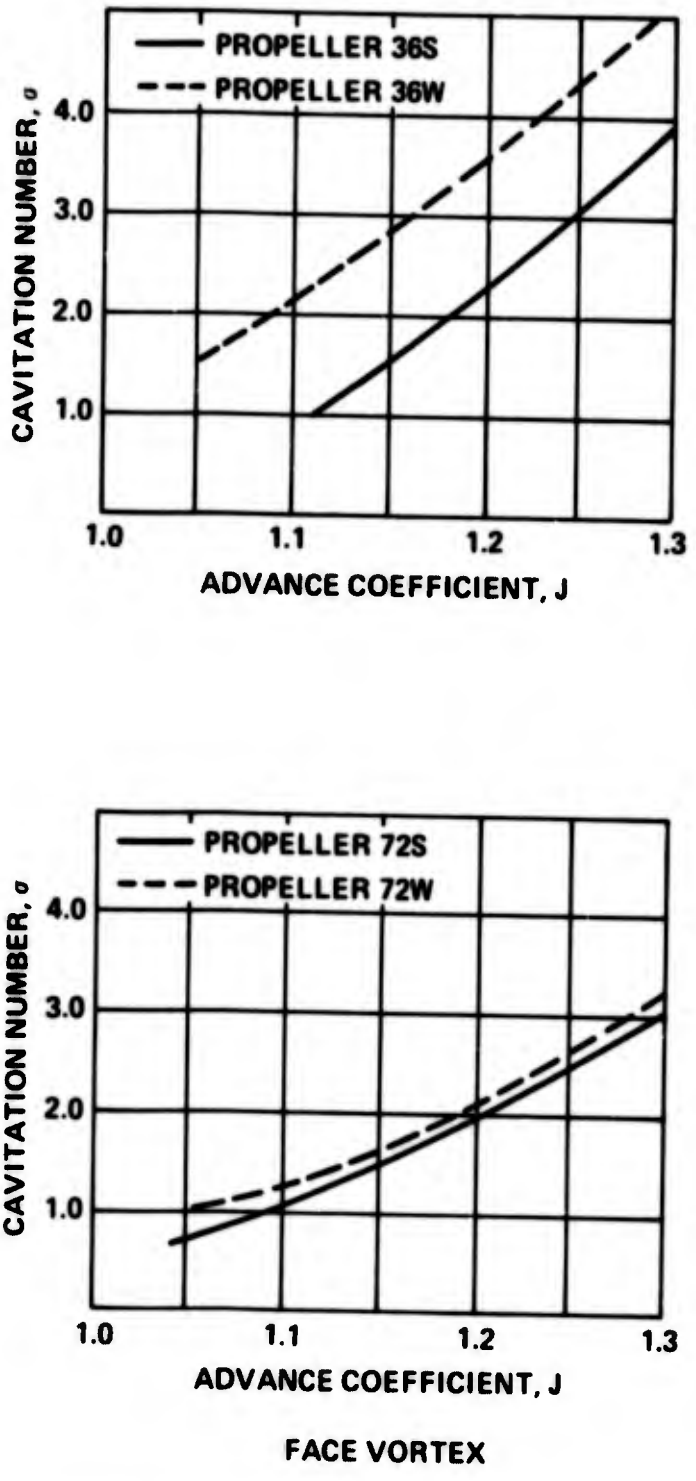

Figure 22 — Comparison of Face Vortex-Cavitation Inception on Propellers 36S, 36W, 72S, and 72W

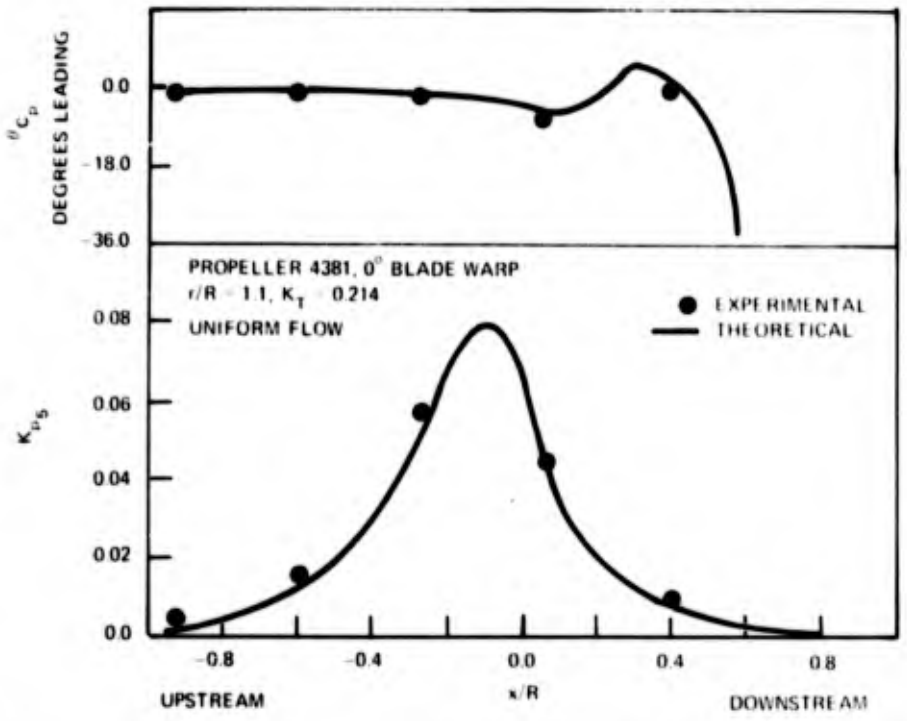

Figure 23 – Comparison of Predicted and Measured Blade-Frequency Pressure Amplitudes and Phases for Design Thrust Coefficients of 0.214, 0° Blade Warp, and 10-Percent Propeller Radius Tip Clearance

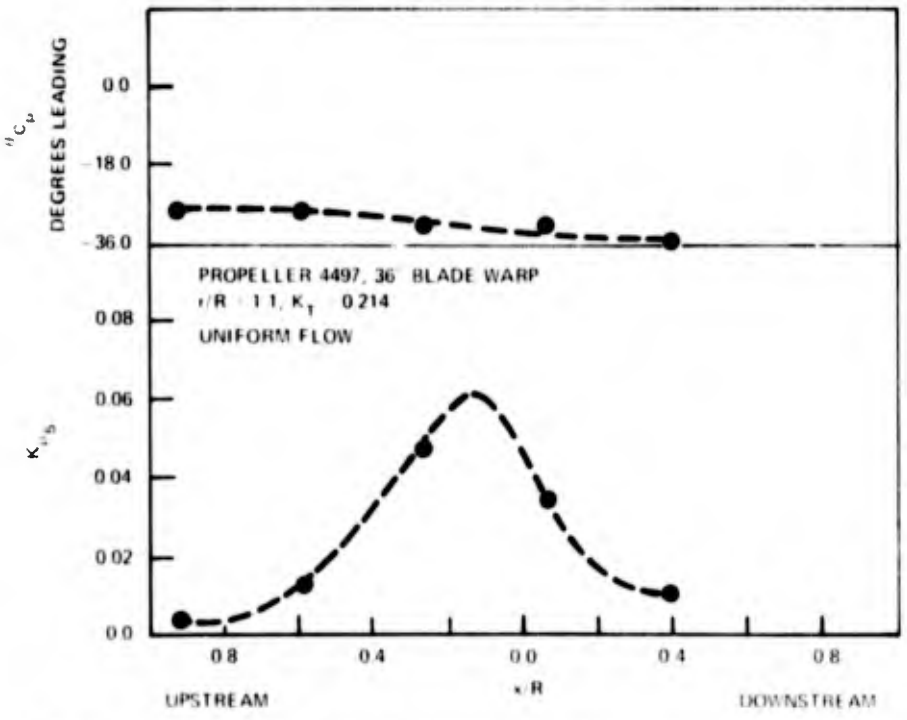

Figure 24 – Measured Blade-Frequency Pressure Amplitudes and Phases for Design Thrust Coefficient of 0.214, 36° Blade Warp, and 10-Percent Propeller Radius Tip Clearance

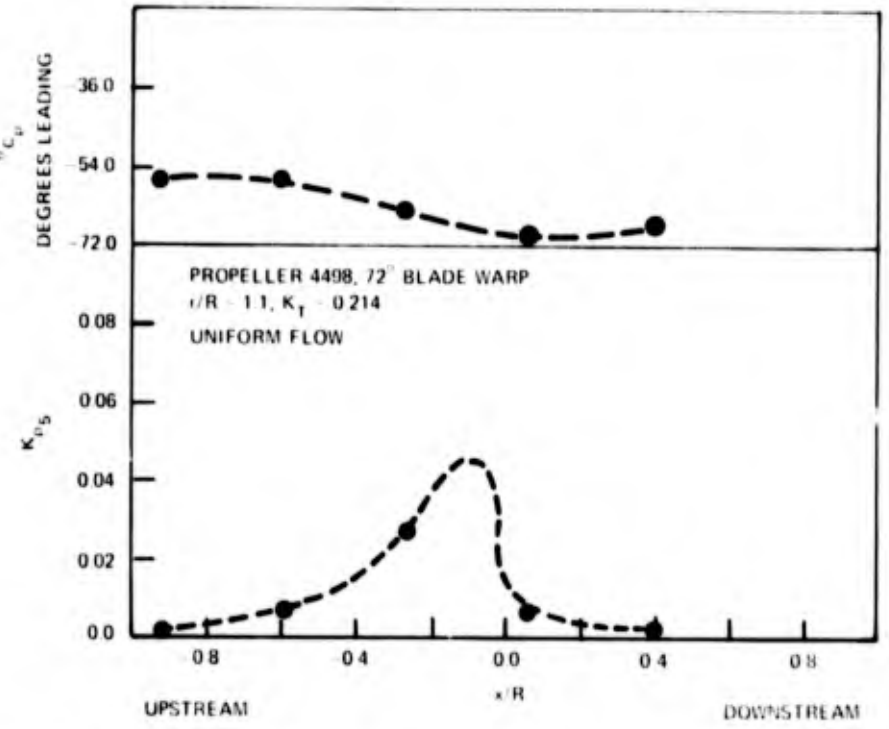

Figure 25 – Measured Blade-Frequency Pressure Amplitudes and Phases for Design Thrust Coefficient of 0.214, 72° Blade Warp, and 10-Percent Propeller Radius Tip Clearance

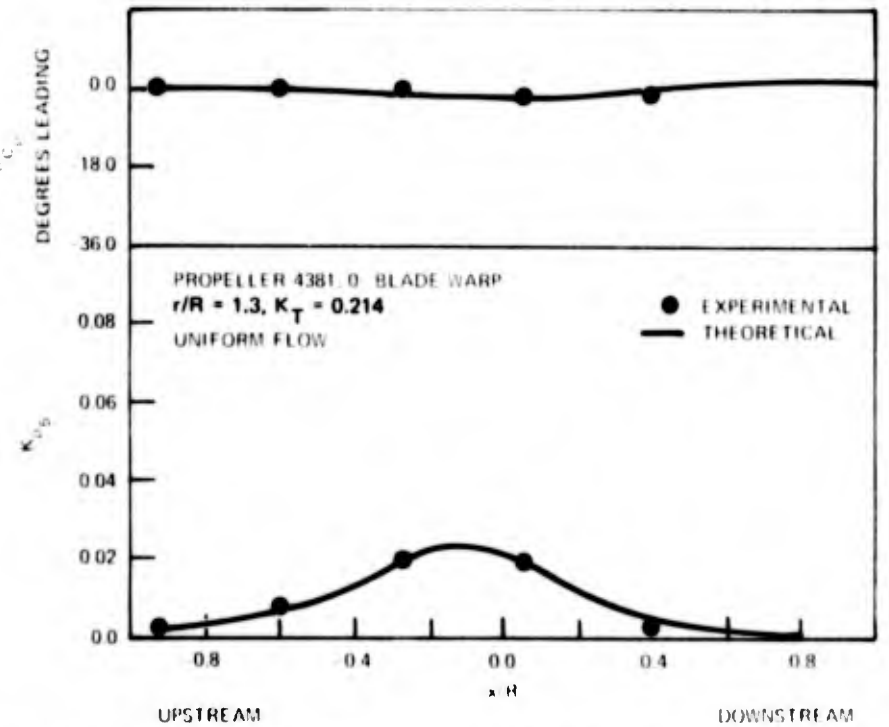

Figure 26 - Comparison of Predicted and Measured Blade-Frequency Pressure Amplitudes and Phases for Design Thrust Coefficient of 0.214, 0° Blade Warp, and 30-Percent Propeller Radius Tip Clearance

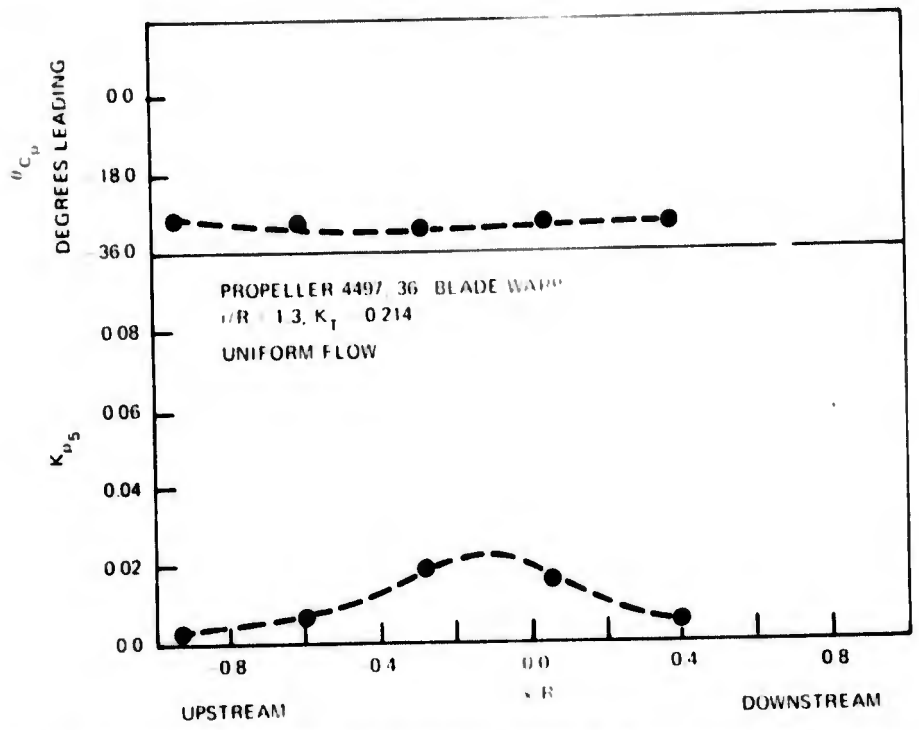

Figure 27 – Measured Blade-Frequency Pressure Amplitudes and Phases for Design Thrust Coefficient of 0.214, 36° Blade Warp, and 30-Percent Propeller Radius Tip Clearance

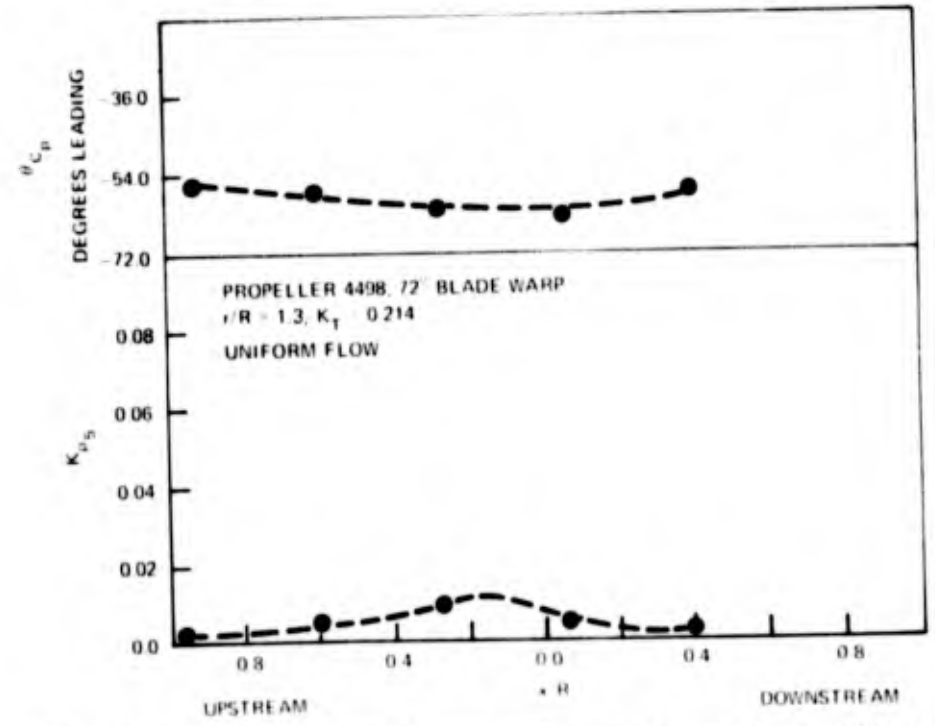

Figure 28 – Measure Blade-Frequency Pressure Amplitudes and Phases for Design Thrust Coefficient of 0.214, 72° Blade Warp, and 30-Percent Propeller Radius Tip Clearance

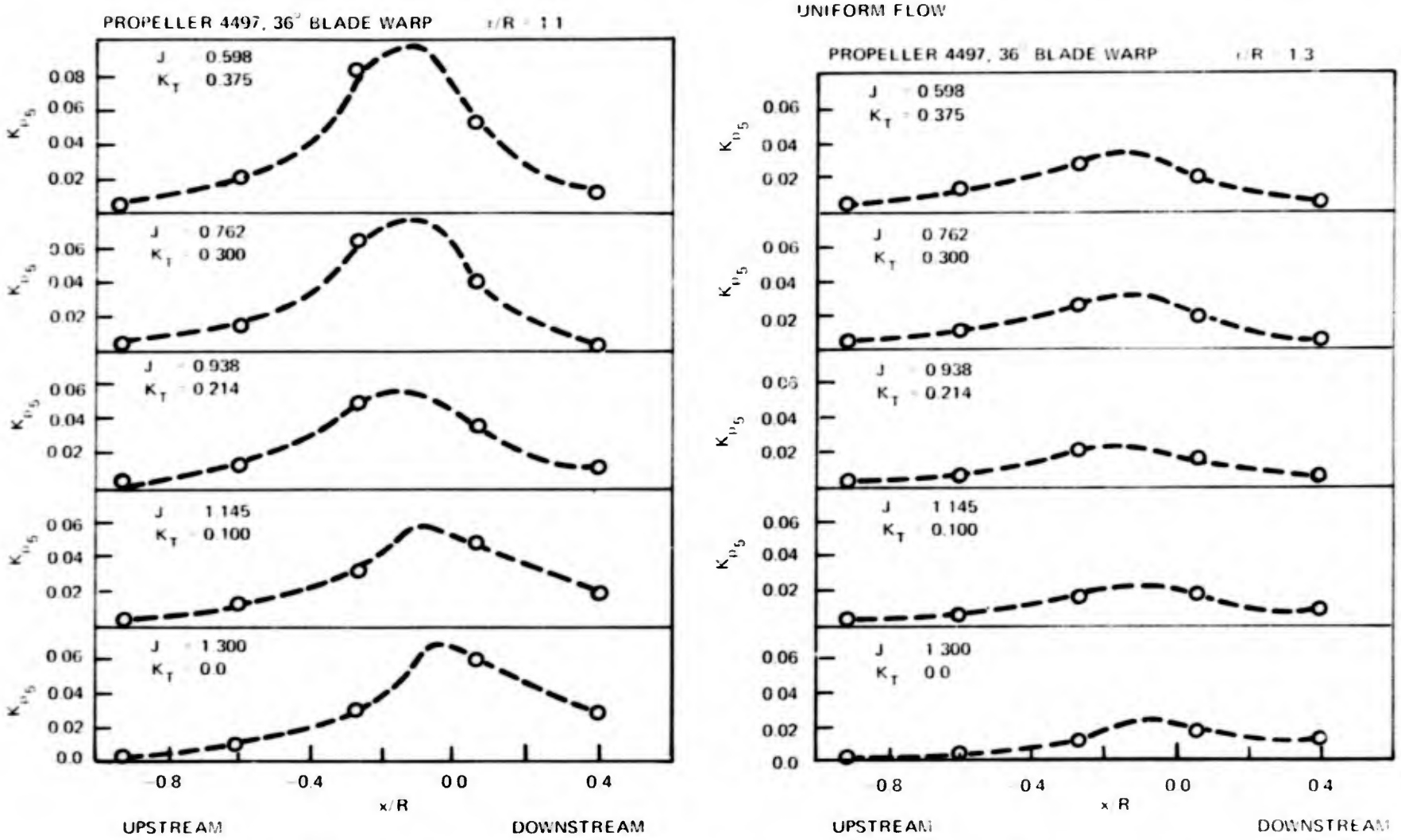

Figure 29 – Measured Blade-Frequency Amplitudes for 36° Warped Propeller at Five Advance Conditions and 10- and 30-Percent Propeller Radius Tip Clearance

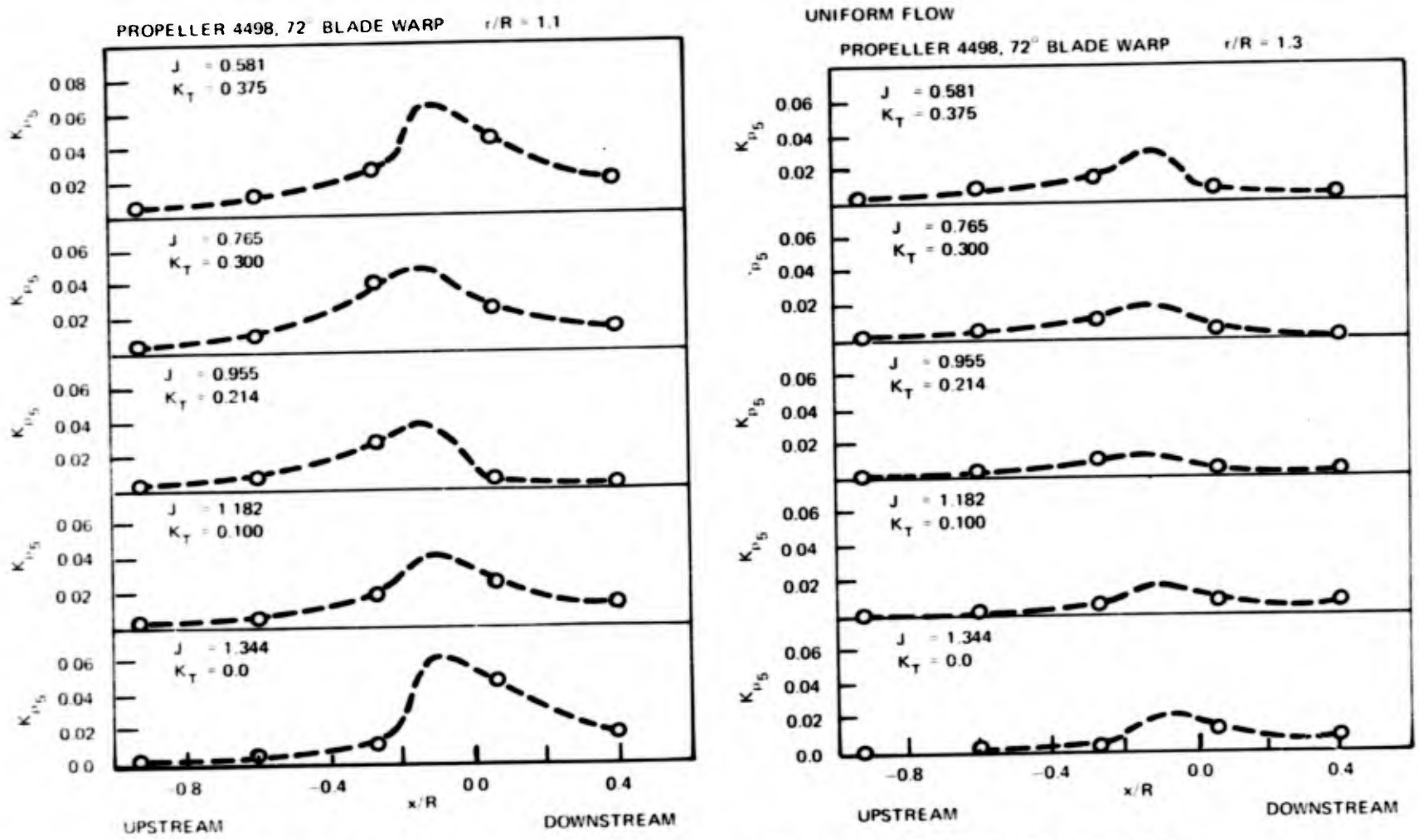

Figure 30 – Measured Blade-Frequency Amplitudes for 72° Warped Propeller at Five Advance Conditions and 10- and 30-Percent Propeller Radius Tip Clearance

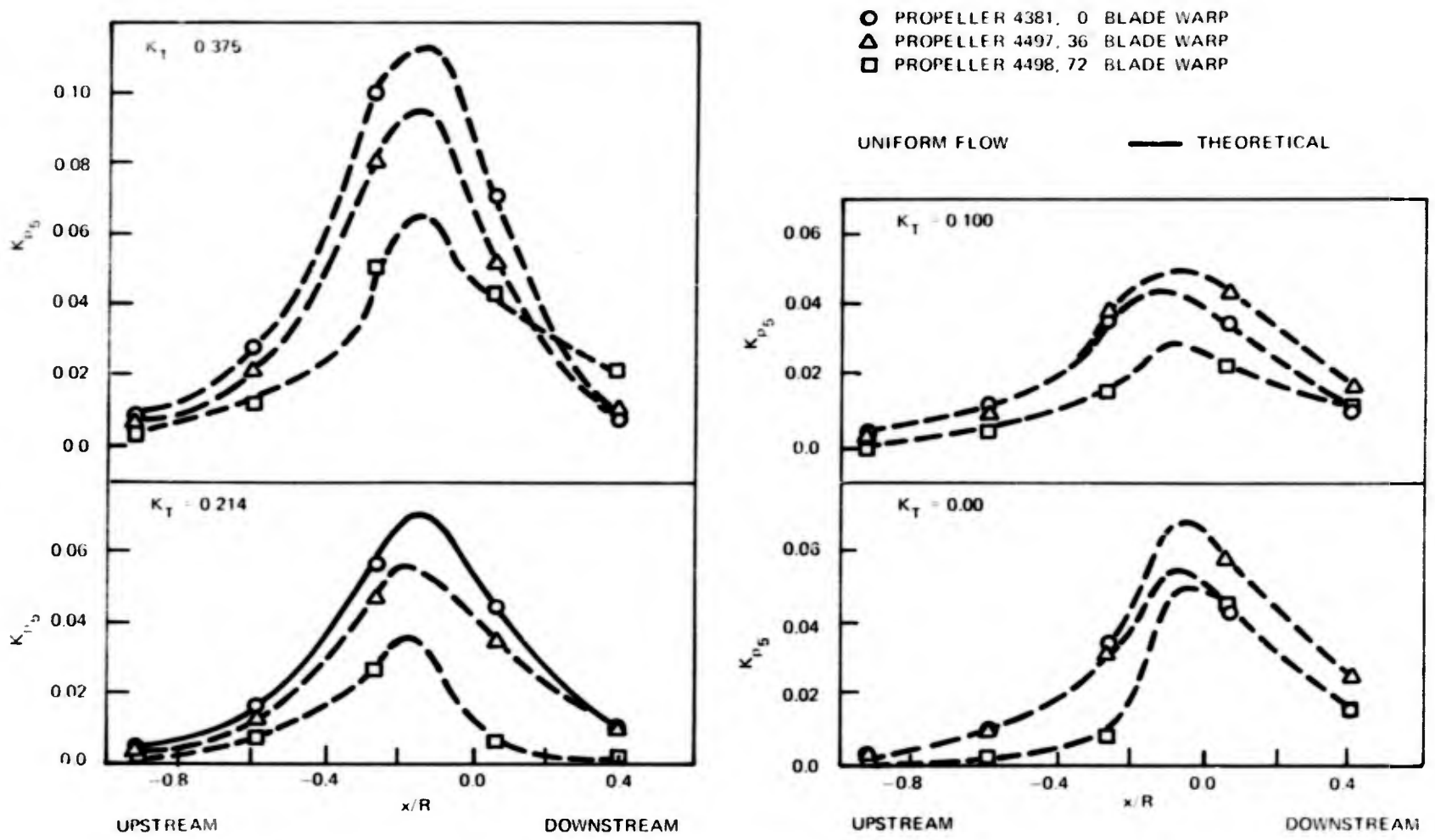

Figure 31 – Measured Blade-Frequency Amplitudes for Warped Propeller Series at Thrust Coefficient Values of 0.375, 0.214, 0.100, 0.00 for 10-Percent Propeller Radius Tip Clearance

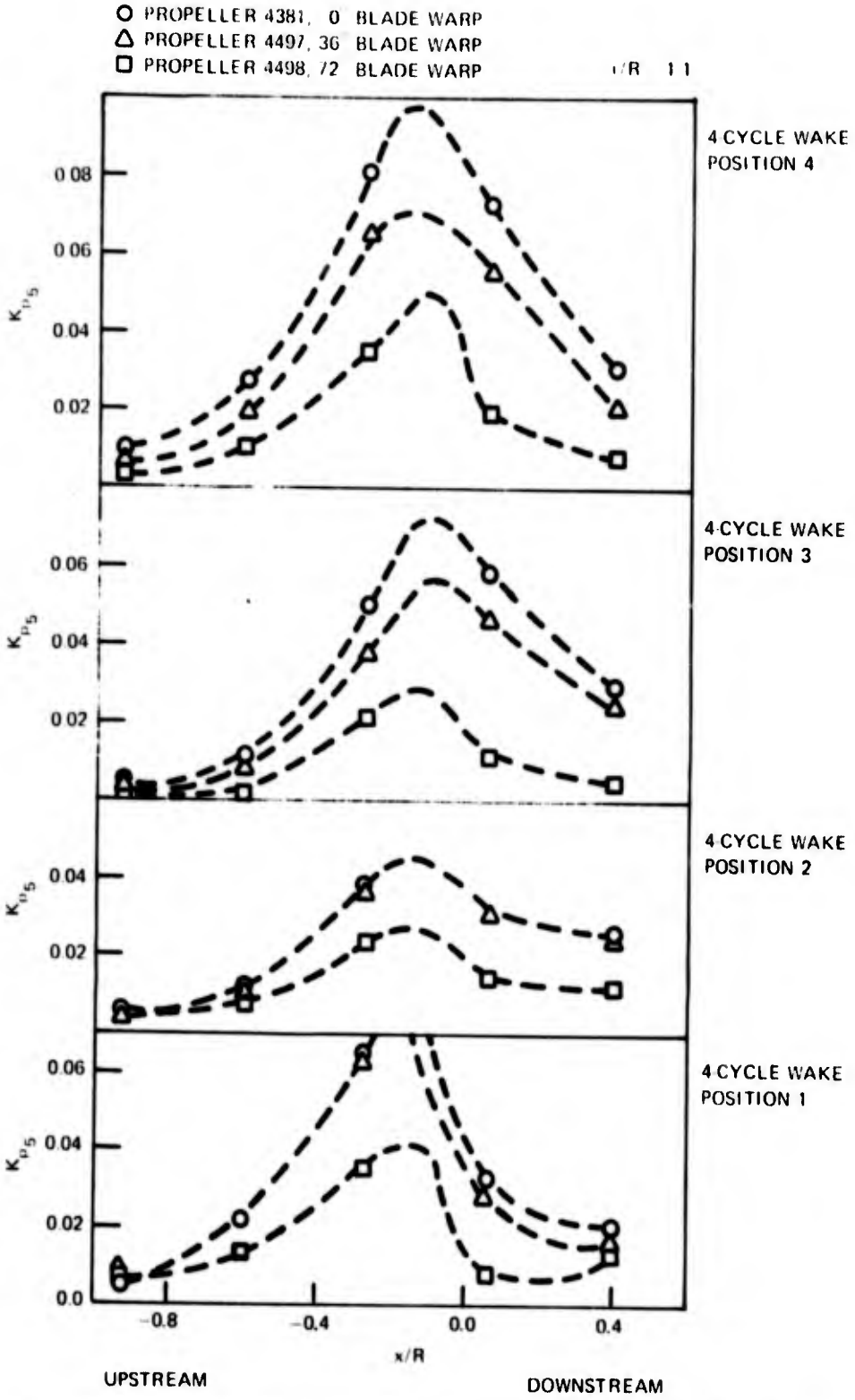

Figure 32 – Measured Blade-Frequency Pressure Amplitudes for the 0°, 36°, and 72° Warped Propellers at Mean-Thrust Coefficients of 0.214, 10-Percent Propeller Radius Tip Clearance, and Four Distinct Positions of the 4-Cycle Wake Screen

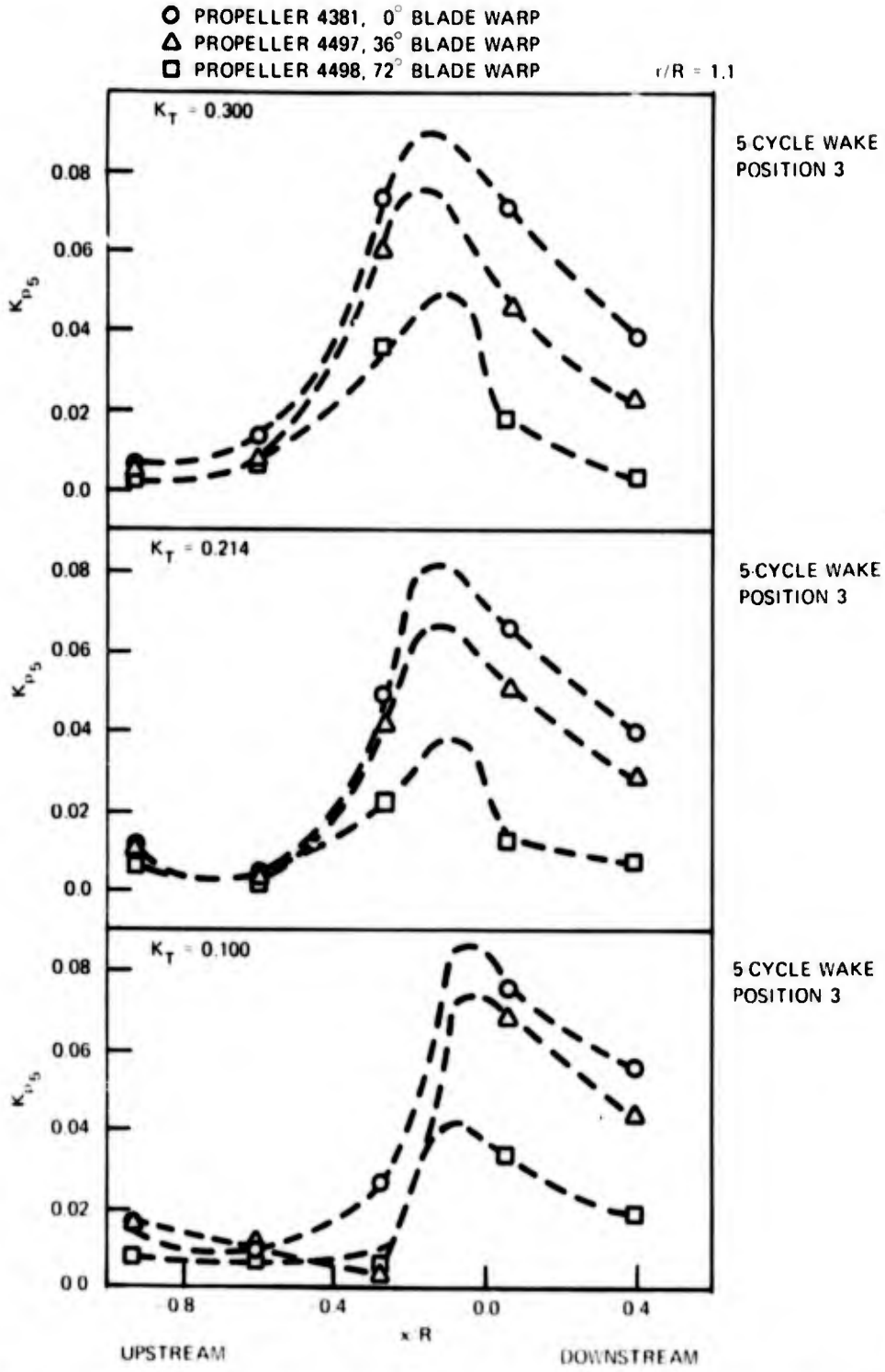

Figure 33 – Measured Blade-Frequency Pressure Amplitudes for the 0°, 36°, and 72° Warped Propellers at Mean-Thrust Coefficient Values of 0.300, 0.214, and 0.100 for Position 3 of the 5-Cycle Wake Screen, and 10-Percent Propeller Radius Tip Clearance

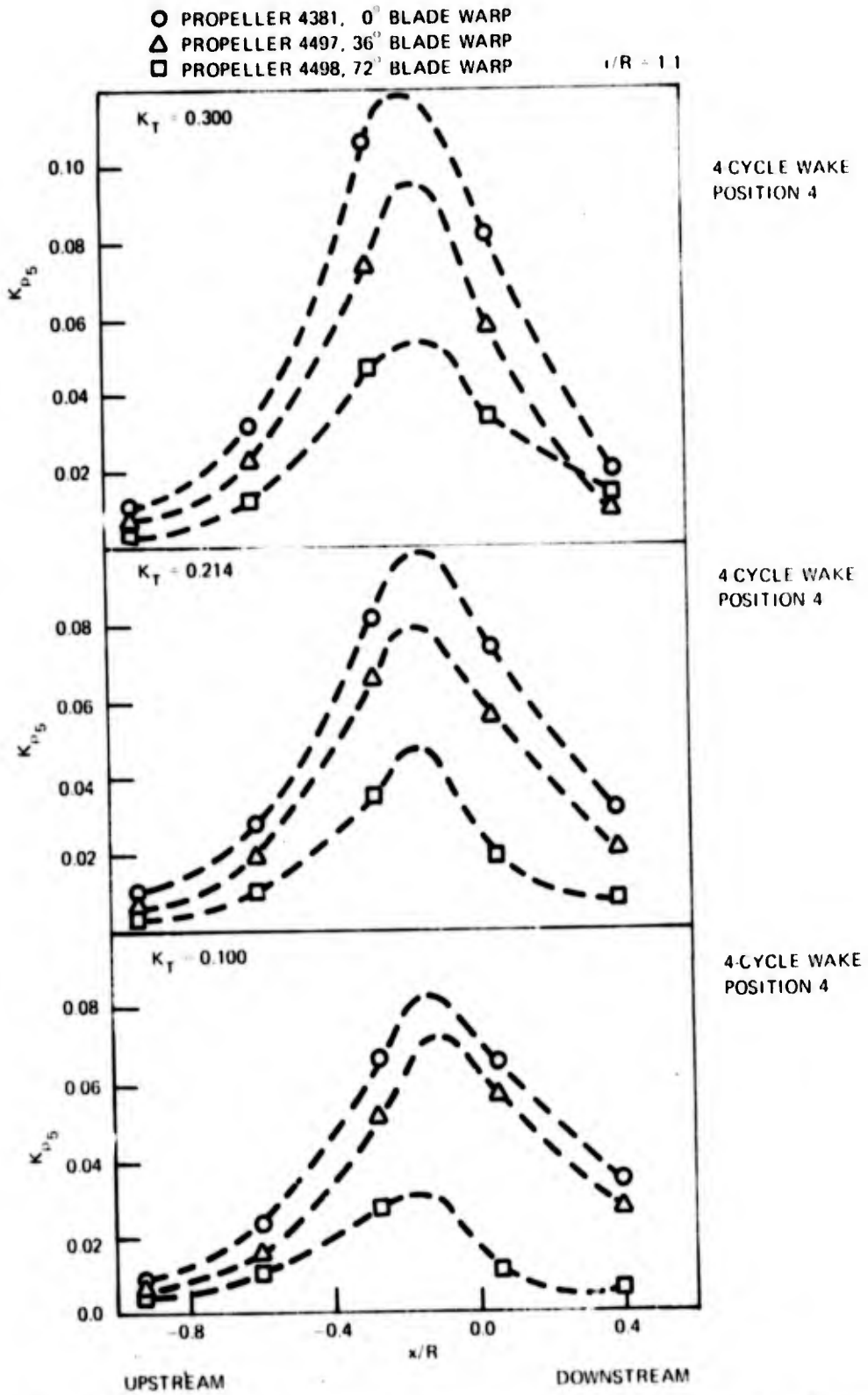

Figure 34 – Measured Blade-Frequency Pressure Amplitudes for the 0°, 36°, and 72° Warped Propellers at Mean-Thrust Coefficient Values of 0.300, 0.214, and 0.100 for Position 4 of the 4-Cycle Wake Screen, and 10-Percent Propeller Radius Tip Clearance

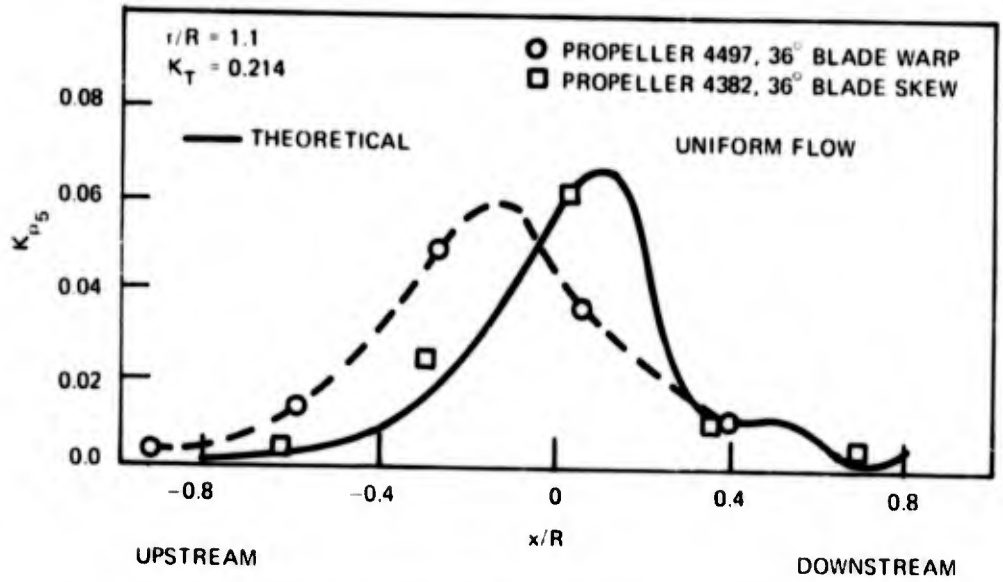

Figure 35 – Measured Blade-Frequency Pressure Amplitudes for Skewed and Warped Propellers of 36° at Design Thrust Coefficient of 0.214 and 10-Percent Propeller Radius Tip Clearance

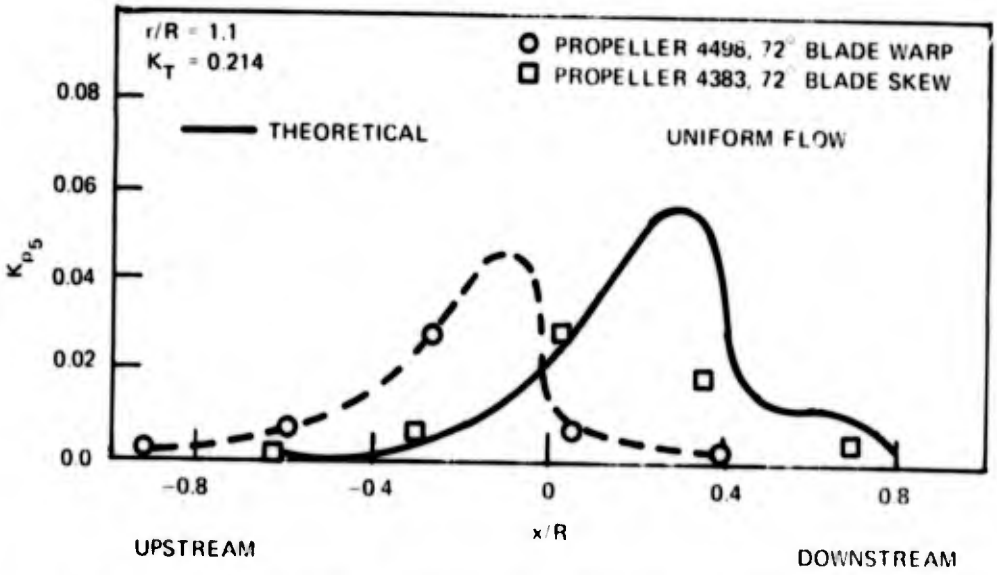

Figure 36 – Measured Blade-Frequency Pressure Amplitudes for Skewed and Warped Propellers of 72° at Design Thrust Coefficient of 0.214 and 10-Percent Propeller Radius Tip Clearance

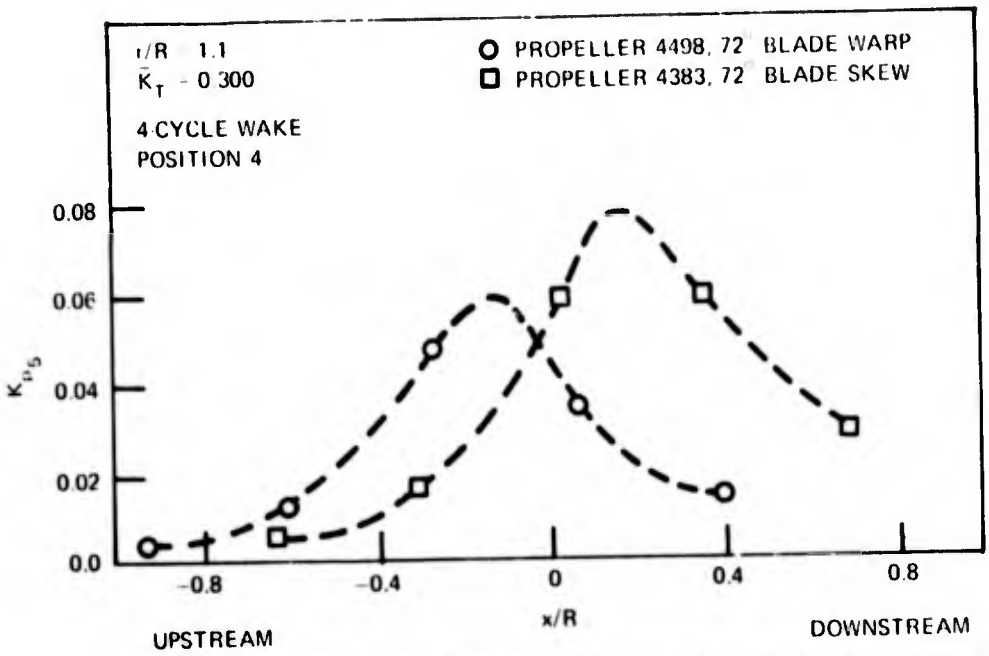

Figure 37 – Measured Blade-Frequency Pressure Amplitudes for Skewed and Warped Propellers of 72° at Mean-Thrust Coefficient of 0.300, 10-Percent Propeller Radius Tip Clearance, and Position 4 of the 4-Cycle Wake Screen

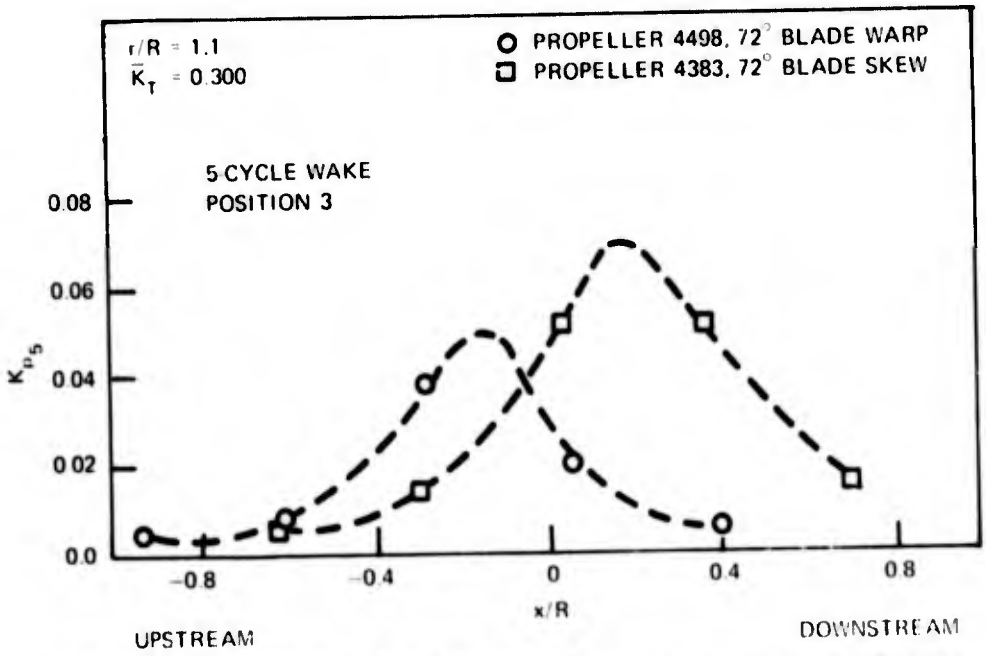

Figure 38 – Measured Blade-Frequency Pressure Amplitudes for Skewed and Warped Propellers of 72° at Mean-Thrust Coefficient of 0.300, 10-Percent Propeller Radius Tip Clearance, and Position 3 of the 5-Cycle Wake Screen

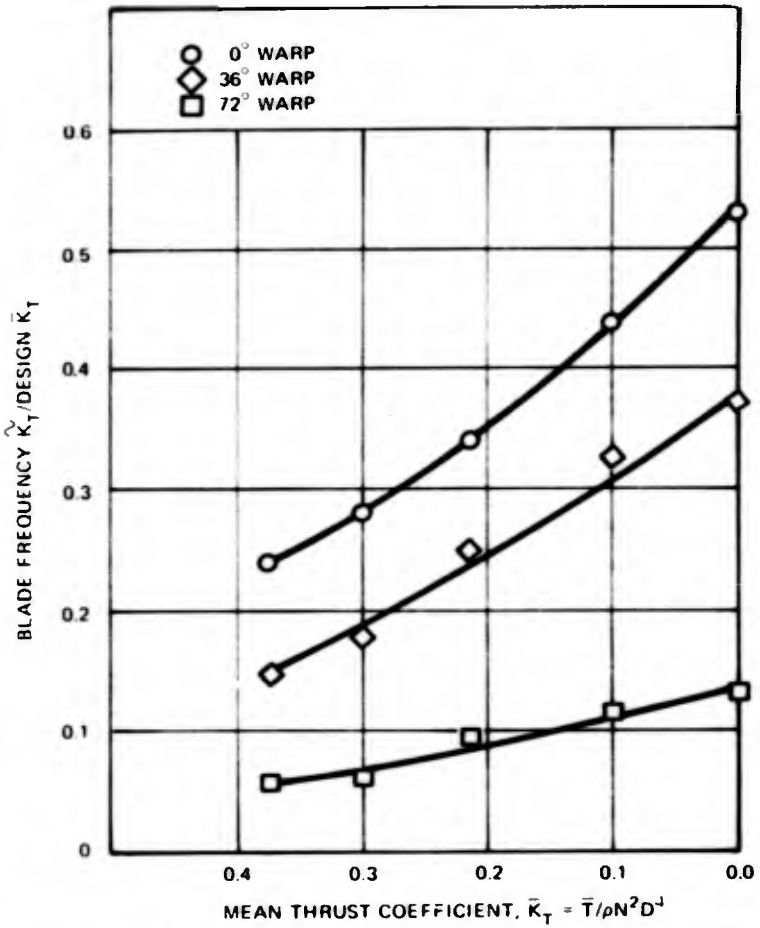

Figure 39 – Blade-Frequency Thrust in 5-Cycle Wake

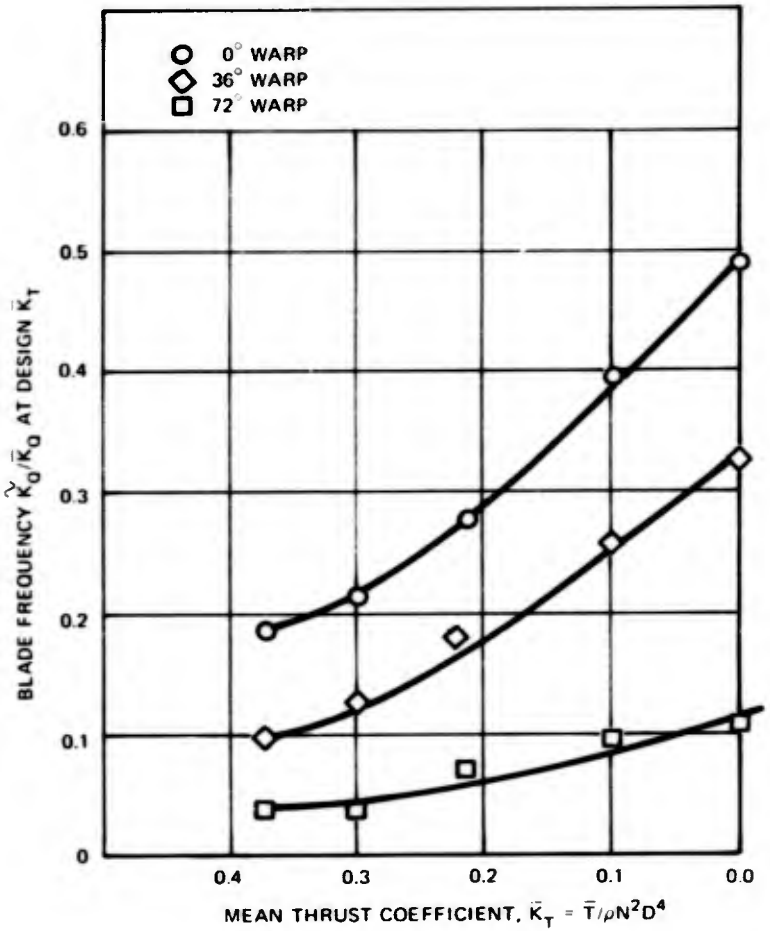

Figure 40 – Blade-Frequency Torque in 5-Cycle Wake

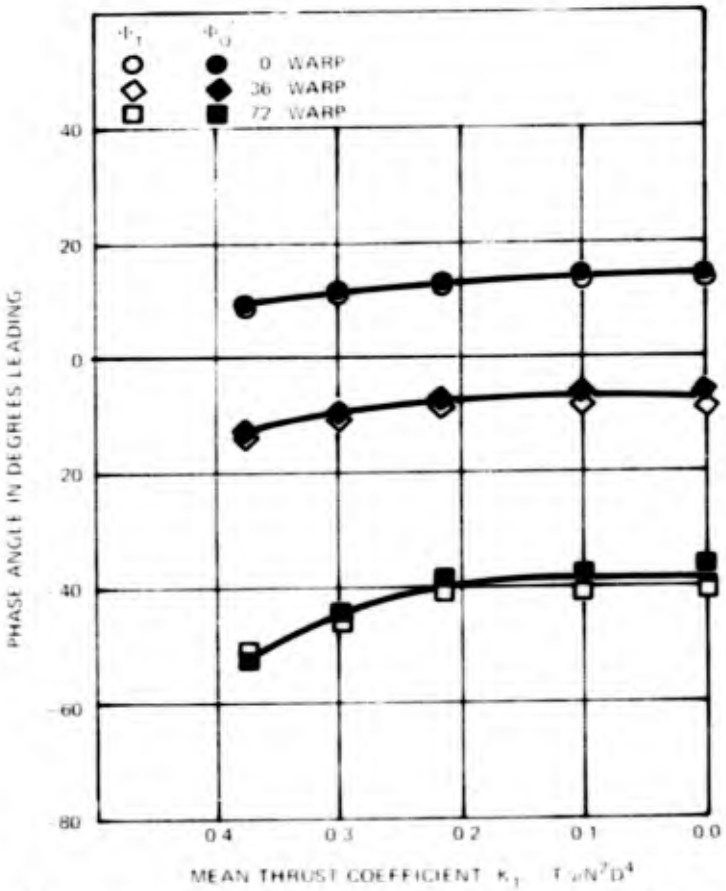

Figure 41 – Phase Angle of Blade-Frequency Thrust and Torque in 5-Cycle Wake

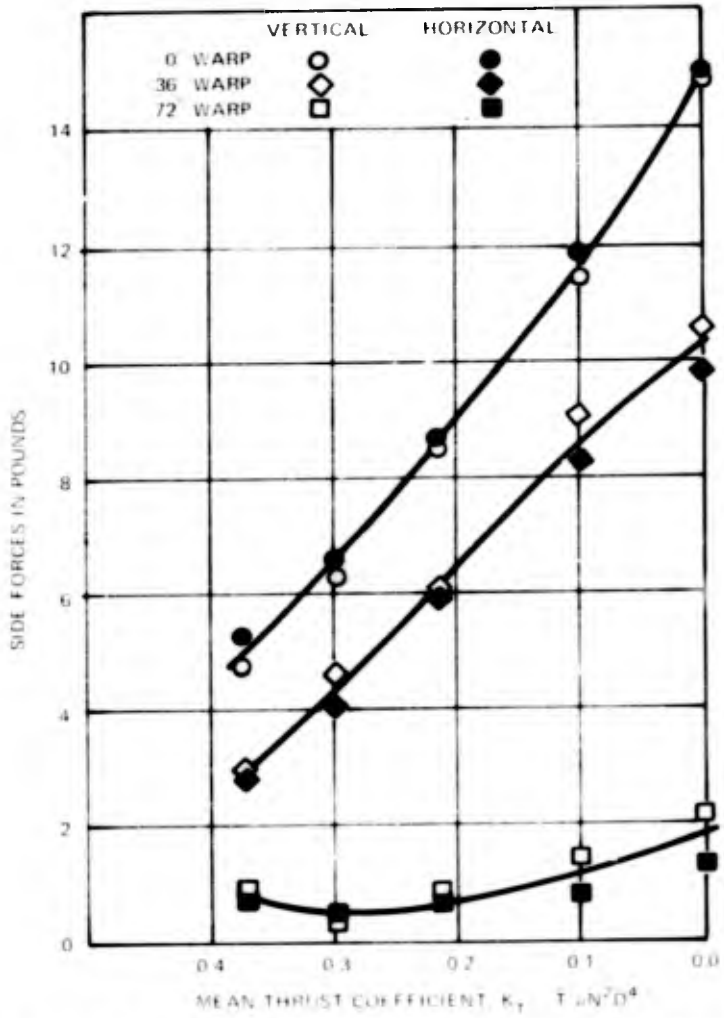

Figure 42 – Blade-Frequency Side Forces in 4-Cycle Wake

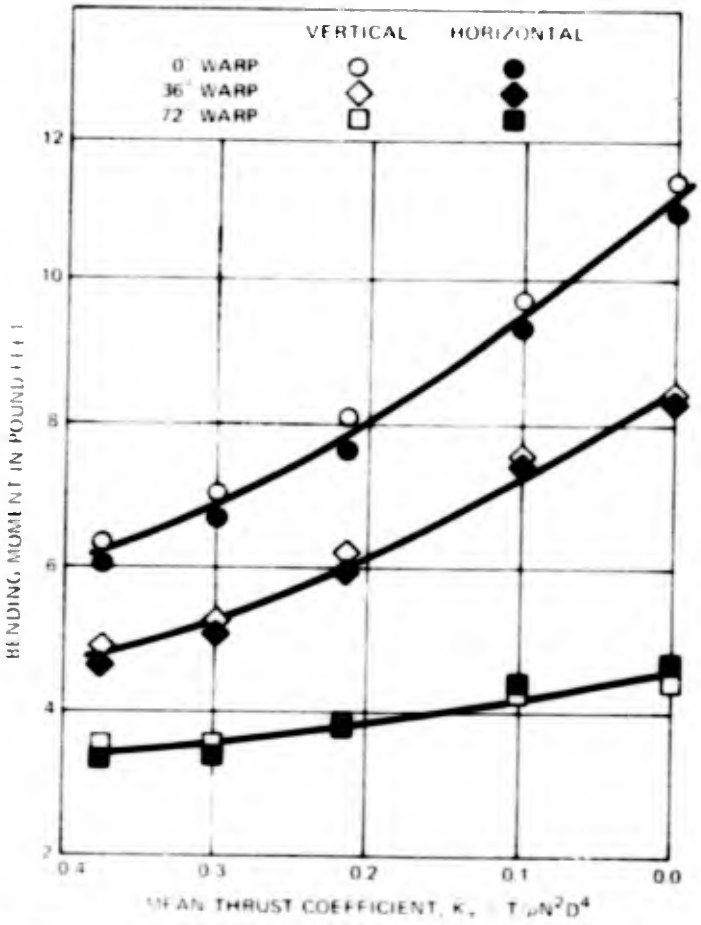

Figure 43 – Blade-Frequency Bending Moments in 4-Cycle Wake

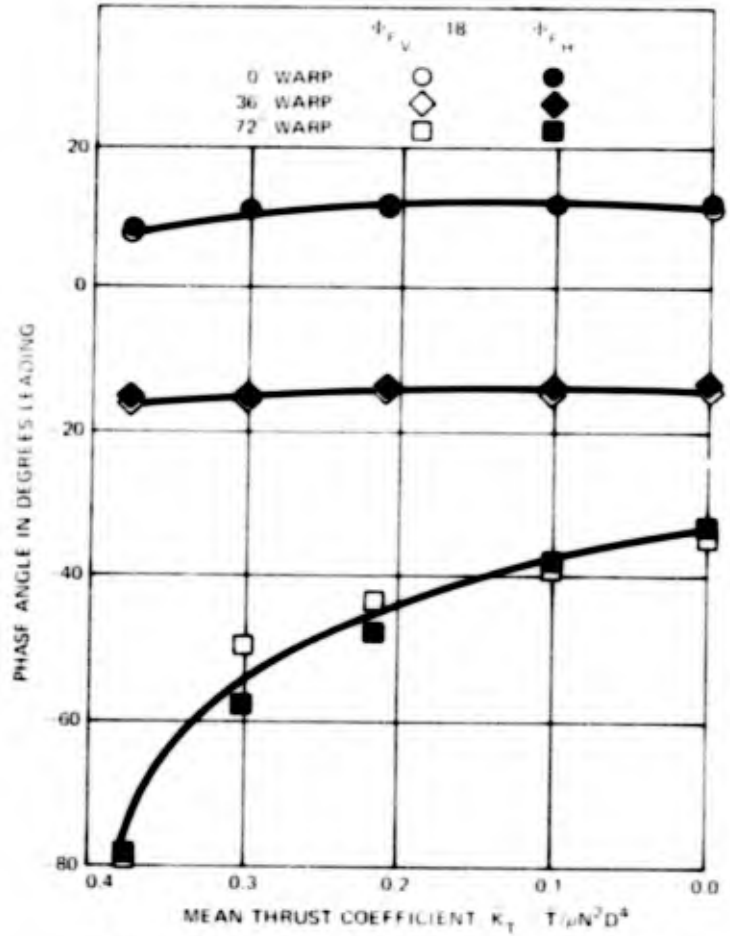

Figure 44 – Phase Angles of Blade-Frequency Side Forces in 4-Cycle Wake

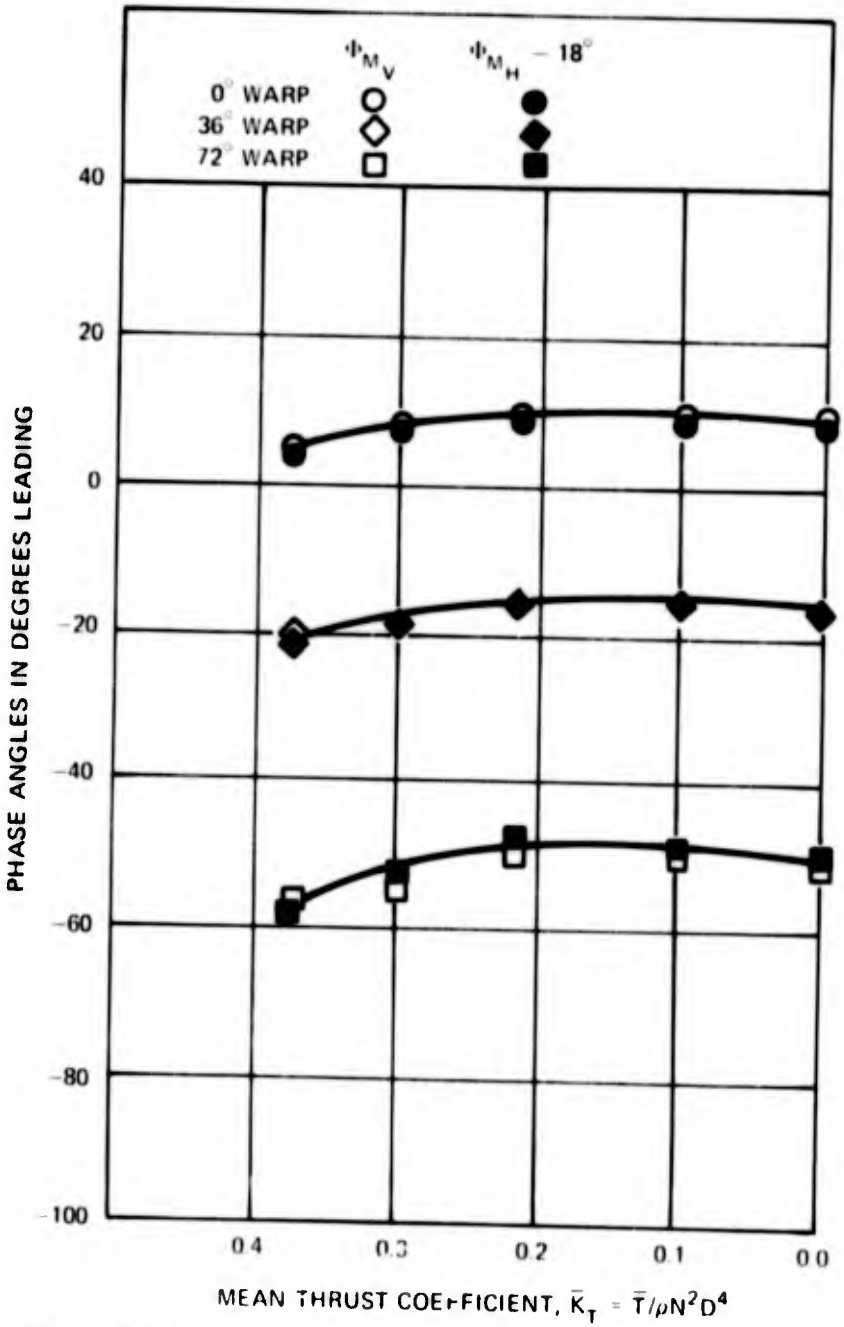

Figure 45 — Phase Angles of Blade-Frequency Bending Moments in 4-Cycle Wake

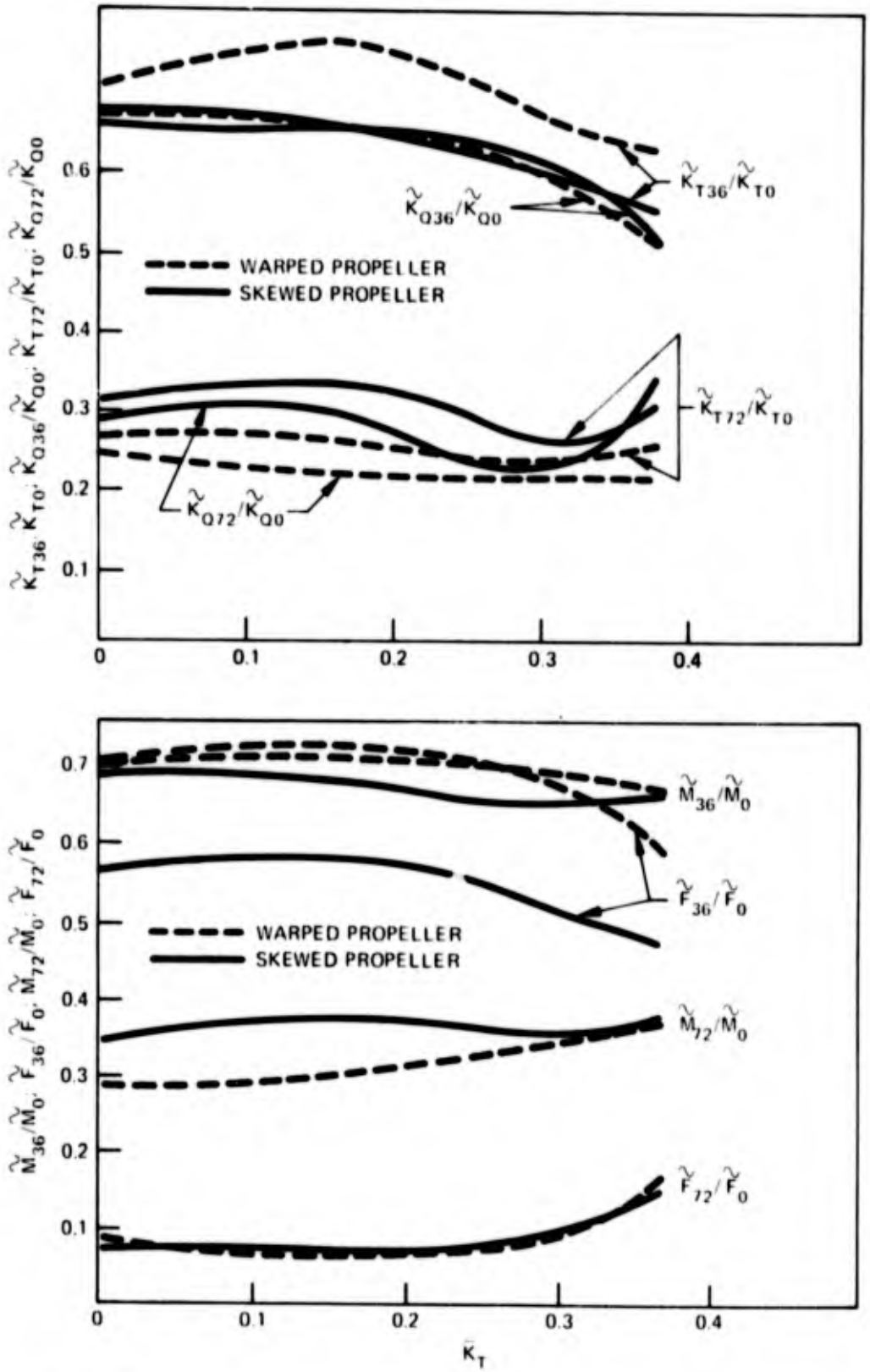

Figure 46 Unsteady Loading of a Series of Warped and Skewed Propellers at Various Mean Loading Conditions

TABLE I – PROPELLER DESIGNATION

Propeller Model Number	Geometric Characteristic	Propeller Designation
4382	36° skew	36S
4383	72° skew	72S
4497	36° warp	36W
4498	72° warp	72W

TABLE 2 – GEOMETRY OF WARPED PROPELLER SERIES

Number of Blades	5
Expanded Area Ratio	0.725
Section Mean Line	**NACA a = 0.8**
Section Thickness Distribution	**NACA 66** with NSRDC modified nose and tail
Design J	0.889
Design C_{Th}	0.686

r/R	tan β_i	c/D	t/c
0.2	1.8256	0.174	0.2494
0.3	1.3094	0.229	0.1562
0.4	1.0075	0.275	0.1068
0.5	0.8034	0.312	0.0768
0.6	0.6483	0.337	0.0566
0.7	0.5300	0.347	0.0421
0.8	0.4390	0.334	0.0314
0.9	0.3681	0.280	0.0239
PROPELLER 4381 – WARP 0 DEGREES			
r/R	θ_S (deg)	P/D	t_M/c
0.3	0.0	1.3448	0.0368
0.4	0.0	1.3580	0.0348
0.5	0.0	1.3361	0.0307
0.6	0.0	1.2797	0.0245
0.7	0.0	1.2099	0.0191
0.8	0.0	1.1366	0.0148
0.9	0.0	1.0660	0.0123

r/R	θ_S (deg)	P/D	t_M/c
PROPELLER 4497 – WARP 36 DEGREES			
0.3	4.655	1.4332	0.0370
0.4	9.363	1.4117	0.0344
0.5	13.948	1.3613	0.0305
0.6	18.378	1.2854	0.0247
0.7	22.747	1.1999	0.0199
0.8	27.145	1.1117	0.0161
0.9	31.575	1.0270	0.0134
PROPELLER 4498 – WARP 72 DEGREES			
0.3	9.293	1.5124	0.0407
0.4	18.816	1.4588	0.0385
0.5	27.991	1.3860	0.0342
0.6	36.770	1.2958	0.0281
0.7	45.453	1.1976	0.0230
0.8	54.245	1.0959	0.0189
0.9	63.102	0.9955	0.0159

TABLE 3 – AXIAL LOCATION OF PRESSURE TRANSDUCERS WITH RESPECT TO REFERENCE PLANE OF PROPELLER

Transducer	x/R
1	−0.93
2	−0.60
3	−0.27
4	+0.06
5	+0.40

TABLE 4 – OPEN-WATER ADVANCE COEFFICIENTS AT THE THRUST COEFFICIENTS SELECTED FOR WATER TUNNEL EXPERIMENTS

Propeller Number	Propeller Blade Warp deg	Thrust Coefficients				
		0.00	0.100	0.214	0.300	0.375
		Advance Coefficients				
4381	0	1.280	1.118	0.873	0.688	0.538
4497	36	1.300	1.145	0.938	0.762	0.598
4498	72	1.344	1.182	0.955	0.765	0.581

TABLE 5 – FORWARD OPEN-WATER PERFORMANCE AT DESIGN THRUST COEFFICIENT AND DESIGN SHAFT HORSEPOWER

Design Conditions: SHP_D = 32,000
n_D = 105 rpm = 1.75 rps
V_D = 35.78 fps
D = 23.00 ft
J_D = 0.889
C_{Th} = 0.686
K_{TD} = 0.214
$10K_{QD}$ = 0.447

$$\frac{n}{n_D} = \left[\frac{K_{QD}}{K_Q}\right]^{1/3}$$

$$\frac{V_A}{V_D} = \frac{JnD}{V_D}$$

Propeller	J	K_T	$10K_Q$	J/J_D	n/n_D	V_A/V_D
36S	0.896	0.215	0.436	1.007	1.008	1.016
72S	0.910	0.222	0.460	1.023	0.990	1.013
36W	0.917	0.226	0.483	1.032	0.974	1.005
72W	0.925	0.230	0.513	1.040	0.955	0.994

TABLE 6 – EFFECT OF SKEW AND WARP ON STEADY BACKING SPEED AT CONSTANT POWER

C_{Th}	$\frac{V_A \text{ (skew = 36 deg)}}{V_A \text{ (skew = 0 deg)}}$	$\frac{V_A \text{ (skew = 72 deg)}}{V_A \text{ (skew = 0 deg)}}$	$\frac{V_A \text{ (warp = 36 deg)}}{V_A \text{ (warp = 0 deg)}}$	$\frac{V_A \text{ (warp = 72 deg)}}{V_A \text{ (warp = 0 deg)}}$
0.2	0.997	0.939	0.949	0.940
0.4	0.984	0.932	0.941	0.924
0.8	0.991	0.940	0.948	0.923
1.2	0.992	0.948	0.954	0.921
1.6	0.997	0.956	0.953	0.930

TABLE 7 – BACK BUBBLE CAVITATION NUMBER AT DESIGN THRUST LOADING

Propeller Number	Propeller Designation	Cavitation Number	Advance Coefficient
4382	36S	1.38	0.896
4383	72S	1.30	0.910
4497	36W	1.60	0.9175
4498	72W	2.04	0.925

REFERENCES

1. Cumming, R. A. et al., "Highly Skewed Propellers," Transactions of Society of Naval Architects and Marine Engineers, Vol. 80 (1972).

2. Boswell, R. J. and M. L. Miller, "Unsteady Propeller Loading Measurement, Correlation with Theory, and Parametric Study," NSRDC Report 2625 (Oct 1968).

3. Denny, S. B., "Comparisons of Experimentally Determined and Theoretically Predicted Pressures in the Vicinity of a Marine Propeller," NSRDC Report 2349 (May 1967).

4. Teel, S. S. and S. B. Denny, "Field Point Pressures in the Vicinity of a Series of Skewed Marine Propellers," NSRDC Report 3278 (Aug 1970).

5. Denny, S. B., "Cavitation and Open-Water Performance of a Series of Propellers Designed by Lifting-Surface Methods," NSRDC Report 2878 (Sep 1968).

6. Boswell, R. J., "Design, Cavitation Performance and Open-Water Performance of a Series of Research Skewed Propellers," NSRDC Report 3339 (Mar 1971).

7. Boswell, R. J., "Static Stress Measurements on a Highly Skewed Propeller Blade," NSRDC Report 3247 (Dec 1969).

8. Boswell, R. J. et al., "Experimental Measurements of Static Stresses in a Series of Research Skewed Propellers with and without Forward Rake," NSRDC Report 3804 (in preparation).

9. Ma, J. H., "Stress Analysis of Complex Ship Components by Numerical Procedure Using Curved Finite Elements," NSRDC Report 4057 (Jul 1973).

10. Kerwin, J. E., "Computer Techniques for Propeller Blade Section Design," Presented at Second LIPS Propeller Symposium, Drunen, Netherlands (May 1973).

11. Pien, P. C., Discussion of Paper, "Highly Skewed Propellers," by Cumming, R. A. et al., Transactions of Society of Naval Architects and Marine Engineers, Vol. 80 (1972).

12. Cheng, H. M., "Hydrodynamic Aspect of Propeller Design Based on Lifting-Surface Theory, Part II Arbitrary Chordwise Load Distribution," David Taylor Model Basin Report 1803 (Jun 1965).

13. Kerwin, J. E. and R. Leopold, "Propeller-Incidence Correction Due to Blade Thickness," Journal of Ship Research, Vol. 7, No. 2 (Oct 1963).

14. McCarthy, J. H., "A Method of Wake Prediction in Water Tunnel," David Taylor Model Basin Report 1785 (Oct 1963).

15. Hadler, J. B. and H. M. Cheng, "Analysis of Experimental Wake Data in Way of Propeller Plane of Single and Twin-Screw Ship Models," Transactions of Society of Naval Architects and Marine Engineers, Vol. 73 (1965).

16. Cox, G. G. and Wm. B. Morgan, "The Use of Theory in Propeller Design," Marine Technology, Vol. 9, No. 4 (Oct 1972).